BUTYL RUBBER-CERAMIC COMPOSITES FOR FLEXIBLE ELECTRONIC APPLICATIONS

THESIS SUBMITTED TO
COCHIN UNIVERSITY OF SCIENCE AND TECHNOLOGY
IN PARTIAL FULFILLMENT OF REQUIREMENTS
FOR THE DEGREE OF
DOCTOR OF PHILOSOPHY IN CHEMISTRY

UNDER THE FACULTY OF SCIENCE

CHAMESWARY J.

Under the guidance of
Dr. M. T. Sebastian
&
Co-guidance of
Dr. S. Ananthakumar

Materials Science and Technology Division
NATIONAL INSTITUTE FOR INTERDISCIPLINARY SCIENCE AND TECHNOLOGY

Council of Scientific and Industrial Research
Thiruvananthapuram, Kerala, India – 695019

May 2014

Dedicated to My Beloved Son

Parthiv……..

DECLARATION

I hereby declare that the work embodied in the thesis entitled **"BUTYL RUBBER-CERAMIC COMPOSITES FOR FLEXIBLE ELECTRONIC APPLICATIONS"** is the result of investigations carried out by me at Materials Science and Technology Division, National Institute for Interdisciplinary Science and Technology (CSIR-NIIST), Thiruvananthapuram, under the supervision of Dr. M. T. Sebastian and the co-supervision of Dr. S. Ananthakumar and the same has not been submitted elsewhere for any other degree.

Thiruvananthapuram **Chameswary J.**

Dated:

राष्ट्रीय अंतर्विषयी विज्ञान तथा प्रौद्योगिकी संस्थान
NATIONAL INSTITUTE FOR INTERDISCIPLINARY SCIENCE AND TECHNOLOGY
वैज्ञानिक तथा औद्योगिक अनुसंधान परिषद् | Council of Scientific and Industrial Research
इंडस्ट्रियल इस्टेट पी. ओ, पाप्पनंकोड, तिरुवनंतपुरम, भारत - 695 019 | Industrial Estate P.O., Pappanamcode,Thiruvananthapuram, India-695 019

CERTIFICATE

This is to certify that the work embodied in the thesis entitled **"BUTYL RUBBER-CERAMIC COMPOSITES FOR FLEXIBLE ELECTRONIC APPLICATIONS"** has been carried out by Mrs. Chameswary J. under my supervision and the co-supervision of Dr. S. Ananthakumar at Materials Science and Technology Division, National Institute for Interdisciplinary Science and Technology, (CSIR-NIIST), Thiruvananthapuram, in partial fulfillment of the requirements for the award of the Degree of Doctor of Philosophy in Chemistry, under the Faculty of Science, Cochin University of Science and Technology, Cochin and the same has not been submitted elsewhere for any other degree. All the relevant corrections and modifications suggested by the audience and recommended by the doctoral committee during the pre-synopsis seminar of Mrs. Chameswary J. have been incorporated in the thesis.

Dr. S. Ananthakumar
Principal Scientist
National Institute for Interdisciplinary Science and Technology (CSIR),
Thiruvananthapuram

Dr. M. T. Sebastian
Chief Scientist
National Institute for Interdisciplinary Science and Technology (CSIR),
Thiruvananthapuram

CONTENTS

CHAPTER 2

Materials and Experimental Techniques

CHAPTER 3

Butyl Rubber-Low Permittivity Ceramic (Al_2O_3, SiO_2 and $Ba(Zn_{1/3}Ta_{2/3}O_3)$) Composites

CHAPTER 4

Butyl Rubber-High Permittivity Ceramic (TiO_2, $Sr_2Ce_2Ti_5O_{15}$ and $SrTiO_3$) Composites

CHAPTER 5

Butyl Rubber-Very High Permittivity Ceramic ($BaTiO_3$ and $Ba_{0.7}Sr_{0.3}TiO_3$) Composites

PREFACE

Flexible electronics is a rapidly growing area in the microelectronics industry. The assemblage of electronic components on flexible printed circuit boards is a new way to fabricate electronic systems in stationary, mobile and automotive applications. Flexible electronics are being extensively used in flexible displays, sensor arrays or skins, curved circuits, curved detector arrays and other large area electronics. The flexible circuit connectors find applications in stretchable thermometers, biomedical devices and electronic clothing etc. The soft and rubbery future of electronic industry needs new materials to satisfy their requirements. For some applications, particularly in the biomedical field, electronic circuits are to be conformally wrapped around curved surfaces. The dielectric materials used for flexible electronic applications must have mechanical flexibility, optimum relative permittivity, low loss tangent, temperature stability of relative permittivity, low coefficient of thermal expansion (CTE) and high thermal conductivity. It's very difficult to get a single phase material with all the required properties. Most of the elastomers show good flexibility and even stretchability. But their very low relative permittivity, low thermal conductivity and large CTE are unfavorable for practical applications. On the other hand, ceramics show promising thermal and dielectric properties. But their inherent brittleness precludes them from direct use. The most convenient way to obtain all the requisite properties together is by the formation of elastomer–ceramic composites. In such systems, the circuits must be not only flexible but also stretchable.

The thesis entitled **"BUTYL RUBBER-CERAMIC COMPOSITES FOR FLEXIBLE ELECTRONIC APPLICATIONS"** is divided into 6 chapters. It is the outcome of a detailed investigations carried out on the synthesis and characterization of butyl

rubber composites with low, high and very high permittivity ceramic for flexible substrate, electronic packaging and waveguide applications.

The first chapter of the thesis gives a general introduction about flexible electronics, dielectrics and composites. The recent developments in flexible electronics also discussed in this chapter. The preparation and characterization techniques used for the butyl rubber-ceramic composites are given in chapter 2.

The synthesis and characterization of butyl rubber filled with low permittivity ceramic composites are described in chapter 3. The low permittivity ceramics used for the present study are alumina, silica and barium zinc tantalate. The dielectric, thermal and mechanical properties of the composites was investigated as a function of filler volume fraction. The effect of filler particle size on these properties of butyl rubber-alumina composites is also studied. The measured properties suggest that butyl rubber-$Ba(Zn_{1/3}Ta_{2/3})O_3$, butyl rubber-SiO_2 and butyl rubber-micron Al_2O_3 composites are suitable candidates for microwave substrate and electronic packaging applications.

The chapter 4 deals with the synthesis and characterization of butyl rubber-high permittivity ceramic composites. The effect of high permittivity ceramic fillers such as TiO_2, $Sr_2Ce_2Ti_5O_{15}$ and $SrTiO_3$ on dielectric, thermal and mechanical properties was studied. The influence of filler particles size on these properties is investigated in butyl rubber-TiO_2 composites. The maximum filler loaded butyl rubber composites are possible candidates for flexible dielectric waveguide applications and other compositions can be used as microwave substrate and electronic packaging applications and find application as cladding of flexible dielectric wave guide. A flexible monopole antenna is fabricated using BR/ST-4 composite.

The synthesis and characterization of butyl rubber-very high permittivity ceramic composites are discussed in chapter 5. $BaTiO_3$ and $Ba_{0.7}Sr_{0.3}TiO_3$ are the very high permittivity ceramics used and their effect on dielectric, thermal and mechanical properties of the composites are investigated. The effect of filler particles size on these properties is studied in butyl rubber-$BaTiO_3$ composites.

Chapter 6 primarily highlights the summary of the results made in this thesis with an outline of future work.

Acknowledgements

I present this thesis, in the name of God, the Almighty, the most beneficent and merciful who showered HIS unperturbed love and blessings throughout my life and provided me physical, mental and spiritual support for the successful completion of this work.

I have great pleasure to express my deepest sense of gratitude to my research supervisor Dr. M. T. Sebastian for suggesting me an interesting problem. His effective guidance, creative discussions, constant support and encouragement helped me a lot in formulating the thesis in time.

I would like to express my sincere thanks to Dr. S. Ananthakumar, my co-guide for his constant support and inspiration during the period of my research.

I am grateful to Dr. Suresh Das, Director, National Institute of Interdisciplinary Science and Technology (NIIST), Thiruvananthapuram, Dr. B. C. Pai and Prof. T. K. Chandrasekhar, (Former Directors, NIIST, Thiruvananthapuram) for kindly providing the necessary facilities for carrying out research work.

I wish to thank Dr. K. G. K. Warrier (Former Head, MSTD), Dr. U. Shyama Prasad, Dr. P. Prabhakar Rao (Scientists, NIIST, Thiruvananthapuram) and Dr. Peter Koshy for their help rendered during the course of this work.

I am indebted to Dr. K. P. Surendran, Dr. Manoj Raama Varma and Dr. Jose James (Scientists, NIIST, Thiruvananthapuram), Dr. J. D. Sudha, Dr. C. Pavithran, Dr. A. R. R. Menon and Dr. V. S. Prasad (Polymer section, NIIST, Thiruvananthapuram) for all the help rendered by them during my research work.

I would like to acknowledge Prof. P. Mohanan (Department of Electronics, CUSAT, Kochi) for antenna measurements.

I am immensely thankful to Mr. P. Chandran, Mr. P. Gurusamy, Mr. M. Brahmakumar and Mr. A. Peer Mohamed for extending the SEM, XRD, mechanical

and thermal measurement facility for my research work. I am thankful to all the office and library staff at NIIST for all the help and cooperation.

I am extremely thankful to my seniors, Dr. G. Subodh, Dr. P. S. Anjana, Dr. Sumesh George, Dr. Sherin Thomas, Dr. Tony Joseph, Dr. T. S. Sasikala, Dr. Dhanesh Thomas and Dr. K. S. Deepa for their creative suggestions, timely advice and constant support which paved way for the completion of my work. I am also thankful to Dr. V. L. Reena, Dr. Bindhu P. Nair for their love, care and support during the research work.

I express my hearty thanks to Ms. Nina Joseph for her loving companionship, valuable suggestions and constant mental support throughout the period of my work. I would like to thank my collegues and friends in NIIST especially Mr. K. M. Manu, Mr. Jobin Varghese, Mr. Abhilash. P, Ms. Namitha L. K, Ms. Gayathri T. H, Ms. P. Nisha, Ms. C. P. Resmi, Ms. P. Neenulekshmi, Mr. Jithesh K, Mr. Binu Mohanan, Mr. Dijith K. S, Ms. Aiswarya R., Mr. Arun B., Ms. Angel Mary Joseph, Ms. Lekshmi D. R., Mr. Arun S., Ms. Indhuja I. J., Ms. Roshni S. Babu, Ms. Kanagangi S. Nair, Dr. Savitha S. Pillai, Mr. M. A. Sanoj, Ms. Anlin Lazar and Ms. K. T. Rethika, Ms. Varsha Viswanath, Ms. Ann Rose Sunny, Mr. Arun, Ms. Raji G. R, Ms. Y. Jasna, Ms. U. Bhagya, Ms. Chinthu sukumar, Ms. Deepa J. P., Ms. Resmi V. G, Ms. Krishnapriyanka, Ms. Raseena, Ms. B. Sayoojyam, Ms. Mridhula, Ms. Shani, Ms. Gopika, Ms. Sachana, Mr. Sumesh Gopinath, Ms. Gopika, Mr. Mathew Presumie, Mr. Taylor Djaafer, Mr. Romain Bonnet, Ms. Sivabharathy, Ms. Varsha, Ms. Sreelekshmi, Ms. Sreena, Ms. Sreejitha, Ms. Anumol Varkey, Mr. Hemanth, and Mr. Anoop who helped me in many ways during my research work.

I also extend my sincere thanks to Ms. Sumy Mathew and Mr. Dinesh for their help and support for the successful completion of work.

I would like to thank Department of Science and Technology (DST) and Council of Scientific and Industrial Research (CSIR), Government of India for providing me the research fellowship.

I owe an unlimited debt of gratitude to my father N. Janarthanan, my mother J. Padmavathy and dearest sister J. Sindhu for their love, encouragements and prayers throughout my research life. I wish to express my special thanks to my husband Mr. V. Saravanan for his understandability, love, inspiration and constant support during the course of my work. He stood with me in my thick and thin and provided lots of encouragements that lead to the successful completion of my research work. At this moment, I also remember my beloved son Parthiv for his indefinable patience and love.

Last but not least, I want to express my thanks to all those who have helped me in many ways for the successful completion of this work.

Chameswary J.

Chapter 1

Introduction

The first chapter gives a general introduction about flexible electronics, dielectrics and also recent developments in this field. This chapter also cites the importance of elastomer-ceramic composites in today's electronic world.

1.1 Introduction

Wireless communication is one of the most vibrant areas in the communications field in this era. Wireless communications involves the transfer of information between two points without direct connection. The first radio communication was born when Marconi demonstrated the radio transmission from Isle of Wight to a tugboat 18 miles away in 1895 [1]. Later radio technology advanced rapidly to enable transmissions over large distances with better quality, less power and smaller, cheaper devices. By far, the most successful application of wireless communication is cellular telephone system [2]. The number of mobile subscribers has been growing tremendously in the past decades. The number of mobile phone subscribers is about 6.8 billion with a world population of about 7 billion. In India we have about 900 million mobile subscribers which are much more than that predicted five years ago.

Most modern wireless systems rely on (radiofrequency) RF or microwave signals because they offer wide bandwidths. The majority of wireless systems operate at higher frequencies due to the crowding of spectrum and the need for higher data rates. RF frequencies range from very high frequency (VHF) (30–300 MHz) to ultra high frequency (UHF) (300–3000 MHz). The microwave is typically used for frequencies between 0.3 GHz (300 MHz) and 300 GHz with a corresponding wavelength between 1 m and 1 mm [3].

The microwave region is divided into different bands as per the recommendation of Institute of Electrical and Electronics Engineers (IEEE) and is given in Table 1.1.

Table 1.1 Licensed spectrum allocated to major commercial wireless systems.

Wireless system	Frequency range
AM radio	535-1605 KHz
FM radio	88-108 MHz
Broadcast TV	54-88 MHz, 174-216 MHz
Broadcast TV (UHF)	470-806 MHz
3G broadband wireless	746-764 MHz, 776-794 MHz
1G and 2G digital cellular phones	806-902 MHz
Satellite digital radio	2.32-2.325 GHz
Satellite TV	12.2-12.7 GHz
Fixed wireless services	38.6-40 GHz

Today's wireless systems include broadcast radio and television, cellular telephone and networking systems, direct broadcast satellite (DBS) television service, wireless local area networks (WLANs), paging systems, global positioning system (GPS) service and radio frequency identification (RFID) systems [4]. Recently, interest in wireless systems for medical applications has been rapidly increasing. Wireless devices have invaded the medical area with a wide range of capability. Portable devices such as heart rate monitors, pulse oximeters, spirometers and blood pressure monitors use wireless technology in medical field [5]. RF and microwave communication systems are pervasive, especially today when wireless connectivity promises to provide voice and data access to "anyone, anywhere, at any time." Figure 1.1 shows the location of the RF and microwave frequency bands in the electromagnetic spectrum.

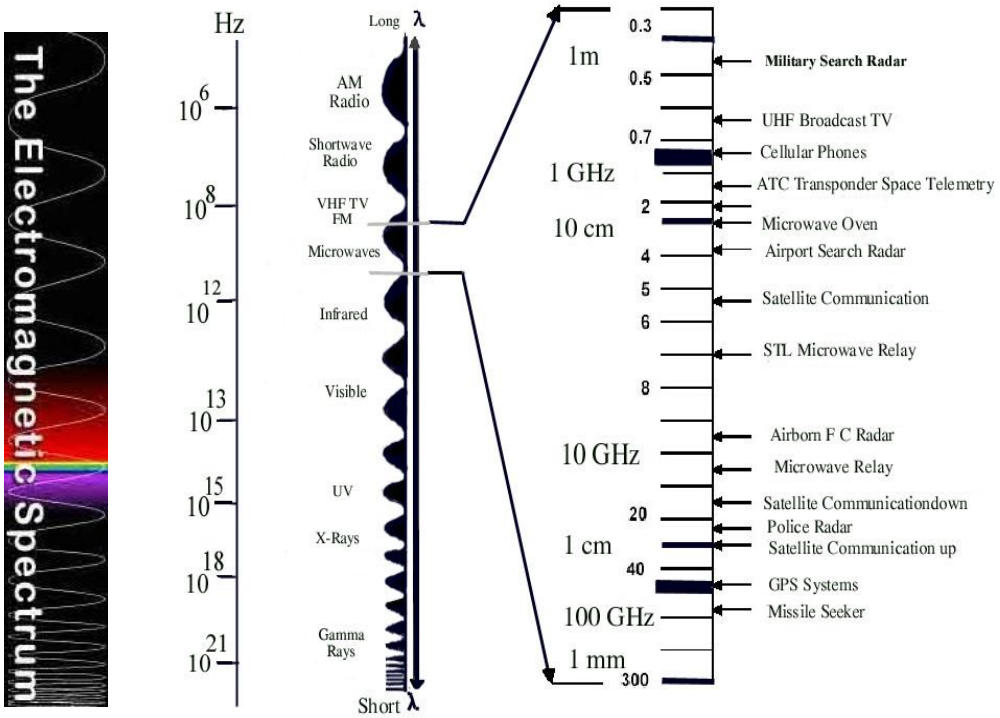

Fig. 1.1 The electromagnetic spectrum and its applications (Ref. 6)

Moore's law predicts that the number of components in a module doubles in two years. The researchers are urged to develop novel materials for microwave components as the clock speeds of electronic devices are approaching microwave frequencies.

1.2 The need for flexible electronics

Flexible electronics enable new applications such as flexible displays, flexible and conformal antenna arrays, electronic solar cell arrays, RFID tags, flexible batteries, electronic circuits fabricated in clothing, aerospace and biomedical devices [5,7]. Flexible electronics is a technology for assembling electronic circuits by mounting electronic devices on flexible substrates. It is also known as flex circuits. The development of flexible electronics dates back to the 1960s. The first flexible solar cell arrays were made by thinning single crystal

silicon wafer cells to ≈100 μm and then assembling them on a plastic substrate to provide flexibility. The first flexible thin film transistor (TFT) of tellurium was developed by Brody and collegues in 1968. Brody's group later made TFTs on wide range of flexible substrates such as mylar, polyethylene and anodized aluminium wrapping foil [8]. Mechanical flexibility in electronic devices would enable new applications which are incompatible with conventionally integrated rigid circuits. In recent years, a radically growing research are focused towards the development of flexible electronics, since it offers many advantages like lightweight, thin, robust and conformable and have the ability to be rolled when not in use [9]. Flexibility can provide many different properties to manufacturers and users and it is conveniently classified in three categories, permanently shaped, bendable or rollable and elastically stretchable. Technologies based on organic materials, reel-to-reel printed polymers, inkjet-printed chemicals, carbon nanotubes and thin-film semiconductors have all contributed to the development of flexible electronics [10,11]. In order to incorporate electronic monitoring devices inside a human body such as heart patients, the electronics must take the shape of the object in which they are integrated and must even follow all complex movements of these objects explaining the need for stretchability. Elastically stretchable electronics can undergo large and reversible deformation which is suitable for biomedical applications. Two basic approaches have been employed to make flexible electronics: (1) transfer and bonding of completed circuits to a flexible substrate which have the advantage of providing high performance devices on flexible substrate and (2) fabrication of the circuits directly on the flexible substrate [8].

The most significant contribution to flexible and stretchable electronics was made by Roger's group at University of Illinois, Urbana Champaign who proposed fully integrated

stretchable electronics. They made stretchable and foldable silicon integrated circuits on wavy silicon ribbons in Polydimethyl siloxane (PDMS) and have demonstrated appealing devices including electronic eye sensor, smart gloves, implanted medical devices and wearable ergonomic biomedical sensors [12]. For stretchable electronic applications, the carrier substrate is an elastic or viscoelastic polymer, e.g., silicones or polyurethanes. PDMS and silicone elastomer are frequently used as stretchable substrates, scaffolds or transfer media for flexible and stretchable devices [13]. Polytetrafluoroethylene (PTFE), polystyrene, polyethylene, liquid crystal polymer, parylene-N etc. are widely used as flexible substrates [14-17]. DuPont™ Kapton® polyimide film has been used in the electronic industry for over 40 years as a dielectric substrate for flexible copper clad laminate. Experts predict that global flexible electronics market will grow to $ 250 billion by 2025 [18].

As the research on flexible electronics has expanded rapidly, many groups and companies have demonstrated flexible displays. Philips demonstrated a prototype rollable electrophoretic display and Samsung announced a 7” flexible liquid crystal panel in 2005. In 2006 Universal Display Corporation and the Palo Alto Research Center presented a prototype flexible organic light emitting diode (OLED) display with a poly-Si TFT backplane made on steel foil [8]. Samsung officially released their first flexible mobile phone called "Youm" on January 2013. In October 2013, Samsung announced the world's first flexible OLED display-the Galaxy Round curved smartphone [19]. Recently Northwestern university scientists have developed first stretchable lithium ion battery. Now it is possible to use stretchable electronic devices anywhere, even inside the body and they can monitor brain waves to heart activity where flat, rigid batteries would fail [20]. Jan Vanfleteren et al. have developed a stretchable thermometer which can wrap around patient’s forehead like a headband [21].

It is anticipated that more than 50 billion devices will be wirelessly connected by 2020 which would involve units as intelligent as smartphones/tablets and as soft as elastomeric electronics.

1.3 Dielectrics for microelectronic industry

The rapid development of mobile communication and satellite broadcasting necessitated the development of microwave electronic devices with high speed. Low loss dielectric materials are needed for microwave frequency applications and frequency selectivity of microwave devices. In electronic industry, dielectric materials have been used as electronic packages, substrates, wave guides, capacitors, resonators, filters etc.

1.3.1 Electronic packaging applications

The electronic packaging is an important factor which decides the ultimate performance of an integrated circuit (IC). Electronic packages are structures that seal a circuit from the environment and make it a single, compact unit [22]. The role of packaging materials is to ensure the electrical insulation of the silicon chip and of circuit pins [23]. The evolution of electronic packaging can be categorized into three generations. The first generation of package called discrete board package which used discrete components to fulfill the supporting function to IC. The second generation used technologies such as chip scale packaging (CSP) and multi- chip-module (MCM) to increase the IC efficiency to 30-40%. The third generation is based on single level integrated module (SLIM) technology called system on package (SOP) proposed by the Packaging Research Center of Georgia Tech. In multilayer printed circuit boards, packaging materials separate interlayers and provide isolated pathways for electronic devices connection [24]. The actual applications of

materials in electronic packaging include interconnections, printed circuit boards, substrates, encapsulations, interlayer dielectrics, die attach, electrical contacts, connectors, thermal interface materials, heat sinks, solders, brazes, lids, housings and so on [25]. High density and high frequency as well as high speed have been the representative characteristics of future microelectronic packaging [26]. The signal attenuation, propagation velocity and cross talk of the microelectronic devices are influenced by the dielectric properties of the packaging material [27]. The propagation delay time (t_d) of electromagnetic waves in a dielectric is given by the equation,

$$t_d = \frac{l\sqrt{\varepsilon_r}}{c} \text{------(1.1)}$$

where l is the line length, ε_r is the relative permittivity of the substrate and c is the speed of light [6]. Hence the relative permittivity must be as low as possible to reduce propagation delay and must have low loss factor to reduce electrical loss for electronic packaging applications.

1.3.2 Substrate applications

A substrate is also called a chip carrier, is the base on which the microscopic electronic components and their connections are built. A substrate is either a single layer or multilayer. Substrates have been used for hybrid integrated circuits (HIC) and for packaging semiconductor IC chips [25]. Dielectric substrates are also used for fabricating transmission line media including microstrip, strip line, coax and even waveguide. This found applications in printed circuit board, microstrip patch antenna, monopole antenna etc.

A monopole antenna is a class of radio antenna consisting of a rod shaped conductor often mounted over a conductive surface called ground plane, the rod functions as a resonator for radio waves. The most common form is the quarter-wave monopole in which the length of antenna is approximately $1/4^{th}$ of a wavelength of the radio waves [28]. The equations of electromagnetic waves derived from Maxwell equations are

$$\nabla^2 E = \frac{1}{c^2}\frac{\partial^2 E}{\partial t^2} \text{------(1.2)} \qquad \nabla^2 H = \frac{1}{c^2}\frac{\partial^2 H}{\partial t^2} \text{------(1.3)}$$

where E is the electric field, H is the magnetic field strength and c is the velocity of electromagnetic wave in vacuum [29].

If the medium is dielectric, then the velocity of electromagnetic waves through a dielectric medium is given by $\mathbf{v} \propto (\mu\varepsilon_r)^{-1/2}$**.** Substrates having low relative permittivity are desirable which lead to better efficiency, large bandwidth and better radiation. Hence the preferable relative permittivity of substrates is typically in the range 2.2 to 12 [30]. Dielectric substrate materials are classified into hard substrates and soft substrates.

(a) Hard substrates

Hard substrates are ceramics such as alumina, aluminium nitride and beryllium oxide which can withstand extreme heat during wire bonding [25]. The market for these ceramic substrates has increased in recent years with the development of electronic industry. For electronic applications steatite and alumina have been used as the substrate due to its high mechanical strength and low loss tangents.

(b) Soft Substrates

Soft substrates are used in applications where packaged parts are soldered on the board. Generally polymers are used as soft substrates. Polymers like polytetrafluoroethylene (PTFE), polyethylene, polystyrene, polyether ether ketone and epoxy shows excellent dielectric properties [31]. However, their low thermal conductivity and high thermal expansion limits their application as substrate in electronic modules. A third category of substrate materials is the composites in which the soft substrates are loaded with hard ceramic particles.

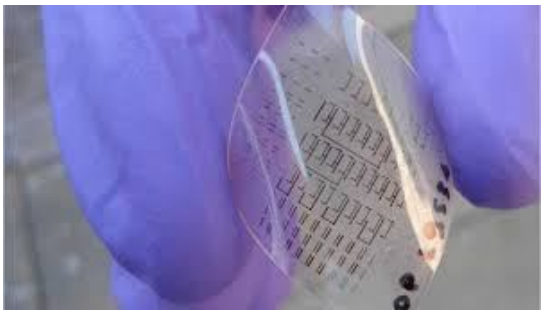

Fig. 1.2 A soft substrate
(Courtesy: www.eetimes.com)

1.3.3 Waveguide applications

Waveguides are a guide for electromagnetic waves and they enable them to feed power from one location to another. Within many electronic circles, waveguides are most commonly used for microwave RF signals and it will only carry or propagate signals above a certain frequency, known as the cut-off frequency. Below this the waveguide is not able to carry the signals. Waveguides are used for transferring both power and communication signals [32]. An ideal dielectric waveguide would have a small core consisting of a flexible, low loss material with large relative permittivity. The cladding would also be flexible and

low in loss and its relative permittivity would be much smaller than that of the core, so that the fields of the guided mode would decrease rapidly with distance in the cladding [33].

1.3.3.1 Types of RF waveguide

(a) Rectangular waveguide: This is the most commonly used form of waveguide and has a rectangular cross section.

(b) Circular waveguide: This is less common than rectangular waveguide. They have many similarities in their basic approach, although signals often use a different mode of propagation.

(c) Circuit board stripline: This form of waveguide is used in printed circuit boards as a transmission line for microwave signals. It typically consists of a line of a given thickness above an earth plane. Its thickness defines the impedance.

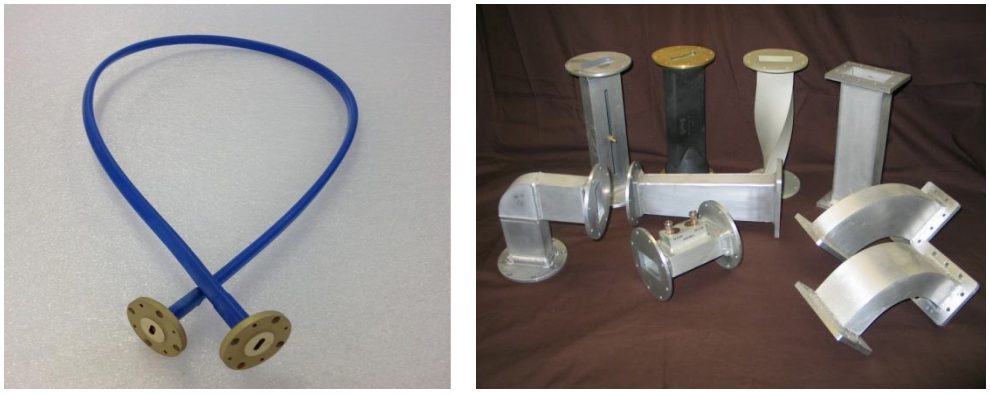

Fig. 1.3 A section of flexible waveguide
(courtesy: www.microwaveengservices.com)

(d) Flexible waveguide

In addition to these basic forms, there are also flexible waveguides. These are most widely seen in the rectangular format. Flexible waveguide is often used to connect to antennas [34].

1.4 Rudiments of dielectrics

The term "dielectric" was coined by William Whewell from "dia-electric" in response to a request from Michael Faraday. The definition of dielectric is a nonconductor of direct electric current [35]**.** The word dielectric and insulator are often used interchangeably. Insulators are substances which allow less amount of current flow through them. A dielectric is an electrical insulator which can be polarized by an applied electric field. When a dielectric is placed in an electric field, electric charges do not flow through the material as in a conductor, but slightly shift from their equilibrium positions causing dielectric polarization. This creates an internal electric field that reduces the overall field within the dielectric itself. Thus a dielectric can be defined as an insulator that can be polarized. All dielectrics are insulators, but all insulators are not dielectrics [36]. When a dielectric is placed between two plates of a capacitor, the capacitance of a capacitor will increase by a factor called relative permittivity (ε_r). The capacitance increases because the material effectively cancels part of the applied field and thus “storing” part of the field or charge. Fig. 1.4 shows the parallel plate capacitor without and with the presence of a dielectric between the plates.

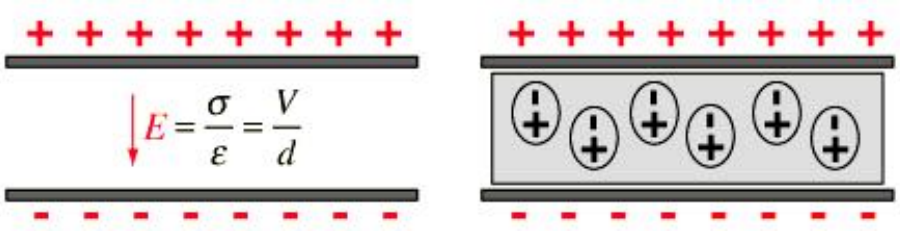

Fig. 1.4 Effect of a dielectric material of relative permittivity ε_r on the capacitance of a parallel plate capacitor

Relative permittivity (ε_r) and loss tangent (tan δ) are the two most important dielectric properties of a material used for high frequencies [37].

1.4.1 Relative permittivity (ε_r)

The permittivity is determined by the ability of a material to polarize in response to the field and thereby reduce the total electric field inside the material. Thus permittivity relates to a materials' ability to transmit an electric field. The relative permittivity (ε_r) is the ratio of permittivity of a substance (ε) to the permittivity of vacuum (ε_0).

$$\varepsilon_r = \varepsilon/\varepsilon_0 \text{ where } \varepsilon_0 = 8.85\text{x}10^{-12}\text{F/m.} \qquad 1.4$$

The relative permittivity of a material under given conditions reflects the extent to which it concentrates electrostatic lines of flux. It is related to the macroscopic properties like polarization or capacitance. The relative permittivity can be defined in terms of capacitance as the ratio of the capacitance of a capacitor with material as a dielectric, compared to a similar capacitor that has a vacuum as its dielectric. The permittivity and capacitance are related as

$$C=\varepsilon(A/d) = \varepsilon_r/\varepsilon_0(A/d). \qquad 1.5$$

where A is the area of cross section and d is the thickness of the sample.

When a dielectric is subjected to an external electric field E, dipole moments are induced inside the material. The dielectric polarization P is equal to the total dipole moment induced in the material by the electric field. Thus

$$P= N_i\mu_i, \qquad 1.6$$

where N_i is the number of dipoles of type i and μ_i is the average dipole moment. The polarization mechanisms operating in a dielectric depend on frequency, temperature and composition. Therefore the permittivity will also be a function of frequency, temperature and composition.

1.4.2 Loss tangent (tan δ)

Relative permittivity can be expressed in complex form as

$$\varepsilon^* = \varepsilon' - j\varepsilon'' \qquad 1.7$$

where ε' is real part which is relative permittivity and ε" is imaginary part which is the dielectric loss. The ratio between the dielectric loss with the relative permittivity is quantified as tan δ ie:

$$\tan\delta = \varepsilon''/\varepsilon \qquad 1.8$$

The loss tangent of a material is quantitatively defined as the dissipation of electrical energy due to different physical processes such as electrical conduction, dielectric relaxation, dielectric resonance and loss from non-linear processes [6]. It occurs due to the inability of polarization process in a molecule to follow the rate of change of the oscillating applied electric field. This arise from the relaxation time which is the time taken for the dipoles to return to its original random orientation. It does not occur instantaneously but the polarization diminished exponentially. The loss will be minimum, if the relaxation time is smaller or comparable to the rate of oscillating electric field. However when the rate of electric field oscillates well faster than the relaxation time, the polarization cannot follow the

oscillating frequency resulting in the energy absorption and dissipated as heat. It normally occurs in the microwave region.

1.4.3 Theory of dielectric properties

1.4.3.1 Polarization mechanisms in dielectrics

The dielectric properties are mainly contributed by the polarization mechanisms arising from the electrical response of individual molecules of a medium. There are basically four kinds of polarization mechanisms viz, interfacial, dipolar, ionic and electronic. The net polarization of a dielectric material is the sum of the contributions from each mechanism.

$$P = P_{electronic} + P_{ionic} + P_{molecular} + P_{interfacial}$$

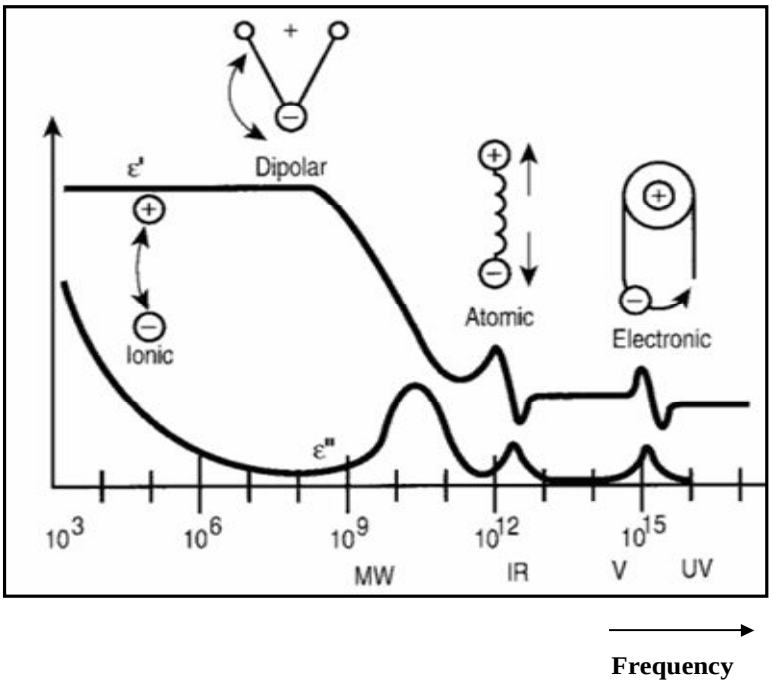

Fig. 1.5 Frequency dependence of polarization and its effects on ε'and ε" (courtesy: www.crops.org)

Figure 1.5 shows the frequency dependence of polarization. Each dielectric mechanism has a characteristic 'cut off frequency'. As frequency increases, the slow mechanisms drop out in turn, leaving the faster ones to contribute to ε_r. The loss tangent will correspondingly have peak at each critical frequency. The magnitude and cut off frequency of each mechanism is unique for different materials. It is clear from the figure that the ionic and electronic polarization contributes to dielectric properties at microwave frequencies.

(a) Interfacial (space charge) polarization: In electrically heterogeneous materials the motion of charge carriers may occur more easily through one phase and therefore are constricted at the phase boundaries. Space charge or interfacial polarization occurs when charge carriers are impeded by physical barriers such as grain boundary, interphase boundary etc. that prevents charge migration leading to piling up of charges at these barriers. When an ac field of sufficiently low frequency is applied, a net oscillation of charge is produced between the barriers as far apart as 1 cm, producing a very large capacitance and relative permittivity. This type involves a longer-range ion movement and may extend to 10^3 Hz.

(b) Dipolar (orientational) polarization: This type of polarization occurs only in polar substances. In zero fields the dipoles will be randomly oriented and thus carry a polarization. When an electric field is applied, the dipoles will tend to align in the direction of applied field and the materials will acquire a net dipole moment. This is called orientational polarization. Two mechanisms can be operative in this case. (a) In linear dielectrics (non-ferroelectrics) dipolar polarization results from the motion of the charged ions between the interstitial positions in ionic structures parallel to the applied field direction. The mechanism is active in the frequency range 10^3-10^6 Hz. (b) Molecules having permanent dipole moment may be rotated about an equilibrium position against an elastic restoring position. Its

frequency of relaxation is very high of the order of ~10^{11} Hz. It is temperature dependent. With increase in temperature the thermal energy tends to randomize the alignment.

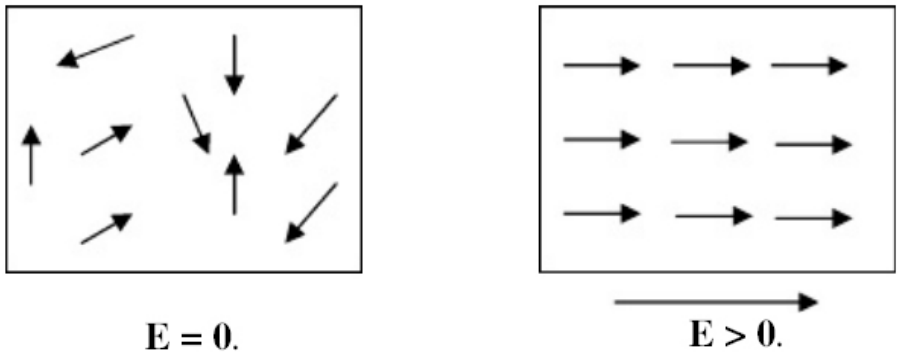

Fig. 1.6 Pictorial representation of dipolar polarization

(c) Ionic polarization: During chemical bonding the atom may acquire an excess of positive or negative charge and form an ionic bond. The displacement of positive and negative ions with respect to each other due to the application of electric field gives rise to ionic polarization. The mechanism contributes to the relative permittivity at infrared frequency range (~10^{12}-10^{13} Hz).

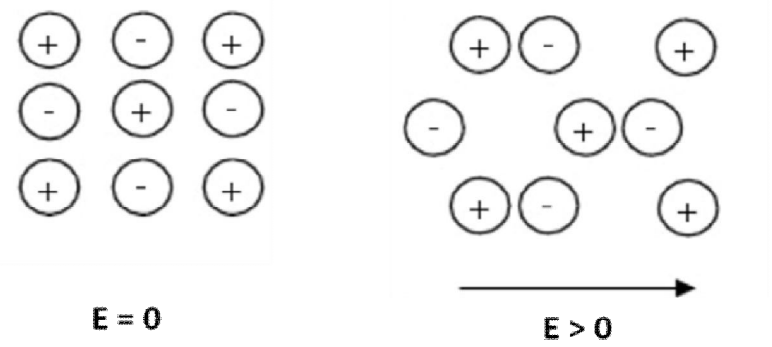

Fig. 1.7 Pictorial representation of ionic polarization

(d) Electronic polarization: When an electric field is applied, the valence electron cloud shifts with respect to nucleus. This occurs at high frequencies of about 10^{15} Hz. It is independent of temperature. Electronic polarization is present in all materials. The relative

permittivity at optical frequencies arises almost entirely from the electronic polarizability. Electronic polarization is responsible for the optical refractive index, η and is a part of relative permittivity in all materials.

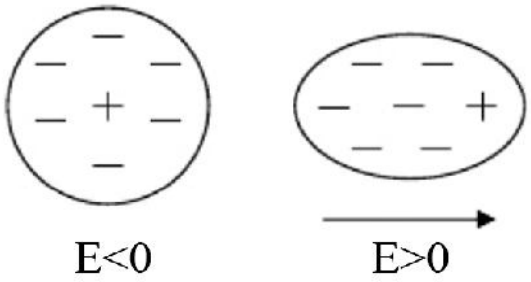

Fig. 1.8 Pictorial representation of electronic polarization

1.4.3.2 Mechanism of interaction of dielectric with electric field

Quantitative treatment of a dielectric in an electric field can be summarized using Clausius–Mossotti equation

$$P = (\varepsilon_r - 1/ \varepsilon_r + 1)(M/\rho) = N_A\alpha/3\varepsilon_0 \qquad 1.9$$

P is the molar polarisability, ε_r is the relative permittivity, ε_0 is the permittivity in vacuum, M is molecular weight of a repeat unit, ρ is density, α is polarizability, Na is the Avogadro constant. This equation shows that relative permittivity is dependent on polarizability and free volume of the constituents present in the materials. Polarizability refer to the proportionality constant for the formation of dipole under the influence of electric field.

1.4.4 Factors affecting the microwave dielectric properties

In polymer-ceramic composites the dielectric properties are controlled by the amount of filler, filler particle size and distribution of the filler, shape and orientation of the filler and

finally dispersion of the filler in the polymer matrix. The response of a polymer–ceramic composite to an external excitation (electric field, temperature, stress, etc.) depends on the response of individual phases, their interfaces as well as the connectivity concept. In heterogeneous systems, the charge accumulation at the interfaces causes a low frequency polarization called the Maxwell–Wagner polarization. The relaxation of this interfacial polarization produces loss at low frequencies [38]. It was found that for the same filler loading, the dielectric characteristics of the composites strongly depend on the type of polymer. Generally polar polymers have relative permittivity between 3 and 9 at low frequencies and between 3 and 5 at high frequencies. The relative permittivity of non-polar polymer is independent of the alternating current frequency because the electronic polarization is effectively instantaneous hence they always have relative permittivity less than 3 [39]. The chain geometry determines whether a polymer is polar or non-polar. Polar polymers increase the ε_r of the composites at low frequencies, but has hardly any effect at microwave frequencies. Temperature also affects dielectric properties. As the temperature is increased the intermolecular forces between polymer chains is broken which enhances thermal agitation. The polar groups will be more free to orient along with the changing electric field. The segmental motion of the chain is practically freezed at lower temperature and this will reduce the relative permittivity. At sufficiently higher temperature, the relative permittivity is again reduced due to strong thermal motion which disturbs the orientation of the dipoles. At this stage the polarization effectively contributes minimal relative permittivity [40]. The origin of loss tangent in polymers is due to the presence of dipolar impurities, end groups, chain fold and branch point. The lower the concentration of the groups, the lower will be the loss tangent [30]. It has been reported that the loss tangent of polymer-ceramic

composite is affected by porosity, water content and interface between two components in the composite [41]. The water content deleteriously affects the dielectric properties of polymer ceramic composites. Since water has both electronic displacement polarization and dipolar orientation polarization at low frequency and mainly has electronic displacement polarization at high frequency [42, 43], it shows high relative permittivity (≈80) and loss tangent (0.015) and hence affects microwave dielectric properties.

1.5 Material requirements for flexible electronic applications:

1.5.1 Dielectric properties: The electrical properties considered in material selection include relative permittivity, loss tangent, frequency and temperature stability of dielectric properties, electrical resistivity and dielectric strength. The relative permittivity of the material should be as low as possible for electronic packaging and substrate applications as the speed of the signal passing through the dielectric medium is inversely proportional to the square root of relative permittivity. A high relative permittivity material is needed for the core of flexible dielectric waveguide. The loss tangent of the material should be low to avoid electrical losses, especially at very high frequencies. The interaction of the signal with a lossy substrate will produce heat and hence signal attenuation [44]. The relative permittivity must be stable within the operational temperature range to control the temperature-induced drift in circuit operating characteristics [45]. High electrical resistivity is also needed to prevent electrical leakage current between the conductor tracks [46]. High dielectric strength is also required for microelectronic applications.

1.5.2 Thermal properties: An electronic material experiences a range of steady-state temperatures, temperature gradients, rates of temperature change, temperature cycles and

thermal shocks through manufacturing, storage and operation. Thermal properties which are significant in enduring such life cycle profiles include thermal conductivity, thermal diffusivity, specific heat capacity and coefficient of thermal expansion (CTE). Materials should have high thermal conductivity for dissipating the heat generated in devices and matched coefficients of thermal expansion to that of silicon (~ 4 ppm/^{o}C) chips to reduce thermal failure.

1.5.3 Mechanical properties: Mechanically flexible materials are needed for flexible electronic applications. Mechanically flexible systems would improve durability and allow enhanced integration. The mechanical properties affect the material's ability to sustain loads due to vibrations, shock and thermo mechanical stresses during manufacture, assembly, storage and operation.

1.5.4 Chemical properties: Chemical properties of the substrate materials are important because of the need to survive manufacturing, storage, handling and operating environments. The chemical properties which are of significance are water absorption, flammability and corrosion resistance. The electrical properties of electronic materials often change as a result of water absorption, swelling and other dimensional instabilities. The corrosion leads to the formation of more stable compounds and can degrade the physical properties of the materials [46].

The composite design is a suitable way to consider all these facts.

1.6 Composites

Composite materials are engineered materials made from two or more constituent materials with significantly different physical or chemical properties and remain separate and

distinct on a macroscopic level within the finished structure [47]. Composite materials can be tailored by appropriately choosing their components, proportions, distributions, morphologies, degree of crystallinity, crystallographic texures as well as the structure and composition of the interface between components for various applications. Due to this strong tailorability, composite materials find applications in various fields such as electronics, aerospace, automobile, construction, biomedical and other industries. The composite materials consist of basically three phases, matrix, reinforcement and interface [48].

1.6.1 Matrix phase

It is a continuous phase or the primary phase. It holds the dispersed phase and shares a load with it. It is made up of metals, ceramics or polymers depending on the type of composite.

1.6.2 Reinforcing (dispersed) phase

It is the second phase (or phases) which is embedded in the matrix in a continuous/ discontinuous form. Dispersed phase is usually stronger than the matrix, therefore it is sometimes called reinforcing phase in case of structural composites. This reinforcement is a strong, stiff integral component which is incorporated into matrix to achieve desired properties. It can be particles of any shape and size including nanoparticles as well.

1.6.3 Interface

Interface is an important zone of composites which determines the properties of the composites and this is the zone across which the matrix phase and reinforcing phases interact. The properties of the composites are the combined behavior of matrix, reinforcing

element and filler/matrix interface. In simple system, bonding at interface is due to adhesion between filler and matrix. Adhesion occurs by four mechanisms namely adsorption and wetting, interdiffusion, chemical bonding and electrostatic attraction. A multiphase material formed from a combination of materials which differ in composition or form, remain bonded together, and retain their identities and properties. Composites maintain an interface between components and act in concert to provide improved specific or synergistic characteristics not obtainable by any of the original components acting alone [49, 50].

1.7 Classification of composites

On the basis of matrix phase, composites can be classified into polymer matrix composites (PMCs), metal matrix composites (MMCs) and ceramic matrix composites (CMCs) as shown in Fig. 1.9. The classifications according to types of reinforcement are particulate composites (composed of particles), fibrous composites (composed of fibers), and laminate composites (composed of laminates) [49].

1.7.1 Polymer matrix composites - Most commercially produced composites use polymer as matrix material. PMCs are very popular due to their low cost and simple fabrication methods. The factors affecting the properties of PMCs are interfacial adhesion, shape and orientation of dispersed phase inclusions, properties of the matrix etc. The main advantages of polymers as matrix are low cost, easy processability, good chemical resistance and low specific gravity. The main disadvantages of PMCs are low thermal resistance and high coefficient of thermal expansion. PMCs are used for manufacturing electrical, biomedical, aerospace structures, marine, automotive, sports goods etc [49].

1.7.2 Metal matrix composites - MMCs are mainly used in the automotive industry. These materials use a metal as the matrix and reinforce it with fibres.

1.7.3 Ceramic matrix composites - Used in very high temperature environments. These materials use a ceramic as the matrix and reinforce it with short fibres or whiskers such as those made from silicon carbide and boron nitride.

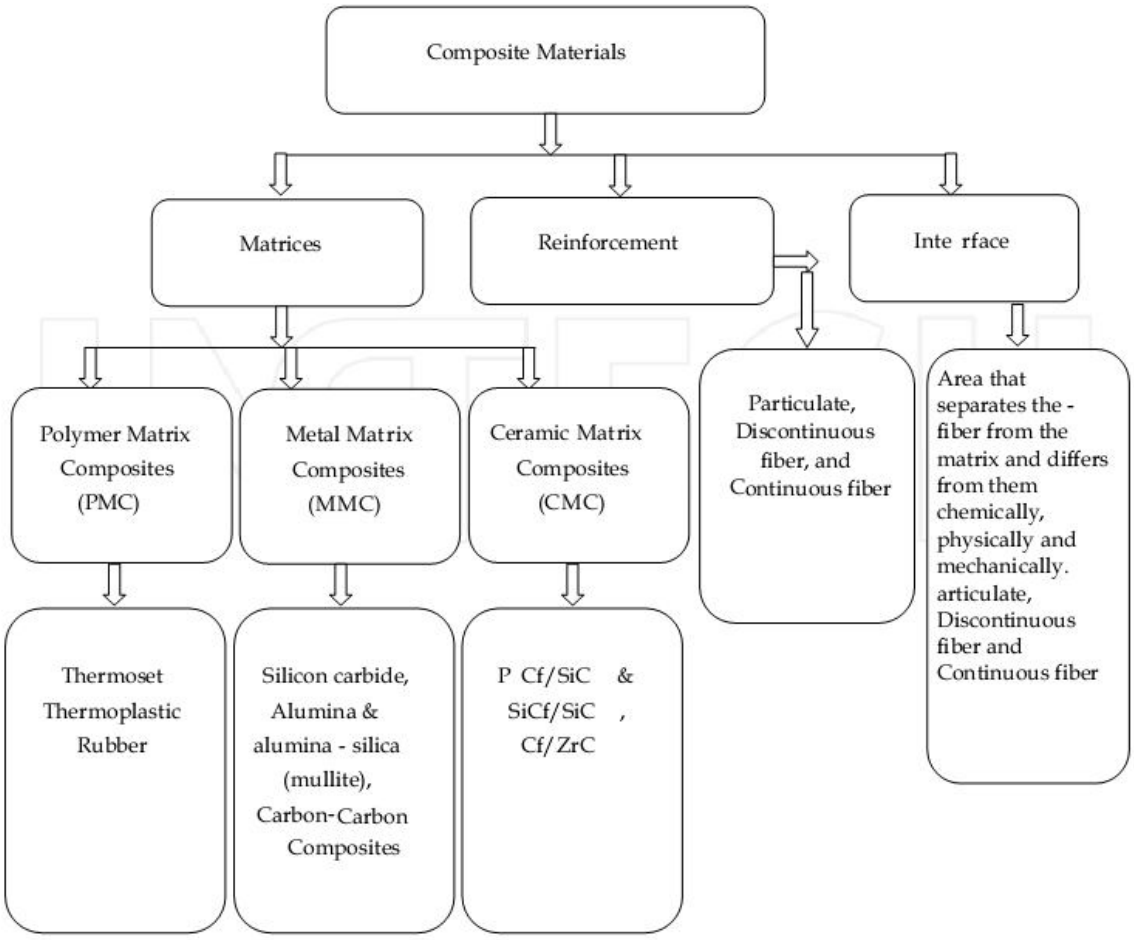

Fig. 1.9 Classification of composites (Ref. 49)

1.7.4 Connectivity

The properties of the composite not only depend on the properties of the components and the amount of each phase present but also depend on how they are

interconnected or the connectivity. Newnham et al. proposed the concept of connectivity. Any phase in a composite is self connected in zero, one, two or three dimensions. In a two-phase composite system, there can be ten different connectivities, which are 0-0, 0-1, 0-2, 0-3, 1-1, 1-2, 1-3, 2-2, 2-3 and 3-3. The first digit represents the connectivity of inclusions and the second digit represents the host. Generally, the host is a polymer in the case of polymer composite. Based on this concept, the 0-3 connectivity composite is a system in which 0D particulate fillers are randomly distributed in a 3D host polymer matrix. ie., the ceramic particles do not contact to each other but the polymer phase is self-connected in all directions in the 0-3 connectivity [51, 52]. This connectivity is easy to fabricate and suitable for mass production. Wang et al. studied the effect of connectivity on the dielectric properties of polymethylmethacrylate-$Ba_{0.6}Sr_{0.4}TiO_3$ composites and found that 1-3 type shows highest permittivity and dielectric tunability [53].

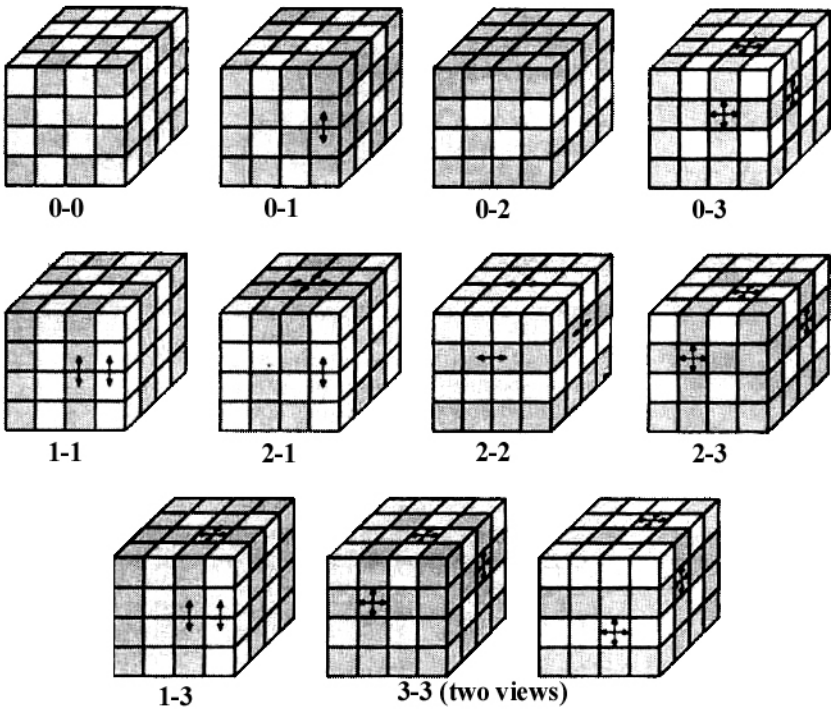

Fig. 1.10 Connectivity patterns in a di-phasic composites systems (Ref. 51)

1.8 Polymer-ceramic composites

The growing demand for low cost, large area, flexible and lightweight devices will pave way for material scientists to develop novel material systems with improved properties. The polymer-ceramic composites have received much attention because of their good performance and low cost, size and weight [54]. In recent decades, a large number of polymer-ceramic electronic composites have been introduced for medical, telecommunication and microelectronics applications [55]. A number of polymer matrices such as epoxy, cyanate ester, polybenzoxazole, polyimide, PTFE, polystyrene and polyethylene with ceramic fillers have been investigated [56-59]. Polymers have been used in electronics as resists, encapsulants, insulators and intermediate dielectrics for more than forty years [60]. Pure polymers have good dielectric properties, flexibility and low processing temperature. But their high CTE and low thermal conductivity restrict their practical use. On the other hand ceramics with desired dielectric properties are available. Due to its high processing temperature and brittle nature, it is often not compatible with current circuit integration technologies. The modern electronic devices and systems require diverse and specific functional properties in materials; which cannot be met in single-phase materials [61]. Hence monolithic ceramics or polymers cannot offer the property requirements for flexible electronics. In this context the polymer-ceramic composites can deliver improved performances by integrating the properties of both the constituents [62]. Hence polymer-ceramic composites can replace the usual ceramics or polymers. The polymers such as polystyrene, polyethylene, PTFE are flexible enough but they are not stretchable. Stretchability is a prime requirement for many applications especially in biomedical field so

that they can cover the curved surfaces and movable parts. Elastomer-ceramic composites can serve this purpose.

1.8.1 Elastomer

The term elastomer is derived from elastic polymer. It is often used interchangeably with the term rubber, although the latter refers to vulcanizates. Elastomers are amorphous polymers with the property of viscoelasticity, generally having low Young's modulus and high yield strain compared with other polymer materials due to its weak intermolecular attractive forces. They are existing above their glass transition temperature and hence considerable segmental motion is possible. At ambient temperatures, rubbers are relatively soft (E≈3 MPa) and deformable; their primary uses are for seals, adhesives and molded flexible parts [63]. They are usually thermosets but may also be thermoplastic. Chain segments of elastomers can undergo high local mobility, but the gross mobility of chains is restricted by the introduction of a few crosslinks into the structure. The long polymer chains crosslink during curing and the process is known as vulcanization. The covalent crosslinkages ensure that the elastomer will return to its original configuration when the stress is removed. In the absence of applied stress, [64] molecules of elastomers usually assume coiled shapes. Consequently, elastomers exhibit high extensibility (up to 1000%) from which they recover rapidly on the removal of the imposed stress. Natural rubber, butyl rubber, synthetic polyisoprene, polybutadiene, chloroprene rubber, ethylene propylene rubber, silicone rubber are some of the examples of elastomers.

Among the elastomers butyl rubber have extreme oxidation, ozone and chemical resistance. Butyl rubber is superior to natural rubber especially in radiation and ageing effects.

1.8.1.1 Butyl rubber

Butyl rubber was developed in 1937 by William J. Sparks and Robert M. Thomas, at Standard Oil research department of New Jersey and commercialised in 1943. Butyl rubber is a copolymer of 98% polyisobutylene with 2% isoprene distributed randomly in the polymer chain. The repeating unit is shown in Fig. 1.11. Polymerization of isoprene results in the incorporation of a double bond or unsaturation into the polymer chain. These double bonds serve as crosslinking sites. Vulcanization of the butyl rubber with sulfur results in the formation of a network structure in the form of a crosslinked rubber (Fig. 1.12). As such butyl rubber is a thermoset polymer and once vulcanized it cannot be reformed into a new shape [65, 66].

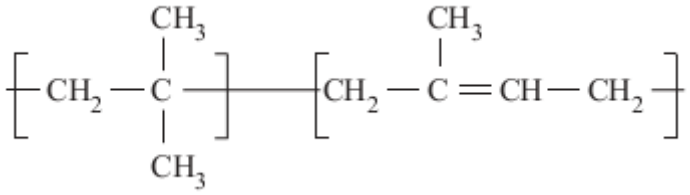

Fig. 1.11 Repeat units for butyl rubber

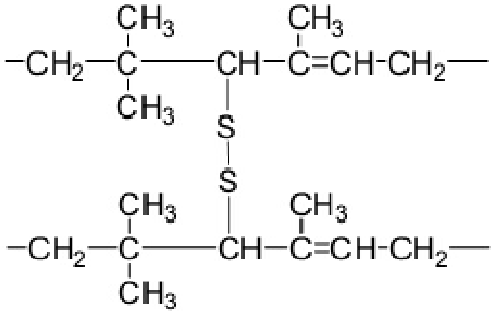

Fig. 1.12 Crosslink of sulfur vulcanized butyl rubber

Commercial processes for the manufacture of butyl rubber are costly and detrimental to the environment as they operate at temperatures ≤-100°C and require the use of toxic methyl chloride. Legislation designed to protect the environment prevents the expanded use of methyl chloride in such processes. Currently > 760,000 metric tons of butyl rubber is produced each year at a price of \$2.8-3 kg^{-1}. Exxon and Lanxess are the major manufacturers of butyl rubber. Among elastomers, vulcanized butyl rubber has lowest gas and moisture permeability, excellent dielectric properties, excellent heat/ozone resistance and high damping properties. The main use of butyl rubber is in tyre-curing bladders and inner tubes [67,68].

1.8.1.2 Advantages of butyl rubber

- Excellent dielectric properties
- Mechanically flexible
- Air tight and gas impermeable
- Low glass transition temperature
- Good resistance to oxidizing chemicals, animal and vegetable oils, silicone fluids etc.
- Good ozone resistance
- Good weathering, heat and chemical resistance
- Displays high damping at ambient temperatures
- Biocompatible

These excellent properties of butyl rubber are the result of low levels of unsaturation between the long rubber chain segments. The molecular structure of butyl rubber can be

oriented to resist stress and thus the mechanical properties are retained over a relatively wide stiffness range since reinforcement is not required for good tensile and tear strength [69].

In most of the industrial applications elastomers are used as composite materials. The incorporation of fillers into rubbery polymer imparts many interesting and useful properties to the particle filled composite materials [13-15]. Elastomer-ceramic composites are important materials suitable for devices where flexibility is an important parameter. These composites can be molded into complex shapes [70]. Moreover, the relative permittivity of filled composites can be tuned by selecting the shape, size and connectivity of the constituents in the polymer matrix [71].

Both dielectrics with low and high relative permittivity are essential in electronic industries. Eventhough butyl rubber is mechanically flexible and has excellent dielectric properties it cannot be used for flexible electronic applications due to its low ε_r and poor thermal properties. The relative permittivity of butyl rubber can be varied over a wide range by selecting ceramics with different range of relative permittivity. A low ε_r ceramics are needed to tune the properties of butyl rubber composites for electronic packaging and substrate applications. High and very high permittivity ceramic materials can be used to make butyl rubber composites for flexible dielectric waveguide applications. In addition, thermal properties of butyl rubber composites can be improved by the addition of ceramics, as ceramics have high thermal conductivity and low coefficient of thermal expansion.

1.9 Scope and objectives of the present investigation

Recently, an increasing interest has been shown in the development of mechanically flexible electronic systems due to their potential applications in various fields including communication, automotive, biomedical and aerospace. For some applications, particularly in the biomedical field, electronic circuits are to be conformally wrapped around curved surfaces. In such systems, the circuits must be not only flexible but also stretchable. The study of elastomer-ceramic composites has received much attention in this context. Among the elastomers, butyl rubber is selected for present study due to its excellent dielectric properties and superior radiation and ageing resistance. Eventhough butyl rubber have good dielectric properties, it has low thermal conductivity and high coefficient of thermal expansion. Moreover, low and high relative permittivity materials are needed for various electronic applications. The dielectric properties of butyl rubber can be tuned by incorporating ceramics with different relative permittivity. For electronic packaging and substrate applications, materials must have a low relative permittivity to minimize capacitive coupling and signal delay along with low loss tangent to reduce signal attenuation. High permittivity and low loss materials are needed to be used as the core of flexible dielectric waveguide. A low ε_r, high ε_r and very high ε_r ceramics are used to tailor the dielectric properties of butyl rubber composites suitable for flexible microwave electronic applications.

Thus the objectives of the present work are

- To develop mechanically flexible, low loss and thermally stable dielectric composites for flexible microwave substrate and electronic packaging applications
- To develop mechanically flexible, low loss and thermally stable dielectric composites for flexible dielectric waveguide applications
- To study the effect of filler particle size on microwave dielectric, mechanical, thermal and other physical properties of butyl rubber composites.

1.10 References

1. D. Tse and P. Viswanath, Fundamentals of wireless communication, Cambridge University Press, New York (2005).
2. A. Goldsmith, Design and performance of 3G wireless networks and wireless lans, Springer, US (2005).
3. D. M. Pozar, Microwave engineering, John Wiley & Sons, New York (1997).
4. M. Schwartz, Mobile wireless communications, Cambridge University Press, New York (2005).
5. M. R. Yuce , S. W. Ng , N. L. Myo, J. Y. Khan and W. Liu, *J. Med. Syst.*, **6,** 467 (2007).
6. M. T. Sebastian, Dielectric materials for wireless communication, Elsevier Publishers, Oxford, UK (2008).
7. D. D. Rossi and C. E. Piaggio, *Nat. Mater.*, **6,** 328 (2007).
8. W. S. Wong and A. Salleo, Flexible electronics: materials and applications, Springer, US (2009).
9. J. M. Cannata, J. A. Williams, Q. Zhou, T. A. Ritter and K. K. Shung, *IEEE Trans. Ultrason. Ferroelect. Freq. Control.*, **53,** 224 (2006).
10. I. Park, S. H. Ko, H. Pan, C. P. Grigoropoulos, A. P. Pisano, J. M. J. Frechet, E. S. Lee and J. H. Jeong, *Adv. Mater.*, **20,** 489 (2008).
11. A. C. Siegel, S. T. Phillips, M. D. Dickey, N. Lu, Z. Suo and G. M. Whitesides, *Adv. Funct. Mater.*, **20,** 28 (2010).
12. J. A. Rogers, *Nat. Nanotechnol.*, **3,** 254 (2008).

13. S. Cheng, Advanced elastomers–technology, properties and applications, Intech (2012).
14. T. Joseph, S. Uma, J. Philip and M. T. Sebastian, *J. Mater. Sci. Mater. Electron.*, **23,** 1243 (2012).
15. K. M. Manu, S. Soni, V. R. K. Murthy and M. T. Sebastian, *J. Mater. Sci. Mater. Electron.*, **24,** 2098 (2013).
16. S. Thomas, S. Raman, P. Mohanan and M. T. Sebastian, *Composites Part A,* **41,** 1148 (2010).
17. D. C. Thompson, O. Tantot, H. Jallageas, G. E. Ponchak, M. M. Tentzeris and J. Papapolymerou, *IEEE Trans. Microwave Theory Tech.,* **52,** 1343 (2004).
18. http://www.transparencymarketresearch.com/flexible-electronics-market.html
19. www.OLED- info.com
20. S. Xu, Y. Zhang, J. Cho, J. Lee, X. Huang, L. Jia, J. A. Fan, Y. Su, J. Su, H. Zhang, H. Cheng, B. Lu, C. Yu, C Chuang, T. Kim, T. Song, K. Shigeta, S. Kang, C. Dagdeviren and I. Petrov, *Nat. Commun.,* **4,** 1543-1 (2013).
21. http://news.softpedia.com/newsImage/Flexible-Washable-Electronics-Made-With-Elastic-Circuit-Connectors-2.jpg/
22. http://www.britannica.com/EBchecked/topic/183875/electronic-substrate-and-package-ceramics
23. P. Gonon, A. Sylvestre, J. Teysseyre and C. Prior, *J. Mater. Sci. Mater. Electron.*, **12,** 81 (2001).
24. Y. Rao, S. Ogitani, P. Kohl and C. P. Wong, *J. Appl. Polym. Sci.,* **83,** 1084 (2002).

25. D. L. Chung, Materials for electronic packaging, Butterworth Heinemann, Washington (1995).

26. W. Ling, A. Gu, G. Liang and L. Yuan, *Polym. Comp.,* **31,** 307 (2010).

27. P. Garrou and I. Turlik, Multichip module technology handbook, Mc Graw-Hill: New York (1998).

28. http://en.wikipedia.org/wiki/Monopole_antenna

29. E. C. Jordan and K. G. Balmain, Electromagnetic waves and radiating systems, Prentice-Hall (1968).

30. N. K. James, S. Rajesh, K. P. Murali, K. S. Jacob and R. Ratheesh, *J. Mater. Sci. Mater. Electron.,* **21,** 1255 (2010).

31. J. A. Bur, *Polymer*, **26,** 963 (1985).

32. http://en.wikipedia.org/wiki/Waveguide

33. W. M. Bruno and W. B. Bridges, *IEEE Trans Microwave Theory Tech.,* **36,** 882 (1988).

34. http://www.radio-electronics.com/waveguide

35. http://www.merriam-webster.com/dictionary/dielectric

36. A. R. V. Hippel, Dielectric Materials and Applications, Technology Press of MIT and John Wiley, New York (1954).

37. C. S. Indulkar and S. Thiruvengadam, An Introduction to electronic engineering materials, S Chand and Company, New Delhi, India (2008).

38. J. Liu, C. G. Duan, W. N. Mei, R. W. Smith and J. R. Hardy, *J. Appl. Phys.*, **98,** 093703 (2005).

39. T. Blythe and D. Bloor, Electrical properties of polymers, 2nd Ed., Cambridge University Press (2005).

40. R. J. Young, Introduction to polymers, Chapman & Hall Ltd, London (1989).

41. N. G. Devaraju, E. S. Kim and B. I. Lee, *Microelect. Eng.*, **82,** 71 (2005).

42. L. Y. Zhang and X. Yao, Dielectric Physics. Xi'an Jiaotong University Press, Xi'an, (1991).

43. J. Molla, M. Gonzalez and R. Vila, *J. Appl. Phys.*, **85,** 1727 (1999).

44. Y. Y. Sun, Z. Zhang and C. P. Wong, *Polymer*, **46**, 2297 (2005).

45. L. M. Walpita, P. N. Chen, H. A. Goldberg, A. Harris and C. Zipp, U.S. Patent No. 5739193 (1998).

46. G. M. G. Pecht, R. Agarwal, P. McCluskey, T. Dishongh, S. Javadpour and R. Mahajan, Electronic packaging materials and their properties, CRC Press, London (1999).

47. D. P. Button, B. A. Yost, R. H. French, W. Y. Hsu, J. D. Belt, M. A. Subrahmanian, H. M. Zhang, R. E. Geidd, A. J. Whittacker and D. G. Onn, *Ceramic substrates and*

packages for electronic applications, Advances in Ceramics, American Ceramic Society, Westerville OH, **26,** 353 (1989).

48. D. L. Chung, Composite materials: science and applications, Springer, London (2010).

49. P. Guggilla and A. K. Batra, Nanocomposites and polymers with analytical methods, *Alabama A&M University, USA* (2000).

50. J. P. Jose, S. K. Malhotra, S. Thomas, K. Joseph, K. Goda and M. S. Sreekala, *Advances in polymer composites: macro and microcomposites–state of the art, new challenges, and opportunities,* Wiley-VCH Verlag GmbH & Co. KGaA (2012).

51. R. E. Newnham, D. P. Skinner and L. E. Cross, *Mat. Res. Bull.,* **13,** 525 (1978).

52. J. F. Tressler, S. Alkoy, A. Dogan and R. E. Newnham, *Composites part A,* **30,** 477 (1999).

53. H. Wang, F. Xiang and K. Li, *Int. J. Appl. Ceram. Technol.*, **7,** 435 (2010).

54. L. A. Ramajo and M. M. Reboredo, M. S. Castro, *J. Mater. Sci.*, **42,** 3685 (2007).

55. M. Taya, Introduction In: electronic composites, Cambridge University Press, UK (2008).

56. D. H. Im, C. J. Jeon and E. S. Kim, *Ceram. Int.*, **38,** S191 (2012).

57. G. Subodh, V. Deepu, P. Mohanan and M. T. Sebastian, *Polym. Eng. Sci.*, **49,** 1218 (2009).

58. S. Thomas, V. Deepu, S. Uma, P. Mohanan, J. Philip and M. T. Sebastian, Mater. Sci. Eng. B, **163,** 67 (2009).

59. C. Janardhanan, D. Thomas, G. Subodh, S. Harshan, J. Philip and M. T. Sebastian, *J. Appl. Polym. Sci.,* **124,** 3426 (2012).

60. R. K. Goyal, P. Jadhav and A. N. Tiwari, *J. Electr. Mater.,* **40,** 1377 (2011).

61. A. K. Batra, M. D. Aggarwal, M. Edwards and A. S. Bhalla, *Ferroelectrics,* **366,** 84 (2008).

62. M. T. Sebastian and H. Jantunen, *Int. J. Appl. Ceram. Technol.,* **7,** 415 (2010).

63. http://en.wikipedia.org/wiki/Elastomer

64. R. O. Ebewele, Polymer science and technology, CRC Press, Florida (2000).

65. R. M. Thomas and W. J. Sparks, U.S. Patent 2, 356, 128 (1944).

66. http://en.wikipedia.org/wiki/Butyl_rubber

67. F. W. Billmeyer, Text book of polymer science, Interscience publishers, John Wiley and Sons, New York and London (1962).

68. J. Duffy and G. J. Wilson, Synthesis of butyl rubber by cationic polymerization in Ullman's Encyclopedia of Industrial Chemistry, 5th ed.; Elseviers, (1993).

69. General properties of elastomers, www.elbex-us.com

70. N. M. R. Siddaramaiah and R. D. S. Samuel, *J. Mater. Sci: Mater. Electron.,* **18**, 635 (2007).

71. S. L. Thomas, Microwave Materials and Fabrication Techniques, Artech House Inc.: USA (1984).

Chapter 2

Materials and Experimental Techniques

This chapter gives a brief description of the synthesis methods and the characterization techniques of ceramic powder and their composites with butyl rubber.

2.1 Materials used

In the present investigation butyl rubber as matrix and ceramic fillers such as Al_2O_3, SiO_2, $Ba(Zn_{1/3}Ta_{2/3})O_3$, TiO_2, $Sr_2Ce_2Ti_5O_{15}$, $SrTiO_3$, $BaTiO_3$ and $Ba_{0.7}Sr_{0.3}TiO_3$ were used for the composite preparation.

2.1.1 Elastomer

2.1.1.1 Butyl rubber (BR)

The butyl rubber used for present investigation was IIR grade. The DSC plot of pure butyl rubber is given in Fig. 2.1. The glass transition temperature of butyl rubber is around -63^oC.

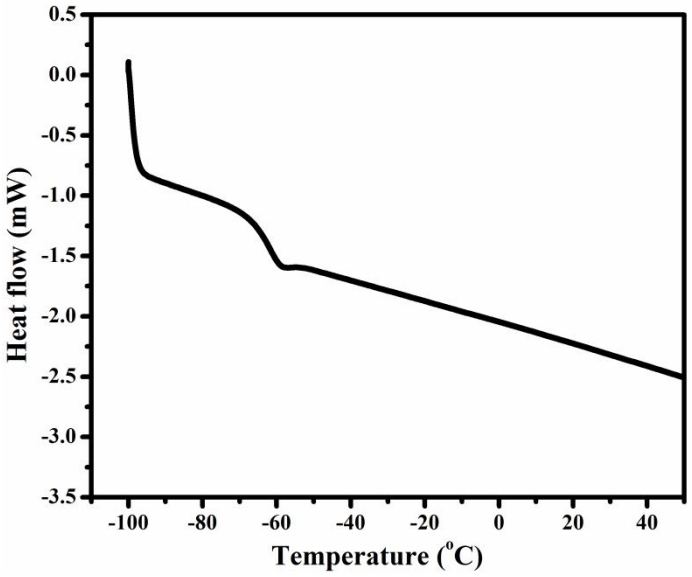

Fig. 2.1 DSC curve of pure butyl rubber

The physical properties of butyl rubber is given in Table 2.1

Table 2.1 Properties of butyl rubber

Density	0.97 gcm^{-3}
Moisture absorption	0.039 vol%
Relative permittivity at 5 GHz	2.4
Loss tangent at 5 GHz	$\approx 10^{-3}$
Thermal conductivity	0.13 $Wm^{-1}K^{-1}$
Coefficient of thermal expansion	191 ppm/^{o}C

2.1.2 Synthesis of ceramics

2.1.2.1 Alumina (Al_2O_3)

Alumina is a well known low loss ceramic packaging material. Micron alumina and nano alumina (<50 nm particle size) procured from Sigma Aldrich, USA were used for the present work. Both the alumina was dried at 100°C for 24 hours before use.

2.1.2.2 Silica (SiO_2)

Silica supplied by Sigma Aldrich dried at 100^{o}C for 24 hours was used.

2.1.2.3 Barium zinc tantalate, $Ba(Zn_{1/3}Ta_{2/3})O_3$ (BZT)

$Ba(Zn_{1/3}Ta_{2/3})O_3$ ceramic was prepared by conventional solid state ceramic route. Stoichiometric quantities of $BaCO_3$, ZnO (99.9 + %, Sigma Aldrich) and Ta_2O_5 (99.99%, Treibacher Industries) were ball milled for 24 hours in distilled water using yttria-stabilized zirconia balls in a plastic container. The slurry was then dried and calcined at 1200^{o}C for 4

hours. The calcined powder was ground well and sintered at 1500^{o}C for 4 hours. The ground powder was then sieved through a 25 μm sieve.

2.1.2.4 Titanium dioxide (TiO_2)

The micron rutile powder was prepared by heating anatase at 1200^{o}C for 4 hours. The powder was then ground well and sieved through a 25 μm sieve. Nano rutile (average size 100 nm) purchased from Sigma Aldrich dried at 100^{o}C for 24 hours was used.

2.1.2.5 Strontium cerium titanate, $Sr_2Ce_2Ti_5O_{15}$ (SCT)

$Sr_2Ce_2Ti_5O_{15}$ ceramic powder was prepared by conventional solid state method as described in section 2.1.2.3 using stoichiometric quantities of $SrCO_3$ and TiO_2 (99.9+%, Sigma Aldrich) and CeO_2 (99.99%, Indian Rare Earths Ltd.). The calcination and sintering temperature of SCT was 1100^{o}C for 4 hours and 1300^{o}C for 4 hours respectively. Finally the sintered and ground powder was sieved through a 25 μm sieve.

2.1.2.6 Strontium titanate ($SrTiO_3$)

High purity $SrCO_3$ and TiO_2 (99.9+%, Sigma Aldrich, USA) reactants were used for the preparation of $SrTiO_3$ ceramic powder. The $SrTiO_3$ preparation followed the same method as described in section 2.1.2.3. The calcination and sintering temperature of $SrTiO_3$ was 1200^{o}C for 4 hours and 1450^{o}C for 4 hours respectively and sieved through a 25 μm sieve.

2.1.2. 7 Barium titanate ($BaTiO_3$)

$BaTiO_3$ micron ceramic powder was also prepared by conventional solid state method. $BaCO_3$ and TiO_2 (99.9+%, Sigma Aldrich) are the precursor powders for $BaTiO_3$

preparation. Stoichiometric amounts of these powders were ball milled for 24 hours in distilled water and was dried and calcined at 1100^{o}C for 4 hours. The calcined powder was ground well and sintered at 1300^{o}C for 4 hours. The sintered and ground powder was sieved through a 25 μm sieve.

$BaTiO_3$ nano powder (<100 nm particle size) was procured from sigma Aldrich dried at 100^{o}C for 24 hours was used.

2.1.2.8 Barium strontium titanate, $Ba_{0.7}Sr_{0.3}TiO_3$ (BST)

$Ba_{0.7}Sr_{0.3}TiO_3$ ceramic was also prepared by following the conventional solid state ceramic route used for other ceramic preparation. Stoichiometric quantities of $BaCO_3$, $SrCO_3$ and TiO_2 (99.9+%, Sigma Aldrich) were ball milled for 24 hours in distilled water. The dried powder was calcined at 1100^{o}C for 6 hours. The calcined powder was ground well and sintered at 1300^{o}C for 4 hours and sieved through a 25 μm sieve.

2.1.3 Other ingredients

Compounding ingredients such as zinc oxide, stearic acid, tetramethylthiuram disulfide (TMTD) and sulfur used were of commercial grade.

2.1.4 Preparation of butyl rubber-ceramic composites

Composite materials play a key role in the modern science and technology, especially in the area of electronics. Polymer based composite materials has a number of applications. Low loss ceramic loaded polymers can be used in most electronic applications.

2.1.4.1 Compounding

The process involving incorporation of ingredients such as activators, accelerators, vulcanizing agent and fillers into the virgin rubber is known as compounding of rubber. In the present investigation, compounding of butyl rubber mix was done by sigma blend method. The mixing was done in a kneading machine. The kneading machine consists of variable speed mixer having two counter rotating sigma blades with a gear ratio of 1:1.2. The formulation of butyl rubber and additives are given in Table 2.2 [1]. The butyl rubber was first masticated through the two counter rotating sigma blades in order to make it soft and more processable. Then the additives are incorporated one by one as per the order given in the Table 2.2. The additives, zinc oxide and stearic acid act as activators for vulcanization, tetramethylthiuram disulfide act as accelerator and sulfur as vulcanizing agent. Finally appropriate amount of ceramic filler was added. The mixing was done for about 30 minutes to get uniform composites. Thus obtained composites were hot pressed at 200^{o}C for 90 minutes under a pressure of 2 MPa. After hot pressing, the composites with desired shapes were used for characterization.

Table 2.2 Formulation of rubber mix

Ingredient	Loading (phr[#])
Butyl rubber	100
Zinc oxide	5
Stearic acid	3
Tetramethylthiuram disulfide	1
Sulfur	0.5

 # parts per hundred rubber

2.2 Characterization

2.2.1 X-Ray Diffraction

The crystal structure of the powdered ceramic samples was analyzed by X-ray diffraction (XRD) techniques. X-ray diffraction method is most useful qualitative, rather than quantitative analysis. The crystal to be examined is ground to a fine powder and placed in a beam of monochromatic X-rays. Each particle of the powder is a tiny crystal, oriented at random with respect to the incident beam. Theoretically the powdered sample provides all possible orientations of the crystal lattice, goniometer provides a variety of angles of incidence and the detector measures the intensity of diffracted beams. The resulting analysis is described graphically as a set of peaks with % intensity on the Y-axis and goniometer angle on the X-axis. The exact angle and intensity of set of peaks is unique to the crystal structure being examined. A monochromator is used to ensure that a specific wavelength reaches the detector, eliminating fluorescent radiation. The resulting trace consists of recording the intensity versus counter angle (2θ). Diffraction data of many different materials are available in a computer searchable powder diffraction file (JCPDS file). Comparing the observed data with that in the JCPDS file allows the phases in the sample to be identified [2, 3].

In the present investigation XRD spectra were recorded in a Philips X-ray Diffractometer (Philips Corp, Almelo, Netherlands) employing Cu Kα (λ= 0.15405 nm) radiation. The measurements were performed over a 2θ range of 10^o to 80^o.

2.2.2 Scanning Electron Microscopy (SEM)

SEM was used to analyze the microstructure of composites. SEM uses a focused beam of high energy electrons to generate variety of signals at the surface of solid specimens. The signals resulted from electron-sample interactions reveal information regarding the sample including texture, chemical composition, crystalline structure and orientation of materials making up the sample. Once the beam hits the sample, electrons and X-rays ejected from the sample. Detectors collect these X-rays, back scattered electrons and secondary electrons and convert them into a signal that is sent to a screen similar to television screen. This produces the final image [4].

In the present study, SEM images were taken in JEOL-JSM 5600 LV, Tokyo, Japan. The fractured surfaces of composite samples for microstructure analysis were prepared by breaking the composite after dipping in liquid nitrogen and coating the fractured surfaces with gold.

2.2.3 Microwave characterization

The microwave characterization of a material plays an important role in microwave electronics. The microwave methods generally fall into two categories: resonant method and non-resonant method. Non-resonant methods are used to get a general idea of electromagnetic properties over a frequency range while resonant methods are used to get accurate knowledge of dielectric properties at a single frequency or at several discrete frequencies. Resonant methods have higher accuracies and sensitivities than non-resonant methods and are most suitable for low loss materials [5, 6].

2.2.3.1 Network analyzer

Network analyzer is the major instrument used in the present work for the characterization of low loss materials. It reveals all the network characteristics of the analog circuit by measuring the amplitudes and phases of transmission and reflection coefficients. Network analyzer is a swept frequency measurement equipment to characterize the complex network parameters in comparatively less time, without any degradation in accuracy and precision [7].

A vector network analyzer (Agilent Technologies, E5071C, ENA Series) is used for the present investigation.

2.2.3.2 Split Post Dielectric Resonator (SPDR)

The SPDR is an accurate method for measuring the dielectric properties of substrates and thin films at a single frequency in the frequency range of 1 to 20 GHz [8, 9]. In this method [10] the sample should be in the form of a flat rectangular piece or a sheet. The SPDR uses a particular resonant mode which has a specific resonant frequency depending on the resonator dimensions and the relative permittivity.

The resonator mainly consists of two dielectric discs in a metal enclosure. The dielectric discs are thin and the height of metal enclosure is relatively small, hence the evanescent electromagnetic field character is strong not only in the air gap region outside the cavity but also in the cavity region for radii greater than the radius of the dielectric resonator. Therefore the electromagnetic fields are also attenuated in the cavity so it is usually not necessary to take into account in the air gap. This simplifies the numerical analysis and reduces possible radiation. The sample under test is placed in the gap between the two parts

of the resonator usually at the place of maximum electric field. The loading of a dielectric sheet sample changes the resonant properties of a split resonator and the dielectric properties of the sample can be derived from the resonant properties of the resonator loaded with sample and the dimensions of the resonator and the sample.

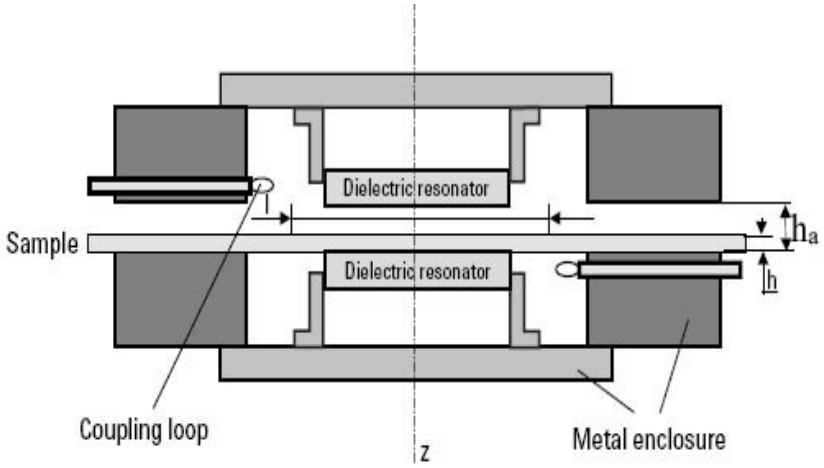

Fig. 2.2 Schematic representation of a split post dielectric resonator (Ref. 11)

The proposed geometry of a split dielectric resonator fixture for the measurement of the complex permittivity of dielectric sheet samples is shown in Fig. 2.2. Split post dielectric resonator usually operates with the $TE_{01\delta}$ mode, which has only azimuthal electric field component. Hence the electric field remains continuous on the dielectric interfaces. The field distributions are affected by the introduction of the sample, which in turn changes the resonant frequency and the unloaded quality factor (Q-factor) of the sample. The dielectric properties of the sample are derived from the changes of resonant frequency and unloaded Q-factor due to the insertion of the sample. For low loss materials, the influence of losses on the resonant frequencies is negligible, so the real part of permittivity of the sample under test is related to the resonant frequencies and physical dimensions of the cavity and sample only. In this method, calibration technique is used and we compare the difference of resonant

frequency of the split dielectric resonator before and after the sample is inserted. The relative permittivity of the sample is an iterative solution to the following equation [11]

$$\varepsilon_r = 1 + \frac{f_o - f_s}{h f_o K_\varepsilon(\varepsilon_r, h)} \tag{2.1}$$

where h is the thickness of the sample under test, f_o is the resonant frequency of empty resonant fixture, f_s is the resonant frequency of the resonant fixture with dielectric sample, K_ε is a function of ε_r and h and has been evaluated using Rayleigh-Ritz technique [11]. The loss tangent of the sample can be determined by

$$\tan\delta = (Q_u^{-1} - Q_{DR}^{-1} - Q_C^{-1})/\rho_{es} \tag{2.2}$$

In equations (2.1) and (2.2)

$$p_{es} = h\varepsilon_r K_1(\varepsilon_r, h) \tag{2.3}$$

$$Q_c = Q_{c0} K_2(\varepsilon_r, h) \tag{2.4}$$

$$Q_{DR} = Q_{DR0} \cdot \frac{f_o}{f_s} \cdot \frac{p_{eDR0}}{p_{eDR}} \tag{2.5}$$

where p_{es} and p_{eDR} are the electric energy filling factors for the sample and for the split resonator respectively; p_{eDR0} is the electric energy filling factor of the dielectric split resonator for empty resonant fixture; Q_{c0} is the quality factor depending on metal enclosure losses for empty resonant fixture; Q_{DR0} is the quality factor depending on dielectric losses in dielectric resonators for empty resonant fixture; and Q_u is the unloaded quality factor of the

resonant fixture containing the dielectric sample. The values of p_{eDR}, p_{es} and Q_c for a given resonant structure can be calculated using numerical techniques.

Fig. 2.3 Photograph of QWED split post dielectric resonator

The sample should be flat and must be positioned such that it extends beyond the diameter of two cavity sections. The position of the sample in z-direction is not sensitive to the measurement results. This provides the accuracy of a resonator technique without machining the sample. The uncertainty of the permittivity measurements of a sample of thickness h is $\Delta\varepsilon/\varepsilon = \pm (0.0015+\Delta h/h)$ and uncertainty in loss tangent measurements are $\Delta (\tan \delta) = 2\times10^{-5}$.

Microwave dielectric properties of butyl rubber-ceramic composites in the present investigation were measured by this method. Samples of dimension (50x50x1.8 mm^3) [6] were employed for measurement. The SPDR operating at 5.155 GHz requires the above mentioned dimensions for accurate measurement.

2.2.3.3 Theoretical modeling of relative permittivity

In order to understand the physical mechanisms controlling the relative permittivity of a heterogeneous system, the experimental values of ε_r were compared with values

predicted using different theoretical models. Several numerical relations have been proposed to predict the relative permittivity of polymer-ceramic composites [12-14]. These models can also be used to determine the extent of filler dispersion and filler/matrix compatibility by comparing the predicted values with the experimental data. The relative permittivity of the composites is influenced not only by the relative permittivity of the individual components but also by other factors such as the morphology, dispersion and the interaction between the two phases and hence the prediction of relative permittivity of composites is very difficult. The following equations are used to predict the relative permittivity of the present composites theoretically:

(a) Lichtenecker equation:

$$\ln \varepsilon_{eff} = (1 - v_f) \ln \varepsilon_m + v_f \ln \varepsilon_f \qquad (2.6)$$

where ε_{eff}, ε_f, ε_m are the relative permittivity of the composites, filler and matrix respectively and v_f is the volume fraction of the filler

The most widely used relation for the prediction of ε_r is Lichtenecker's logarithmic law of mixing. It considers the composite system as randomly oriented spheroids that are uniformly distributed in a continuous matrix. [15].

(b) Maxwell-Garnett equation:

$$\frac{\varepsilon_{eff} - \varepsilon_m}{\varepsilon_{eff} + 2\varepsilon_m} = v_f \frac{\varepsilon_f - \varepsilon_m}{\varepsilon_f + 2\varepsilon_m} \qquad (2.7)$$

The Maxwell-Garnett mixing rule was initially used to calculate the effective permittivity of a system where metal particles are encapsulated in an insulating matrix. This

mixing rule was modified for polymer-ceramic composites incorporating homogeneous distribution of spherical ceramic particles and the excitation of dipolar character is considered [16].

(c) Jayasundere-Smith equation:

$$\varepsilon_{eff} = \frac{\varepsilon_m\left(1-v_f\right)+\varepsilon_f v_f\left[\frac{3\varepsilon_m}{\varepsilon_f+2\varepsilon_m}\right]\left[1+\left(\frac{3v_f\left(\varepsilon_f-\varepsilon_m\right)}{\varepsilon_f+2\varepsilon_m}\right)\right]}{1-v_f+v_f\left[\frac{3\varepsilon_m}{\varepsilon_f+2\varepsilon_m}\right]\left[1+\left(\frac{3v_f\left(\varepsilon_f-\varepsilon_m\right)}{\varepsilon_f+2\varepsilon_m}\right)\right]} \qquad (2.8)$$

Jayasundere-Smith equation is a modification of well-known Kerner equation by including the interactions between neighboring spheres. This equation considers composite as a bi-phase system of dielectric spheres (ε_f) dispersed in a continuous medium (ε_m) and is valid only when $\varepsilon_f >> \varepsilon_m$ [17].

(d) Effective Medium Theory (EMT):

$$\varepsilon_{eff} = \varepsilon_m\left[1+\frac{v_f\left(\varepsilon_f-\varepsilon_m\right)}{\varepsilon_m+n\left(1-v_f\right)\left(\varepsilon_f-\varepsilon_m\right)}\right] \qquad (2.9)$$

where n is the shape factor in EMT model.

In EMT model, composites are treated as an effective medium whose relative permittivity is obtained by averaging over the relative permittivity of the constituents. The basic concept of EMT model is that when a random unit cell (RUC) is embedded in an effective medium it cannot be detected in the electromagnetic experiment. A random unit cell is defined as a core of ceramic surrounded by a concentric shell of the polymer [18]. A

correction factor 'n' is used to compensate for the shape of the fillers and is called morphology factor which is related to ceramic particle and can be obtained empirically.

2.2.3.4 Bending

Bending measurements of the composites were carried out by bending the samples manually in such a way that every part of the sample had undergone 180^{o} bending. The bending cycle was repeated for 125 times and the microwave dielectric properties were measured by SPDR after every 25 cycles.

2.2.4 Radio frequency dielectric measurements

The radio frequency dielectric measurements of composites were done by LCR meter. The working principle of LCR meter is parallel plate capacitor method in which a thin sheet of the material is sandwiched between two electrodes to form a capacitor. The capacitance of a parallel plate capacitor in vacuum is compared with one in the presence of the material for which the dielectric properties are to be measured. Then relative permittivity is calculated using the equation

$$C = \frac{\varepsilon_r \varepsilon_o A}{d} \qquad (2.10)$$

where C is the capacitance of material, ε_r and ε_o are the relative permittivity of material and free space respectively, A is the area of cross section and d is the thickness of the sample.

Fig. 2.4 Photograph of Hioki 3532-50 LCR Tester

In the present study, the dielectric properties at radio frequency were measured using LCR meter (HIOKI 3532-50 LCR Hi TESTER, Japan). Cylindrical discs (11 mm diameter and 1 to 2 mm thickness) were used for measurements.

2.2.5 Temperature coefficient of relative permittivity ($\tau_{\varepsilon r}$)

$\tau_{\varepsilon r}$ of material should be stable within the operational temperature range of electronic devices for practical applications. The temperature coefficient of relative permittivity of the present composites was measured by parallel plate capacitor method. The sample is kept in a chamber and ε_r is measured from 25 to 75^{o}C.

$$\tau_{\varepsilon r} = \frac{1}{\varepsilon_r} X \frac{\Delta \varepsilon_r}{\Delta T} \qquad (2.11)$$

2.2.6 Thermal conductivity (TC)

The thermal conductivity of the composites was measured by laser flash technique using the relation

$$TC = \lambda \times Cp \times \rho \qquad (2.12)$$

where λ is the thermal diffusivity, Cp is the specific heat capacity at room temperature and ρ is the density of the sample.

Fig. 2.5 Photograph of Flash Line™ 2000 thermal properties analyzer

The laser flash method is a vertical set up in which laser flash heats the sample from the bottom side and a detector on top detects the time dependent temperature rise. The thermal diffusivity can be calculated from specimen thickness and the time required for the rear face temperature rise to reach certain percentage of its maximum value [19]. The heat capacity of the sample also measured simultaneously comparing the temperature rise in the sample with that in a reference material [20].

In the present study, thermal conductivity was measured by thermal properties analyzer (Flash Line™ 2000, Anter Corporation, USA). Graphite coated samples of diameter 12.57 mm and thickness 1 mm was used for TC measurements.

2.2.6.1 Modeling of thermal conductivity

The importance of thermal conductivity of polymer-ceramic composites is associated with the need for appreciable levels of thermal conductance in circuit boards, heat

exchangers, etc. Hence it is necessary to model thermal conductivity of composite materials. The effective thermal conductivity of a heterogeneous system is strongly affected by its thermal conductivity of individual components, composition, crystal structure, distribution within the medium and contact between the particles. Numerous theoretical models were proposed for predicting the thermal conductivity of composites [21, 22]. In the present study, following models are used to predict the thermal conductivity of the composites:

(a) Series mixing rule:

$$\frac{1}{k_c} = \frac{v_f}{k_f} + \frac{v_m}{k_m} \tag{2.13}$$

(b) Parallel mixing rule:

$$k_c = v_f k_f + v_m k_m \tag{2.14}$$

where k_c is the effective thermal conductivity of the composite, k_m and k_f are the thermal conductivity of matrix and filler respectively and v_m and v_f are the volume fractions of matrix and filler respectively.

The physical structures assumed in the series and parallel models are of layers of phases aligned either perpendicular or parallel to the heat flow [23]. The series and parallel model of TC gives only lower and upper limits of thermal conductivity values of composites respectively.

(c) Geometric mean model [24]:

$$k_c = k_f^{v_f} k_m^{1-v_f} \tag{2.15}$$

(d) Maxwell-Eucken Model:

$$k_c = k_m \left[\frac{k_f + 2k_m + 2V_f(k_f - k_m)}{k_f + 2k_m - V_f(k_f - k_m)} \right] \qquad (2.16)$$

The Maxwell model assumes a dispersion of small spheres within a continuous matrix of a different phase, where spheres being far enough apart such that the local distortions to the temperature distributions around each of the spheres do not interfere with their neighbors' temperature distributions [24].

(e) Cheng-Vachon Model:

$$\frac{1}{k_c} = \frac{1}{\sqrt{C(k_f - k_m)[k_m + B(k_f - k_m)]}} \ln \frac{\sqrt{[k_m + B(k_f - k_m)]} + \frac{B}{2}\sqrt{C(k_f - k_m)}}{\sqrt{[k_m + B(k_f - k_m)]} - \frac{B}{2}\sqrt{C(k_f - k_m)}} + \frac{1 - B}{k_m}$$

where

$$B = \sqrt{3V_f / 2} \qquad C = -4\sqrt{2 / 3V_f} \qquad (2.17)$$

Cheng and Vachon assumed a parabolic distribution of the discontinuous phase in the continuous phase based on Tsao's model [25]. The constants of this parabolic distribution were determined by analysis and presented as a function of the discontinuous phase volume fraction. Thus the equivalent thermal conductivity of the two phase solid mixture was derived in terms of the distribution function and the thermal conductivity of the constituents.

2.2.7 Coefficient of thermal expansion (CTE)

Dilatometry is a thermoanalytical technique used to measure shrinkage or expansion of materials. Dilatometry [26, 27] is the continuous measurement of the length of the sample as the specimen is subjected to a controlled linear heating rate. In this technique, dimensional

changes in a sample are primarily measured with negligible force acting on it, while the sample is heated.

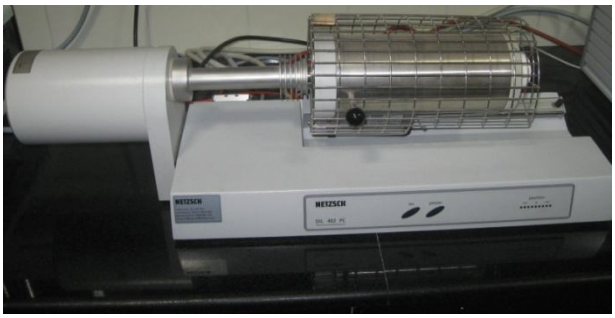

Fig. 2.6 Photograph of DIL 402 PC, NETZSCH dilatometer

The value of coefficient of thermal expansion is calculated using the relation

$$\alpha_l = \frac{1}{L}\frac{\Delta L}{\Delta T} \qquad 2.18$$

where L is the original dimension of the sample and ΔL is the change in length when the change in temperature is ΔT. In the present study, Dilatometer (DIL 402 PC, NETZSCH, Selb, Germany) is employed for thermal expansion measurements of the composites. Cylindrical samples (diameter 8 mm and thickness 10 to 14 mm) are required for dilatometric studies.

2.2.8 Mechanical properties

The mechanical flexibility is the prime requirement for flexible electronic applications. Tensile test is useful to evaluate mechanical properties of materials in which the sample is pulled to failure in a relatively short period of time. The sample is elongated at a constant rate and the load required to produce a given elongation is measured as a dependent variable. A

stress-strain curve may be plotted from the results of a tension test and from the plot the toughness of the material can be assessesd [28, 29]. In the present study the stress-strain properties of the composites were measured using a Universal Testing Machine (Hounsfield, H5K-S UTM, Redhill, U.K.) with a rate of grip separation of 500 mm/min. Tensile tests were conducted using dumb-bell shaped samples of width 4 mm and thickness in the range 1.5–2 mm.

2.2.9 Fourier Transform Infrared Spectroscopy (FTIR)

Infrared spectroscopy exploits the fact that molecules absorb specific frequencies that are characteristic of their structure. Examination of the transmitted light from sample reveals how much energy was absorbed at each wavelength. IR wavelengths absorbed by the sample is obtained from this transmittance or absorbance spectrum. Analysis of these absorption characteristics reveals the molecular structure of the sample in detail. Perkin-Elmer spectrum one FT-IR spectrometer was used to obtain IR spectral data of surface modified ceramic powder [30].

2.2.10 Moisture absorption of composites

The moisture absorption characteristics of the composites were measured using the samples with dimensions 50 mm×50 mm×2 mm. The samples were weighed accurately and immersed in distilled water for 24 hours. The samples were then taken out and again weighed after removing the excess water from the surface. The volume% of water absorption was then calculated using the relation,

$$\text{Volume \% water absorption} = \frac{(W_f - W_i)/\rho_w}{(W_f - W_i)/\rho_w + W_i/\rho_c} \times 100 \qquad 2.19$$

where W_i and W_f are the initial and final weights of the sample and ρ_w and ρ_c are the densities of distilled water and composite respectively.

2.2.11 Antenna measurements

In the present study, the antenna design was done by using Ansoft HFSS (High Frequency Structure Simulator). Ansoft HFSS is an interactive software package for electromagnetic modeling and analyzing 3D structures. This software uses Finite Element Method (FEM) for electromagnetic analysis on arbitrary 3D structures including antennas. The copper was cladded to butyl rubber-ceramic composites by hot pressing as per the simulated design. The copper film was initially roughened by using 60 grit emery paper and then it is hot pressed with butyl rubber composite in the desirable design. The antenna parameters are measured by connecting the fabricated antenna to a network analyzer (PNA E 8362B) by using a SMA (SubMiniature version A) connector.

2.3 References

1. H. Barron, Modern synthetic rubbers, Chapman & Hall Ltd, London (1949).
2. D. L. Bish and J. E Post, Modern powder diffraction. Reviews in mineralogy, Mineralogical Association of America, Boston., **20,** (1989).
3. B. D. Cullity, *Elements of X-ray diffraction*, Addison-Wesley Publishing Company (1978).
4. L. Reimer, Scanning electron microscopy, physics of image formation and microanalysis, Springer, Berlin (1985).
5. J. Krupka, *Meas. Sci. Technol.*, **17,** R55 (2006).
6. M. T. Sebastian, Dielectric materials for wireless communication, Elsevier Publishers, Oxford, UK (2008).
7. L. F Chen, C. K. Ong, C. P. Neo, V. V. Varadan and V. K. Varadan, Microwave electronics: Measurement and material characterization, John Wiley & Sons, England (2004).
8. J. B. Jarvis, R. G. Gayer, J. H. Grosvenor Jr, M. D. Janezic, C. A. Jones, B. Riddle, C. M. Weil and J. Krupka, *IEEE Trans. Dielec. Electrical Insul.*, **5,** 571 (1998).
9. D. G. P. Kajfez, *Dielectric resonators*, Noble Publishing Corporation, Atlanta, US (1998).
10. J. Krupka, *Mater. Chem. Phys.*, **79**, 195 (2003).
11. J. Krupka, A. P. Gregonry, O. C. Rochard, R. N. Clarke, B. Riddle and J. B. Jarvis, *J. Eur. Ceram. Soc.*, **21,** 2673 (2001).
12. B. Sareni, L. Krahenubuh, A. Beroul and C. Brosseau, *J. Appl. Phys.*, **81,** 2375 (1997).

13. A. H. Sihvola, *IEEE Trans. Geosci. Remote Sens.,* **26,** 420 (1988).

14. K. Wakino, *J. Am. Ceram. Soc.,* **76,** 2588 (1993).

15. A. V. Goncharenko, V. Z. Lozovski and E. F. Venger, Opt. Commun., **174,** 19 (2000).

16. F. Claro and R. Rojas, Phys. Rev. B, **43,** 6369 (1991).

17. N. Jayasundere and B. V. Smith, *J. Appl. Phys.,* **73,** 2462 (1993).

18. Y. Rao, J. Qu, T. Marinis and C. P. Wong, *IEEE Trans. Comp. Packag. Tech.,* **23,** 80 (2000).

19. D. P. H. Hasselman, R. Syed and T. Y. Tien, *J. Mater. Sci.*, **20,** 2549 (1985).

20. W. J. Parker, R. J. Jenkins, C. P. Butler and G. L. Abbott, *J. Appl. Phys.,* **32,** 1679 (1961).

21. E. F. Jaguaribe, Int. J. Heat and Mass Transf., **27,** 399 (1984).

22. J. K. Carson, S. J. Lovatt, D. J. Tanner and A. C. Cleland, J. Food. Eng., **75,** 297 (2006).

23. D. W. Richerson, Modern ceramic engineering: properties processing and use in design, Taylor and Francis, CRC Press, London (2006).

24. R. C. Progelhof, J. L. Throne and R. R. Ruetsch, Polym. Eng. Sci., **16,** 615 (1976).

25. G. T. N. Tsao, *Ind. Eng. Chem.*, **53**, 395 (1961).

26. J. Wang, J. K. Carson, M. F. North and D. J. Cleland, *Int. J. Heat and Mass Transf.,* **49,** 3075 (2006).

27. L. Pennisi, The firing process, engineered materials hand book, ceramics and glasses, ASM International, The material information society, SC (1991).

28. K. P. Menard, Dynamic mechanical analysis; A practical introduction, CRC Press, Boca Raton (1999).
29. H. W. Hayden, W. G. Moffatt and J. Wulff, The structure and properties of materials, volume III: Mechanical behaviour, Wiley Eastern Ltd, (1984).
30. C. Banwell and E. Mccash, "Fundamentals of molecular spectroscopy", Tata McGraw-Hill Education, (1994).

Chapter 3

Butyl Rubber-Low Permittivity Ceramic [Al_2O_3, SiO_2 and $Ba(Zn_{1/3}Ta_{2/3})O_3$] Composites

This chapter describes the synthesis, characterization and properties of butyl rubber filled with low permittivity ceramic composites. The low permittivity ceramics used for the present study were alumina, silica and barium zinc tantalate. The dielectric properties both at 1 MHz and 5 GHz, thermal and mechanical properties of these composites as a function of filler volume fraction were investigated. The effect of filler particle size on these properties was studied in butyl rubber-alumina composites. The relative permittivity and thermal conductivity of these composites were compared with theoretical models.

3.1 Introduction

The development of mechanically flexible or even stretchable electronic systems is increasing in recent years due to their attractive features [1]. Today's citizen carries more electronic systems near or even inside the body. Hence, the systems must be light weight, must take the desirable shape of the object and should follow all complex movements of these objects [2]. The soft, stretchable and elastic electronic assemblies can take the shape of the object in which they are integrated [3]. An ideal substrate and packaging material have to satisfy diverse requirements such as low relative permittivity to reduce signal propagation delay, low loss tangent to reduce signal attenuation along with better device performance, mechanical flexibility, high dimensional stability, moisture absorption resistance, high thermal conductivity (TC) to dissipate the heat generated, low coefficient of thermal expansion (CTE) matching to that of silicon etc. [4-6]. Several low permittivity ceramics such as silicates and aluminates with excellent microwave dielectric properties have been developed for substrate and packaging applications [7-9]. Its brittle nature and high processing temperature precludes them from practical use. Polymers are also widely used in the packaging industry [10, 11]. High value of CTE and low surface energy limits their practical applications. Hence, polymers or ceramics cannot be used alone for practical applications. Button et al. proposed a composite strategy of combining the advantages of ceramic and polymer to achieve a superior property balance [12]. Polymers such as polyethylene, polytetrafluoroethylene are flexible but cannot be used for stretchable applications. Stretchability is the prime requirement for biomedical applications where circuits are to be wrapped around curved surfaces. The research on elastomer-ceramic composites has received much attention in this context. The properties of the composites are

very much dependent on the size and shape of the fillers and the interaction between the filler and the polymer matrix. Hence, by the proper design of composites, one can utilize ease of processing and low ε_r of polymers with high thermal conductivity and low CTE of ceramics. Recently, the addition of nanofillers to polymers has attained much attention. An extensive research is going in the field of polymer-nano composites by incorporating nano scale fillers into polymers [13-15]. However, a few reports are available which explores the microwave dielectric properties of polymer-nanocomposites [16, 17]. In order to enhance the compatibility between the polymer phase and filler phase of composite systems chemical coupling agents such as functional silanes, organotitanates etc. are used. The coupling agents will act as a bridge between polymer matrix and filler particles. Studies were reported on the effect of coupling agents on dielectric properties of polymer ceramic composites [18, 19].

The elastomer used for the present study was butyl rubber. Butyl rubber is a synthetic elastomer with excellent dielectric properties in the microwave frequencies (ε_r = 2.4, tan$\delta \approx 10^{-3}$), good mechanical flexibility, ageing resistance, weathering resistance [20] etc. In order to develop low permittivity composites, the relative permittivity of the ceramic should be as low as possible. Numerous low relative permittivity ceramic materials are available. Among the available low permittivity ceramics, Al_2O_3, SiO_2 and $Ba(Zn_{1/3}Ta_{2/3})O_3$ (BZT) are used for the preparation of low permittivity butyl rubber-ceramic composites in the present study since they have relatively low loss factor.

Among the low permittivity ceramics, alumina is a well known low loss ceramic packaging material. The quality factor of alumina depends on the purity and density of the sintered ceramics. The quality factor (Qxf) of alumina is about 1 million with ε_r = 9.8 and τ_f = -60 ppm/^oC at room temperature [21]. The very high thermal conductivity (30 $Wm^{-1}K^{-1}$)

and low CTE (6-7 ppm/^{o}C) of alumina makes it a suitable electronic packaging material. Elastomer-alumina composites were well studied for its mechanical and curing characteristics [22, 23]. Recently, the effect of nano alumina loading on the electrical and mechanical properties of polyvinyl alcohol composites was investigated by Nigrawal et al. [24]. Ratheesh et al. investigated the dielectric properties of alumina and magnesia filled PTFE composites and found that PTFE-alumina composites are excellent candidates for microwave substrate applications [25]. Recently the effect of particle size on dielectric, thermal and mechanical properties of silicone rubber-alumina composites was investigated by Namitha et al. [26]. Zhou et al. synthesized silicone rubber-alumina composites and investigated the effect of alumina filler on the thermal and mechanical properties of silicone rubber composites [27]. Zhou et al. also reported the effect of alumina particle size on the mechanical and physical properties of silicone rubber composites [28]. Eventhough studies were reported on the alumina filled polymer composites, only a few reports are available on the evaluation of microwave dielectric properties of elastomer-alumina composites.

Silica is another low permittivity ceramic with excellent dielectric properties (ε_r = 4, tan$\delta \approx 10^{-3}$) and thermal properties such as thermal conductivity = 1.4 $Wm^{-1}K^{-1}$ and CTE = 0.5 ppm/^{o}C [29]. Silica is an important reinforcing filler of elastomer for industrial applications. Silica loaded polymer composites were also reported for microwave electronic applications [30-32]. Chen et al. studied the effect of filler loading and particle size on the dielectric, mechanical and thermal properties of PTFE-SiO_2 composites [33]. The effect of silica on dielectric properties of styrene butadiene rubber were investigated by Hanna et al. in the frequency range of 60 Hz to 10^8 Hz at room temperature [34].

$Ba(Zn_{1/3}Ta_{2/3})O_3$ is a complex perovskite ceramic with ε_r = 28, tan$\delta \approx 10^{-3}$ and a nearly zero temperature coefficient of resonant frequency (τ_f = 1 ppm/^oC) [35]. It is an ideal dielectric resonator at microwave frequencies. Recently, Manu et al. reported the effect of $Ba(Zn_{1/3}Ta_{2/3})O_3$ ceramic on the dielectric, mechanical and thermal properties of high density polyethylene composites [36]. The microwave dielectric properties of PTFE-$Ba(Mg_{1/3}Ta_{2/3})O_3$ composite were studied by Nijesh et al. and found that PTFE filled with 76 wt% $Ba(Mg_{1/3}Ta_{2/3})O_3$ attained a relative permittivity of 6.7 and a loss tangent of 0.003 in the X-band [37]. Namitha et al. studied the microwave dielectric properties of silicone rubber-BZT composites and found that the dielectric properties of silicone rubber were improved with the addition of BZT [38]. However, a very little attempt has been made to explore the microwave dielectric properties of BZT filled polymer composites.

The present chapter deals with the investigation of the effect of low permittivity ceramic fillers such as Al_2O_3, SiO_2 and $Ba(Zn_{1/3}Ta_{2/3})O_3$ on dielectric, thermal and mechanical properties of butyl rubber-ceramic composites. The effect of filler particle size on properties of the composites was studied by incorporating nano alumina in the butyl rubber matrix. The experimental values of relative permittivity and thermal conductivity of composites were compared with various theoretical models.

3.2 Butyl rubber-Al_2O_3 composites

Since alumina is a widely used ceramic packaging material, the effect of filler particle size on dielectric, thermal and mechanical properties of butyl rubber-ceramic composites was studied in butyl rubber-alumina composites. The alumina (micron and nano) powder was procured from Sigma Aldrich. The powder was dried at 100^oC for 24 hours before using for

composite preparation. The butyl rubber-micron alumina (BR/AL) and butyl rubber-nano alumina (BR/nAL) composites were prepared as described in section 2.1.4.1. The sample designation and the corresponding ceramic volume fraction (v_f) are given in Table 3.1. The BR/AL composites were prepared with a micron alumina loading from 0-0.42 v_f. The nano alumina has high surface area and large ceramic volume. Hence the possibility of agglomeration of nano particles increases with filler loading. This makes the processing of butyl rubber-nano alumina composites difficult at higher filler loading [39]. Hence, a maximum loading of 0.1 volume fraction of nano alumina is possible in the case of BR/nAL composites. The composites thus prepared were characterized for microstructure, dielectric, thermal and mechanical properties using techniques explained in section 2.2.

Figure 3.1 shows the powder XRD pattern of micron alumina and nano alumina. All the peaks are indexed based JCPDS file no. 46-1212. The phase purity of the ceramics was clear from Fig. 3.1.

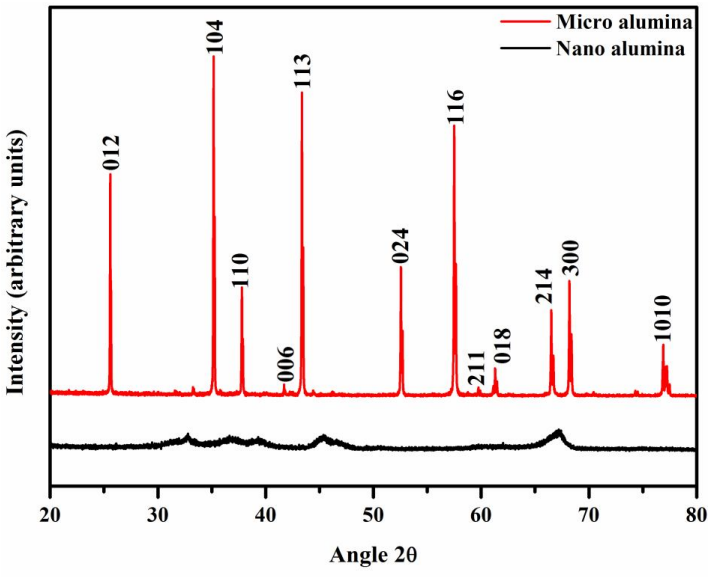

Fig. 3.1 XRD patterns of micron alumina and nano alumina

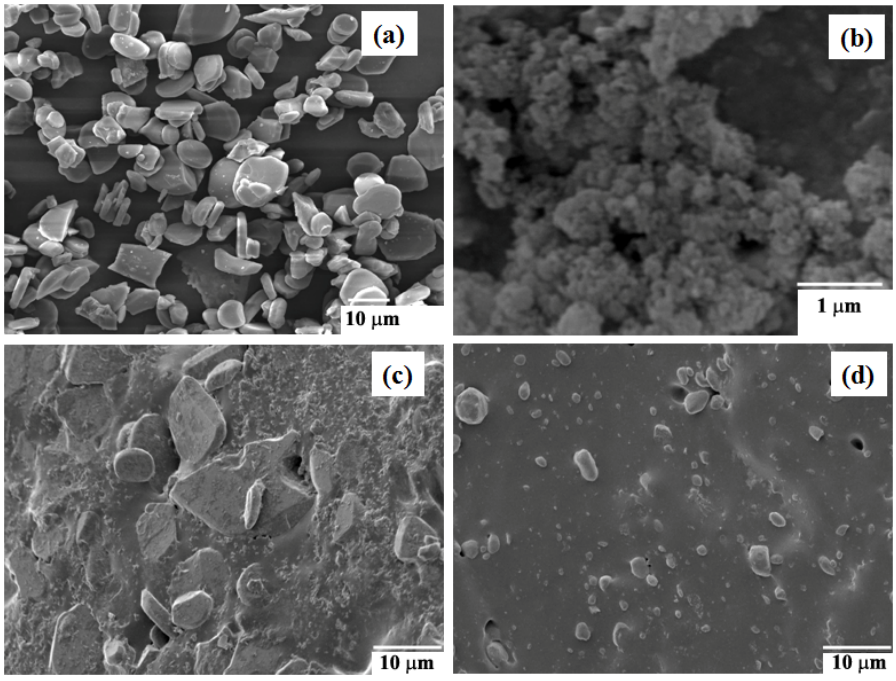

Fig. 3.2 SEM images of (a) micron alumina powder (b) nano alumina powder (c) fractured surface of BR+0.1 v_f of micron alumina and (d) BR+0.1 v_f of nano alumina composites

Figure 3.2 shows the SEM images of micron alumina, nano alumina powder and their composites with butyl rubber. Fig. 3.2 (a) and (b) depicts the morphology of micron alumina and nano alumina powder respectively. Fig. 3.2 (c) is the fractured surface of the BR+0.1 v_f of micron alumina composite which shows a homogeneous dispersion of ceramic particles in the rubber matrix. Some agglomerations are observed for the composites with nano alumina and are clear from the fractured surface of the BR+0.1 v_f of nano alumina composite (Fig. 3.2 (d)).

Table 3.1 gives the dielectric properties at 1 MHz and moisture absorption of BR/AL and BR/nAL composites. The relative permittivity of both composites increases with filler loading. This is due to the high relative permittivity of alumina compared to butyl rubber matrix. From the Table 3.1 it is clear that the BR/nAL composite have high relative

permittivity than that of BR/AL composites. The composites filled with nano particles have large interfacial area for the same filler loading which promotes interfacial polarization mechanism leads to increase in relative permittivity of BR/nAL composites. The loss tangent is the main factor affecting the frequency selectivity of a material and is influenced by many factors such as porosity, microstructure and defects [40]. The loss tangent of both composites shows same trend as that of relative permittivity. The moisture content is an important parameter for materials used for packaging applications. Absorption of moisture from the working atmosphere will degrade the dielectric properties since water is a polar molecule. It is clear from Table 3.1 that as the filler content increases, the volume % (vol%) of water content increases for both composites since the ceramic is hydrophilic in nature. Compared to micron composite, nano composites have a high tendency to absorb moisture due to the large surface area of the nano alumina and also for higher nano filler loading pores are present in the composites due to the agglomeration of the particles. This is evident from the SEM image 3.2 (d). The loss tangent and moisture absorption of butyl rubber-nano alumina composites are much higher as compared to the composites based on micron alumina.

Figure 3.3 (a) and (b) shows the variation of relative permittivity and loss tangent of BR/AL and BR/nAL composites at 5 GHz. As the relative permittivity of alumina is higher than the butyl rubber, the ε_r of BR/AL and BR/nAL composite shows an increasing trend with filler content. The relative permittivity of both composites at microwave frequency is slightly higher than that at 1 MHz. Further studies are needed to understand the increase in ε_r in the microwave frequency range as compared to at low frequency in butyl rubber-alumina composites. The nano alumina filled butyl rubber composites have higher relative permittivity than micron

Table 3.1 Dielectric properties at 1 MHz and moisture absorption of BR/AL and BR/nAL composites

Composite material	Sample Designation	Filler in phr[#] ()[$]	ε_r (1 MHz)	tan δ (1 MHz)	Water absorption (vol%)
Butyl rubber-micron alumina composite	BR-0	0 (0.00)	2.44	0.0003	0.039
	BR/AL-1	10 (0.02)	2.48	0.0011	0.045
	BR/AL-2	20 (0.04)	2.54	0.0012	0.045
	BR/AL-3	30 (0.06)	2.65	0.0021	0.056
	BR/AL-4	40 (0.08)	2.73	0.0032	0.057
	BR/AL-5	50 (0.10)	2.78	0.0046	0.065
	BR/AL-6	100 (0.26)	3.01	0.0051	0.067
	BR/AL-7	200 (0.33)	3.80	0.0063	0.071
	BR/AL-8	300 (0.42)	4.61	0.0083	0.082
Butyl rubber-nano alumina composite	BR/nAL-1	10 (0.02)	2.49	0.0090	0.150
	BR/nAL-2	20 (0.04)	2.55	0.0110	0.220
	BR/nAL-3	30 (0.06)	2.67	0.0160	0.490
	BR/nAL-4	40 (0.08)	2.79	0.0270	0.620
	BR/nAL-5	50 (0.10)	2.81	0.0470	0.700

[#] parts per hundred rubber.

[$] The corresponding ceramic volume fraction is given in parenthesis.

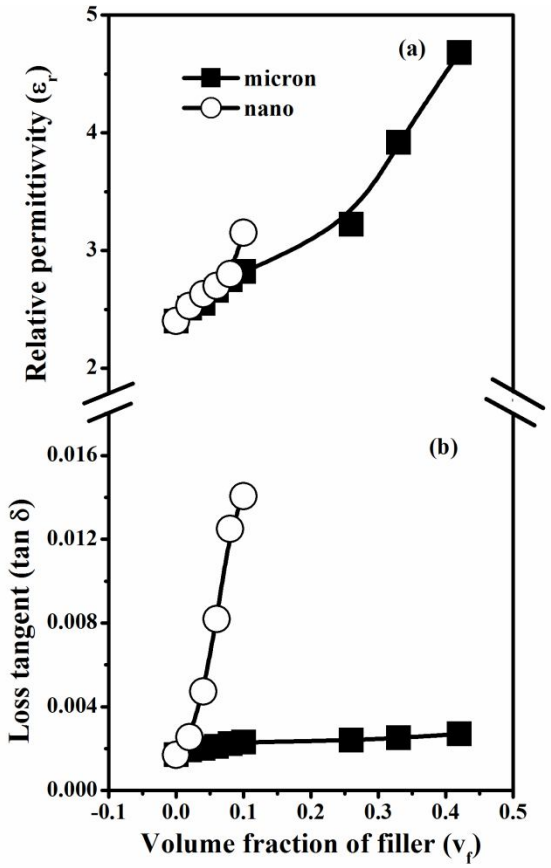

Fig. 3.3 Variation of (a) relative permittivity and (b) loss tangent of BR/AL and BR/nAL composites at 5 GHz

composite. Similar behaviour was observed by Ratheesh et al. in their work on PTFE-rutile, PTFE-silica and PEEK-$SrTiO_3$ composites [14, 30, 41]. They have reported that the nano filler has more polarization at interface region due to its high surface area and also due to large interface region between the filler and matrix. The nano composite also have high moisture content due to its large surface area. These factors will contribute to the high relative permittivity of nano composites. The relative permittivity of BR/AL composite increases from 2.40 to 4.68 as the micron alumina content increases from 0-0.42 v_f and that of BR/nAL composite from 2.40 to 3.15 when the nano alumina loading increases from 0-0.1 v_f. It is also noted that the loss tangent increases with the increase in filler content of both

micron and nano size alumina and a high loss tangent is exhibited by the nano alumina filled composites. The main reason for the higher loss tangent of nano composite is due to its high moisture content. The lattice strain is also higher for nano fillers due to its high surface area. Similar observation is reported in PTFE/rutile, epoxy/SiO_2 and PTFE/alumina composites [14, 31, 42]. The loss tangent of BR/AL composite increases from 0.0017 to 0.0027 as the micron alumina loading increases from 0-0.42 v_f and that of BRnAL composite increases from 0.0017 to 0.0140 as the nano alumina content increases from 0-0.1 v_f at 5 GHz.

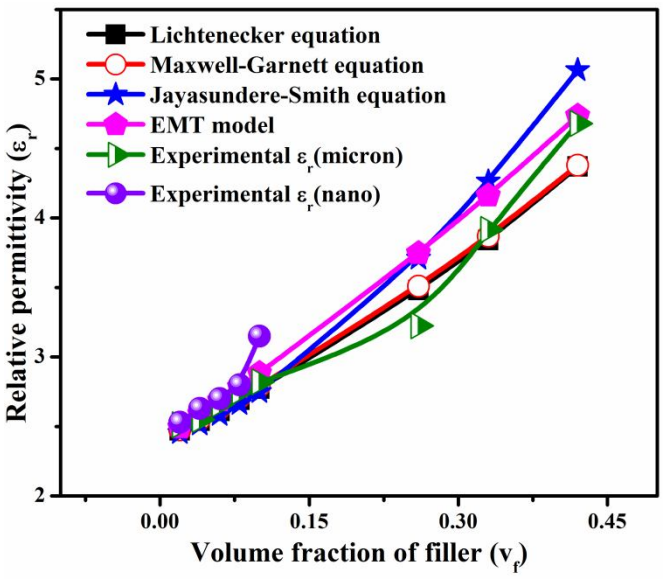

Fig. 3.4 Comparison of theoretical and experimental relative permittivity of BR/AL and BR/nAL composites at 5 GHz

Modeling techniques give relative permittivity of a composite system in terms of the relative permittivity of every constituting component and their volume fractions. Fig. 3.4 shows the comparison between the experimental and theoretical values of relative permittivity of BR/AL and BR/nAL composites at 5 GHz. All the equations are matching with the experimental ε_r of both BR/AL and BR/nAL composites upto 0.1 v_f. Maxwell-

Garnett and Lichtenecker equation shows slight deviation at higher ceramic content. In Maxwell-Garnett model, only the excitation of dipolar character is considered to be important and the correlations between these excitations are not taken into account. The multipolar contributions to the local field are also neglected. But these assumptions are valid only in dilute systems [43]. Hence, Maxwell-Garnett equation shows deviation at higher filler content. The most widely used relation for the prediction of ε_r is Lichtenecker's logarithmic law of mixing. It considers the composite system as randomly oriented spheroids that are uniformly distributed in a continuous matrix [44]. The deviation of experimental ε_r of both composites from Lichtenecker's equation at higher filler loadings may be due to the lack of consideration of interfacial interaction between the polymer and the filler particles. The experimental values of ε_r of both composites are matching with those values calculated from Jayasundere-Smith equation and shows deviation only at 0.42 v_f of micron alumina content and at 0.1 v_f of nano alumina content. The Jayasundere-Smith equation considers the particulate filled composite as a binary system and is valid only when $\varepsilon_f >> \varepsilon_m$ where ε_f and ε_m is the relative permittivity of filler and matrix respectively [45]. The EMT model is also in agreement with experimental ε_r of both composites at lower filler loadings and shows deviation at higher filler content. The deviation of all theoretical models at higher filler loading is due to the imperfect dispersion of filler particles in the butyl rubber matrix. The effective permittivity of a composite depends on the various factors such as relative permittivity of individual components in the system, their volume fractions, shape, size, porosity, interphase polarizability and interphase volume fractions. All these parameters cannot be accounted in a single equation. Hence, the experimental results show deviation from the theoretical values at higher filler content.

The bending effect on dielectric properties is important as far as flexible electronic applications concerned. Figures 3.5 and 3.6 show the variation of dielectric properties of butyl rubber-micron alumina and butyl rubber-nano alumina composites with bending. It is clear from the Fig. 3.5 (a) and (b) that the relative permittivity of all the composites is nearly independent of bending. It is evident from the Fig. 3.6 (a) and (b) that the loss tangent of the nano composites is almost independent of bending and that of micron composite shows slight variation with bending. Hence, these are suitable for flexible electronic applications.

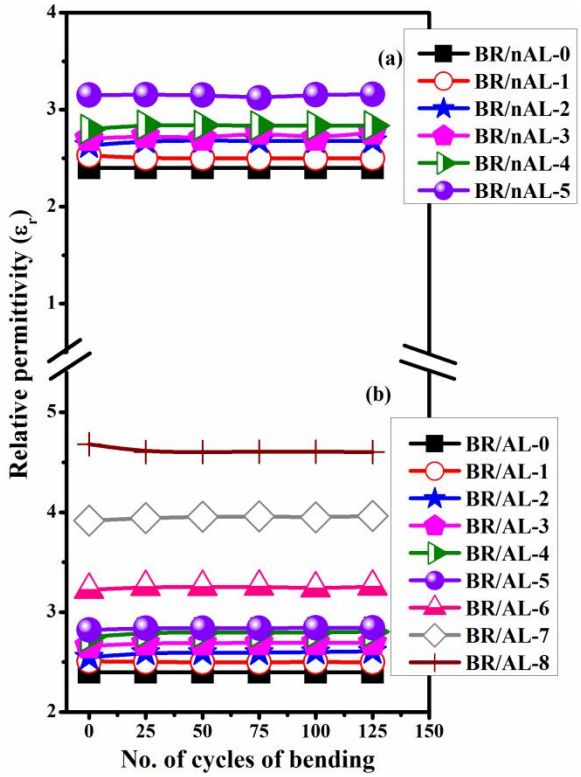

Fig. 3.5 Variation of relative permittivity of (a) BR/nAL and (b) BR/AL composites with bending

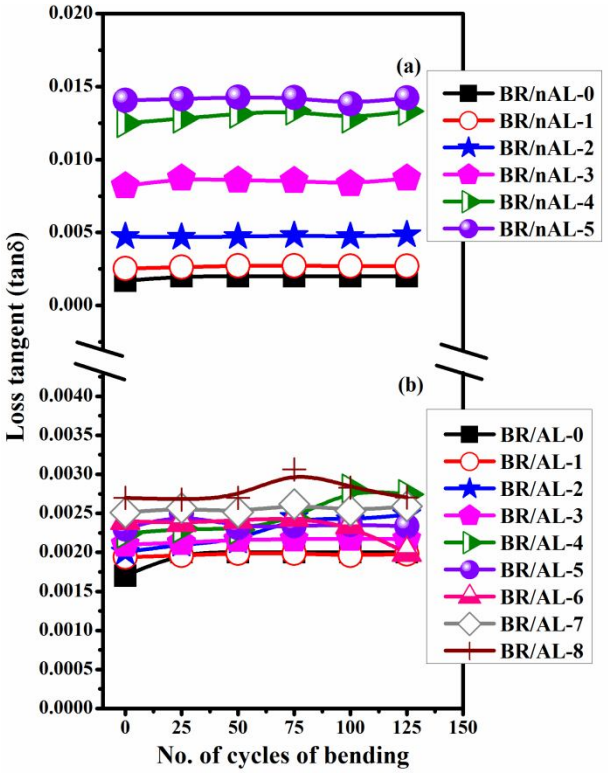

Fig. 3.6 Variation of loss tangent of (a) BR/nAL and (b) BR/AL composites with bending

Figure 3.7 (a) and (b) shows the temperature dependence of butyl rubber-nano alumina and butyl rubber-micron alumina composite respectively. The thermal stability of relative permittivity is one of the important properties of the substrate materials that control the overall performance of the materials. From the figure it is clear that all the composites are almost thermally stable within the measured temperature range. The small decrease in relative permittivity with temperature may be due to the large difference in thermal expansion coefficient of butyl rubber and the alumina [46, 47].

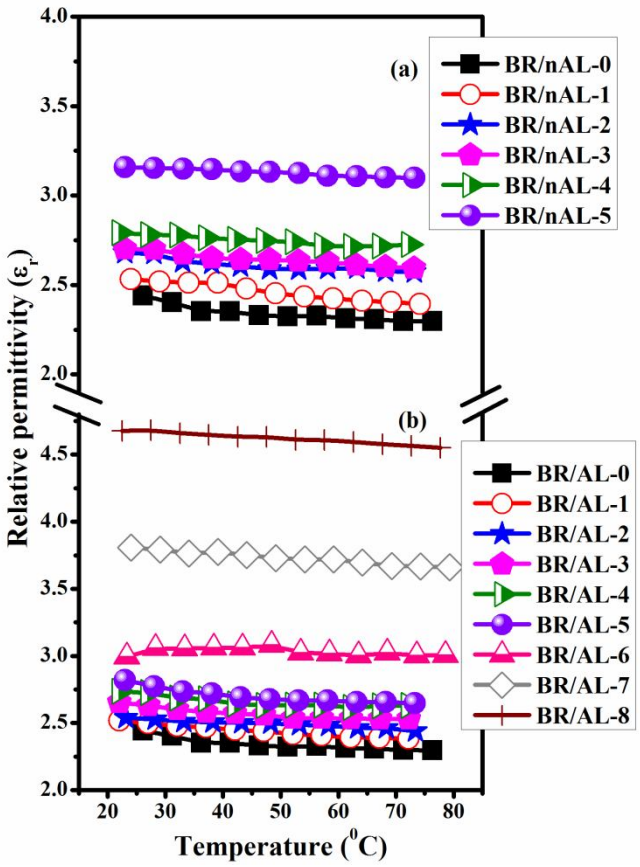

Fig. 3.7 Variation of relative permittivity of (a) BR/nAL and (b) BR/AL composites with temperature

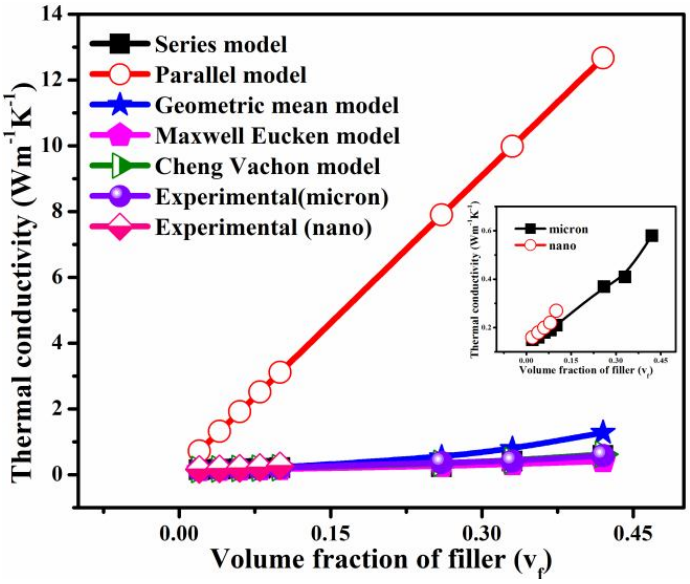

Fig. 3.8 Variation of thermal conductivity of BR/AL and BR/nAL composites with filler content

Heat dissipation from integrated circuits is a crucial problem for electronic industry that affects potential miniaturization, speed and reliability**.** The thermal conductivity (TC) of polymers is very low, ranging from 0.14 to 0.60 $Wm^{-1}K^{-1}$ [48] and can be improved by the addition of ceramic fillers as the TC of ceramic is higher than that of polymers. The thermal conductivity of the composites depends on the intrinsic thermal conductivities of filler and matrix, shape and size of the filler and the loading level of filler [49]. The variation of thermal conductivity of both BR/AL and BR/nAL composites with filler content is shown in Fig. 3.8. The TC of both composites shows increasing trend with ceramic loading. This is quite expected since the thermal conductivity of alumina (30 $Wm^{-1}K^{-1}$) is higher than that of butyl rubber matrix (0.13 $Wm^{-1}K^{-1}$). From the inset plot in Fig. 3.8 it is clear that the TC of nano alumina loaded composites is slightly higher than that of micron composite. The matrix/filler interface plays a critical role in nano composites due to its large surface area.

The number of particles increases with decreasing particle size for the same filler content [50]. This will leads to the formation of large number of conductive channels in nano filler added composites. Hence, the BR/nAL composites show high thermal conductivity than that of BR/AL composites. Many theoretical models have been published for predicting the thermal conductivity of composites [51]. The experimental thermal conductivity of present composites was compared with that values calculated using equations (2.13)-(2.17). Fig. 3.8 also compares the experimental thermal conductivity of both micron and nano composite with theoretical models. The physical structures assumed in the series and parallel models are of layers of the phases aligned either perpendicular or parallel to the heat flow respectively. The series and parallel model of TC gives only lower and upper limits of thermal conductivity values of composites respectively [52]. The experimental TC values of both composites are within the range of series and parallel model. The geometric mean model is in good agreement with experimental thermal conductivity of both composites upto a volume fraction of 0.1 and has a lower value than predicted thermal conductivity at higher micron alumina loading. This may be due to the agglomeration of filler particles at higher filler loadings. The other two models such as Cheng-Vachon and Maxwell-Eucken model are matching with experimental TC of both composites. Cheng and Vachon assumed a parabolic distribution of the discontinuous phase in the continuous phase based on Tsao's model [53]. The constants of this parabolic distribution were determined by analysis and presented as a function of the discontinuous phase volume fraction. Maxwell-Eucken model considers the composite system as randomly distributed and non-interacting homogeneous spheres in a homogeneous medium.

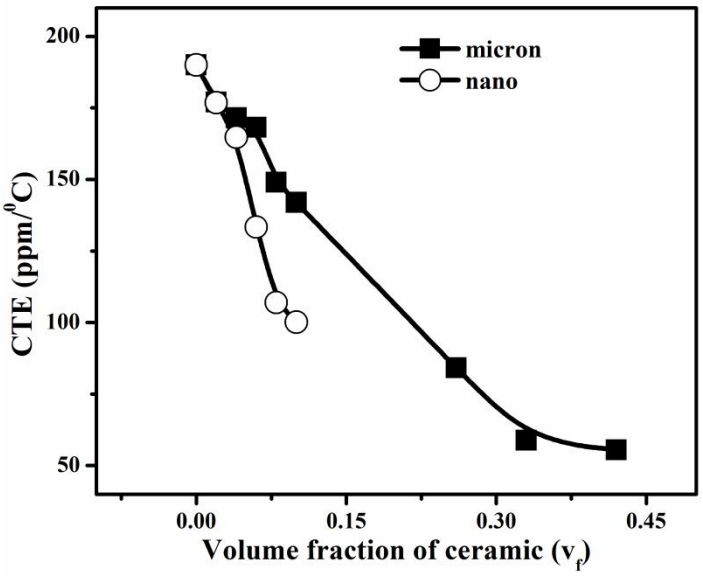

Fig. 3.9 Variation of CTE of BR/AL and BR/nAL Composites with filler content

Figure 3.9 shows the variation of coefficient of thermal expansion of butyl rubber-micron alumina and butyl rubber-nano alumina composites with filler content. The CTE of both the composites decreases with ceramic loading since the CTE value of alumina is smaller than that of rubber matrix and also the mobility of loose molecular bonds in the polymer chains are restrained by the ceramic loading [54]. The BR/nAL composites show much lower CTE value compared to that of BR/AL composites. The physical cross linking points are more in the case of nano particles because of its high specific surface area and this will increase the mechanical interaction between the filler and rubber matrix [27]. Hence the nano composites have lower CTE than that of micron composites

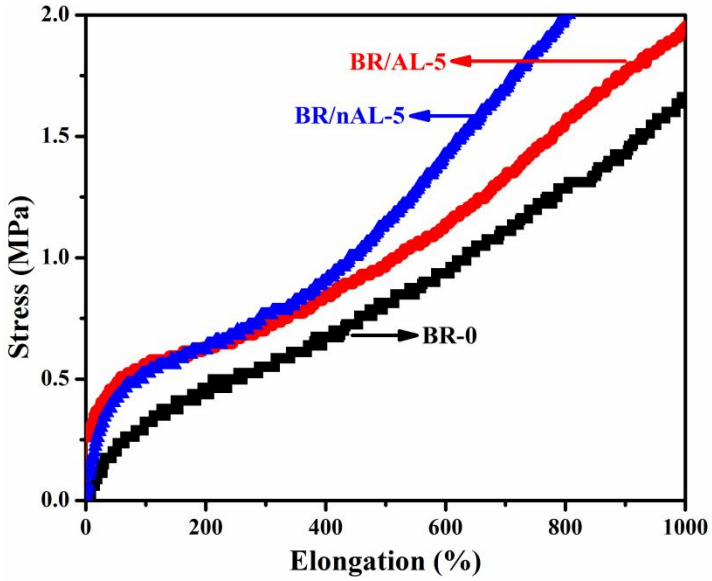

Fig. 3.10 Stress-strain curves of BR/AL and BR/nAL composites

Figure 3.10 shows the stress-strain curve of BR/AL and BR/nAL composites. The mechanical properties of a particulate composite depend on the strength of the adhesive bond between the different phases, the type of dispersion and the amount of particle agglomeration. From the figure it is clear that the stress needed for ceramic filled butyl rubber composite is greater than that of unfilled sample. Among BR-0, BR/AL-5 and BR/nAL-5, the stress required for BR/nAL-5 composite is high. This may be due to more homogeneous dispersion of nano particles in the rubber matrix. Chee et al. reported that at lower filler loading the nano alumina particle orient along the direction of stress and this would reinforce and increase the stiffness of the nano composite [55].

3.3 Butyl rubber-SiO_2 and butyl rubber-$Ba(Zn_{1/3}Ta_{2/3})O_3$ composites

Silica was procured from Sigma Aldrich. $Ba(Zn_{1/3}Ta_{2/3})O_3$ ceramic was prepared by conventional solid state route as described in section 2.1.2.3. The butyl rubber-silica (BR/S) and buty rubber-BZT (BR/BZT) composites were prepared as described in section no.

2.1.4.1. The density of silica ($\rho \approx 2.6$ g/cm^{-3}) is lower than that of BZT ($\rho \approx 7.96$ g/cm^{-3}). Hence, the silica filled composites were prepared upto a loading of 0.42 v_f (200 phr) and that of BR/BZT composites upto a filler loading of 0.32 v_f (400 phr). The sample designation and the corresponding ceramic volume fraction are given in Table 3.2. The composites were then hot pressed at 200^{o}C for 90 minutes under a pressure of 2 MPa. The phase purity of silica and BZT were confirmed by XRD analysis. The composites were characterized for microstructure, dielectric, thermal and mechanical properties using techniques explained in section 2.2.

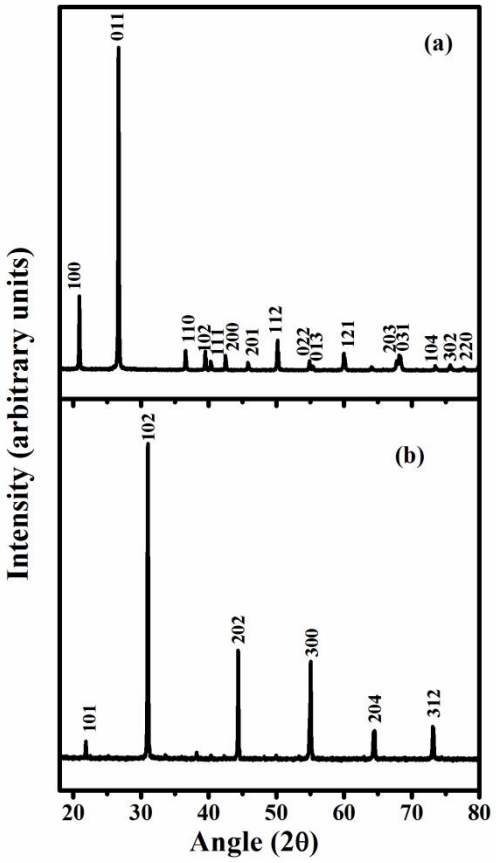

Fig. 3.11 XRD patterns of (a) SiO_2 and (b) $Ba(Zn_{1/3}Ta_{2/3})O_3$

Figure 3.11 shows the XRD patterns of silica heat treated at 100^{o}C for 24 hours and BZT sintered at 1500^{o}C for 4 hours. The peaks were indexed based on the JCPDS file no. 89-8934 and 18-0201 for silica and BZT respectively. The phase purity of both the ceramics were obvious from the XRD patterns.

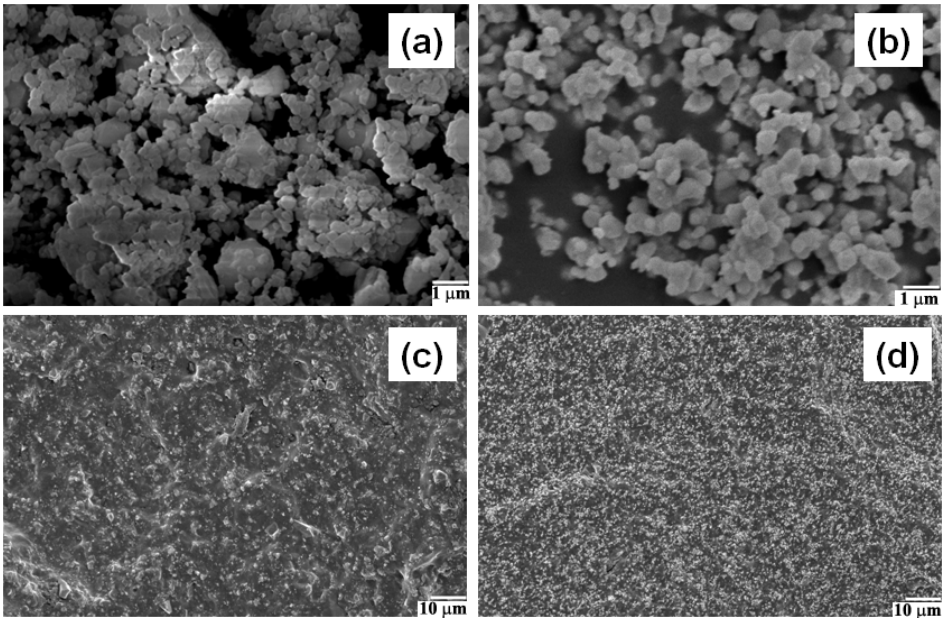

Fig. 3.12 SEM images of (a) SiO_2 powder (b) $Ba(Zn_{1/3}Ta_{2/3})O_3$ powder (c) fractured surface of BR+0.42 v_f of SiO_2 and (d) BR+0.32 v_f of $Ba(Zn_{1/3}Ta_{2/3})O_3$ composites

Figure 3.12 (a) and (b) shows the SEM images of silica and BZT powder respectively. Both silica and BZT particles are irregularly shaped and are less than 1μm in size. Fig. 3.12 (c) and (d) represents fractured SEM images of BR+0.42 v_f of SiO_2 and BR+0.32 v_f of $Ba(Zn_{1/3}Ta_{2/3})O_3$ respectively. From the figure it is clear that the filler particles are uniformly distributed in the rubber matrix of both composites.

Table 3.2. Dielectric and water absorption properties of butyl rubber-silica and butyl rubber-BZT composites

Composite material	Sample designation	Filler in phr[#] ()[$]	ε_r (1 MHz)	tan δ (1 MHz)	Water absorption (vol%)
Butyl rubber-silica composites	BR-0	0 (0.00)	2.44	0.0003	0.039
	BR/S-1	10 (0.03)	2.51	0.0020	0.048
	BR/S-2	25 (0.08)	2.75	0.0050	0.052
	BR/S-3	50 (0.15)	2.83	0.0060	0.059
	BR/S-4	100 (0.26)	3.10	0.0080	0.078
	BR/S-5	200 (0.42)	3.37	0.0100	0.091
Butyl rubber-BZT composites	BR/BZT-1	10 (0.01)	2.45	0.0010	0.040
	BR/BZT-2	25 (0.03)	2.50	0.0012	0.041
	BR/BZT-3	50 (0.06)	2.71	0.0015	0.043
	BR/BZT-4	100 (0.10)	3.11	0.0016	0.044
	BR/BZT-5	200 (0.19)	3.49	0.0018	0.045
	BR/BZT-6	300 (0.26)	4.45	0.0019	0.047
	BR/BZT-7	400 (0.32)	5.46	0.0021	0.057

[#] parts per hundred rubber.

[$] The corresponding ceramic volume fraction is given in parenthesis.

Table 3.2 shows the dielectric and water absorption properties of butyl rubber-silica and butyl rubber-BZT composites. The relative permittivity and loss tangent of both the composites increases with filler content. The increase in ε_r of the composites is mainly due to the high relative permittivity of silica and BZT as compared to rubber matrix. The connectivity among the filler particles increases at higher filler content which in turn

increases the relative permittivity of the composites [56]. The interfacial area and the possibility of accumulation of space charges at interface of polymer-ceramic composite increases with increase in the ceramic loading which in turn increases the loss tangent of the composites. The tanδ of BR/S composite is found to be higher than that of BR/BZT composites. This may be due to the presence of more moisture content in the silica powder. The moisture content significantly influences the electrical properties of the composites since the relative permittivity and loss tangent of water is high [57]. Hanna et al. reported a similar observation in styrene butadiene rubber-silica composites [34]. It is also evident from the Table 3.2 that the volume % of moisture content increases with filler content for both BR/S and BR/BZT composites. This may be due to the hydrophilic nature of ceramic. It has been reported that materials with moisture absorption upto about 0.1% can be used for electronic packaging applications [58]. The present composites exhibit moisture absorption within this limit.

Figure 3.13 (a) and (b) depicts the microwave dielectric properties of BR/S and BR/BZT composites at 5 GHz. The relative permittivity of both the composites increases with filler loading. The increase in total polarizability of composite material with filler content contributes to the increase in relative permittivity of the composites. The relative permittivity of BR/S composites at 5 GHz is less than that at 1 MHz as expected due to the absence of certain polarization mechanisms at microwave frequencies. But the ε_r of BR/BZT composites at 5 GHz is higher than that at 1 MHz. The relative permittivity of BR/S composite is 3.09 for the maximum silica loading of 0.42 v_f. The relative permittivity of BZT filled butyl rubber composites has ε_r of 5.72 for the maximum filler loading of 0.32 v_f. The BZT based composite has higher relative permittivity since silica has a lower relative

permittivity. From the figure it is also clear that the loss tangent of BR/S and BR/BZT composites shows similar trend as that of relative permittivity with increase in filler loading. The tanδ of BR/S composites is higher than that of BZT filled composites. The tanδ of BR/S-5 and BR/BZT-7 composites at 5 GHz are 0.0045 and 0.0025 respectively. The increase in loss of BR/S composites is due to the presence of more moisture content in silica composites than that of BR/BZT composites which is evident from Table 3.2. The dipole relaxation of water molecule in the microwave frequency contributes to loss tangent of the composites [59].

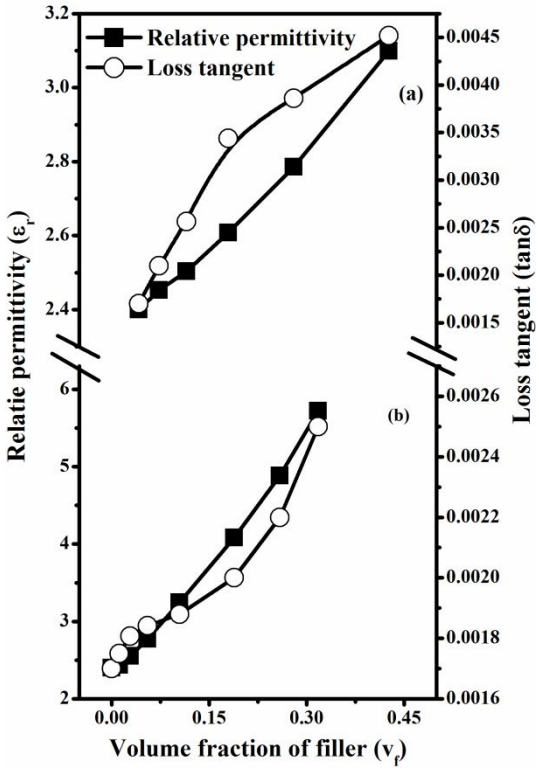

Fig. 3.13 Variation of ε_r and tan δ of (a) BR/S and (b) BR/BZT composites with filler content at 5 GHz

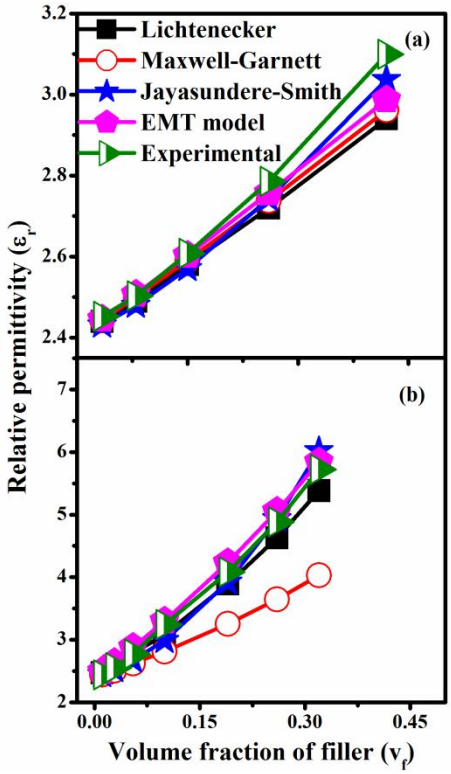

Fig. 3.14 Comparison of theoretical and experimental relative permittivity of (a) BR/S and (b) BR/BZT composites at 5 GHz

The precise prediction of effective relative permittivity of the composites is very important for electronic packaging applications. Fig. 3.14 shows the comparison of experimentally observed relative permittivity with the values predicted using the equations (2.6) to (2.9). It is clear from Fig. 3.14 (a) that the experimental relative permittivity of butyl rubber-silica composites are in agreement with theoretical models upto a filler loading of 0.15 v_f and shows deviation at higher silica content. Among the theoretical models, the EMT model proposed by Rao et al. [60] holds good for BR/S composites. EMT model considers the composite as an effective medium in which random unit cell (RUC) is embedded. The RUC is defined as a core of filler surrounded by a concentric matrix layer. The basic assumption of EMT model is that the RUC embedded in effective medium cannot be detected in an electromagnetic experiment which makes it possible to predict the relative permittivity of the composite. The importance of EMT model is that shape of the filler particles is taken into account through the morphology factor 'n' in calculations. Therefore no restrictions are imposed on the shape of the particles to be used. The shape factor, 'n' for BR/S composites is 0.2. It is evident from Fig. 3.14 (b) that the values of ε_r predicted by Maxwell-Garnett equation shows considerable deviation from the experimental values of BR/BZT composites except at very low filler loading. As the interparticle distance decreases with the increase in filler volume fraction, Maxwell-Garnett formula may not yield accurate results. Lichtenecker's equation is valid upto a volume fraction of 0.19 and shows deviation at higher BZT loading. This may be due to the lack of consideration of interfacial interaction between the polymer and the filler particles. The Jayasundere-Smith equation is in agreement with experimental data since this equation considers the interactions between the fields of neighbouring filler particles [61]. The experimental relative permittivity of BR/BZT

composites are also very well fit with EMT model. The 'n' value is determined empirically and the value of 'n' for BR/BZT composite is 0.2.

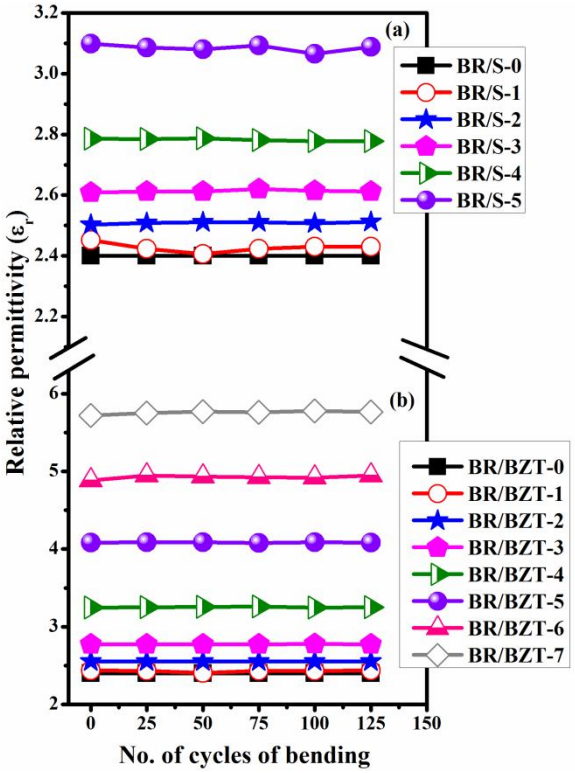

Fig. 3.15 Variation of relative permittivity of (a) BR/S and (b) BR/BZT composites with bending

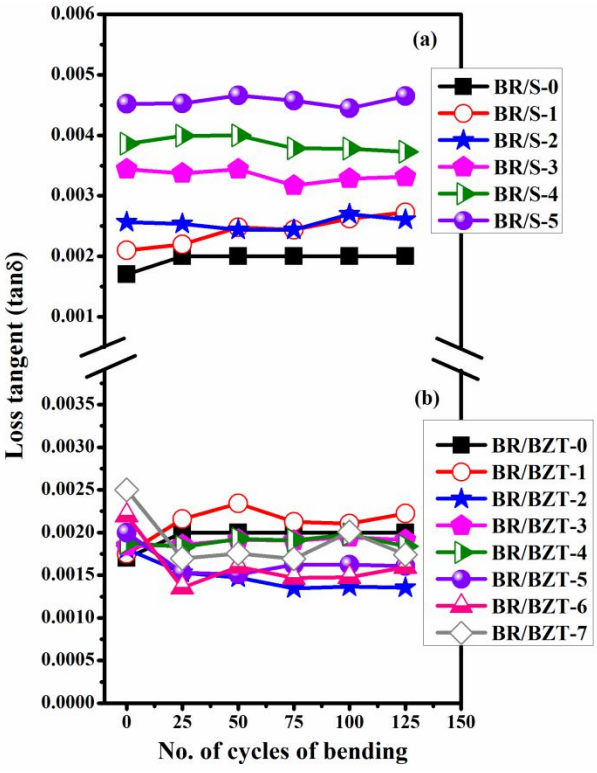

Fig. 3.16 Variation of loss tangent of (a) BR/S and (b) BR/BZT composites with bending

The effect of bending on microwave dielectric properties of butyl rubber-silica and butyl rubber-BZT composites is shown in Fig. 3.15 and 3.16. It is evident from the Fig. 3.15 (a) and (b) that the ε_r of BR/S composites shows a slight decrease after a bending cycle of 75 for butyl rubber loaded with 0.42 v_f of silica content. This may be due to the aggregating tendency of silica at higher loading. The relative permittivity of BR/BZT composites is nearly independent of repeated bending. From the Fig. 3.16 (a) and (b) it is clear that the tanδ of silica filled composites shows small variation with bending. The loss tangent of the butyl

rubber- BZT composites also shows a small variation with repeated bending. But the variation is only marginal [62].

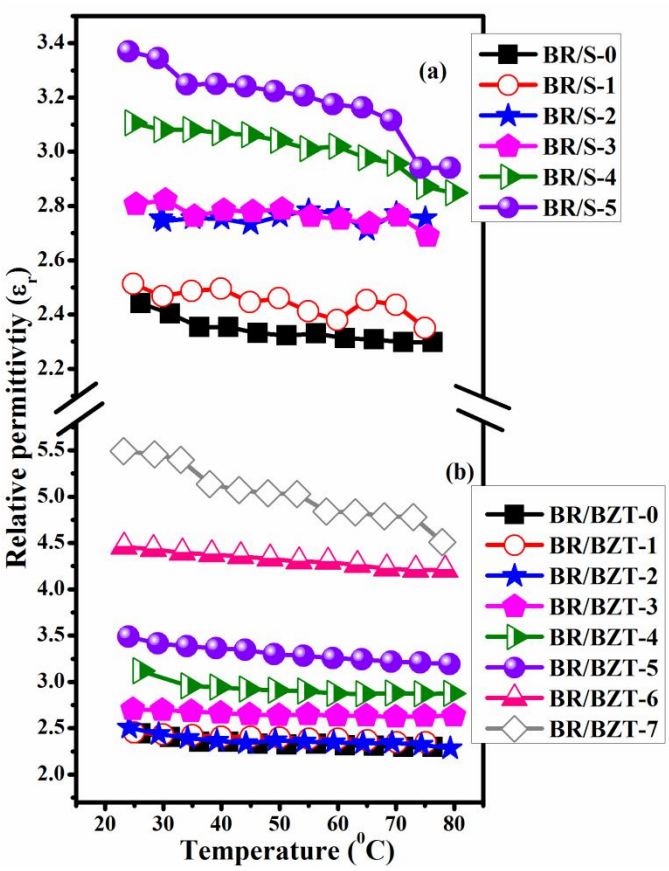

Fig. 3.17 Temperature dependence of relative permittivity of (a) BR/S and (b) BR/BZT composites at 1 MHz

Figure 3.17 (a) and (b) shows the variation of relative permittivity of butyl rubber-silica and butyl rubber-BZT composites with temperature at 1 MHz. It is noted that the variation of relative permittivity with temperature is small and the relative permittivity of both the composites decreases with temperature. This may be due to the difference in the thermal expansion coefficient of the matrix and the filler and also due to the decrease in polarizability of dipoles with temperature. The large difference in CTE may prevent the aggregation of the polar components and this might lead to a reduction in relative

permittivity with increase in temperature [63]. Both BR/S and BR/BZT composites are almost thermally stable in the measured temperature range.

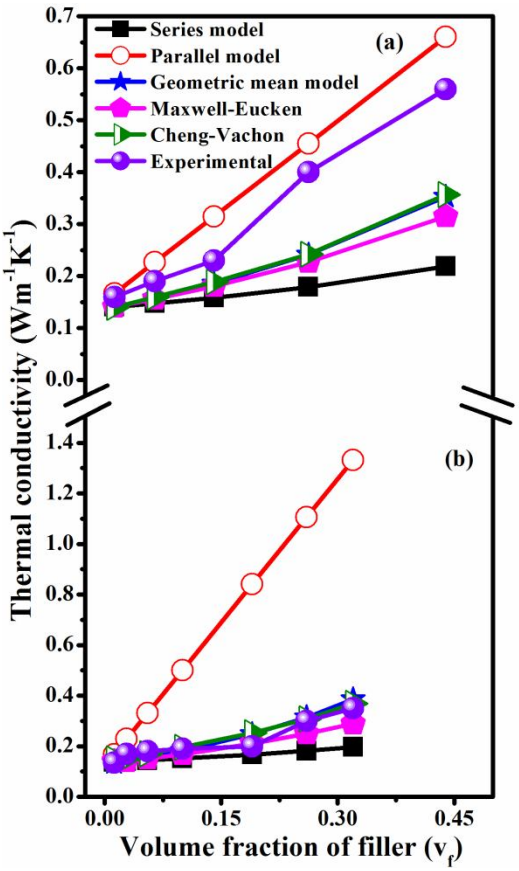

Fig. 3.18 Variation of thermal conductivity of (a) BR/S and (b) BR/BZT composites with filler loading

The variation of thermal conductivity of BR/S and BR/BZT composites with filler content are shown in Fig. 3.18. The thermal conductivity of butyl rubber is 0.13 $Wm^{-1}K^{-1}$. As the thermal conductivity of fillers silica (1.4 $Wm^{-1}K^{-1}$) and BZT (3.9 $Wm^{-1}K^{-1}$) are higher than that of matrix, the thermal conductivity of both BR/S and BR/BZT composites increased with filler content. The increase in thermal conductivity of both the composites at higher filler content is due to the presence of more connecting paths between the filler particles [16]. The thermal conductivity of BR/S composites increases from 0.13 to 0.56 as the silica loading increases from 0-0.42 v_f and that of BR/BZT composites from 0.13 to 0.35 as the

filler loading increases from 0-0.32 v_f. The thermal conductivity of the composite can be further enhanced by adding high thermal conductivity fillers such as aluminium nitride, silicon nitride etc. Fig. 3.18 also compares the experimental thermal conductivity with those calculated using equations 2.13 to 2.17. From Fig. 3.18 (a) it is evident that all the theoretical models match with measured thermal conductivity of butyl rubber-silica composites at lower silica loading and deviates from predicted values after a filler loading of 0.15 v_f. The wide variations in filler geometry, orientation and dispersion makes it difficult to compare composites filled with different materials. Moreover, the interfacial boundary thermal resistance between the filler particles and the matrix, referred to as Kapitza resistance, [64] is not taken into account while calculating the thermal conductivity of composites. It is not possible to measure it at the molecular level where it takes place. As a result, experimental and theoretical thermal conductivity data are often not in agreement. From the Fig. 3.18 (b) it is clear that the TC values of BR/BZT composites lies within the range of series and parallel models. It is worth to be noted that the geometric mean model and Cheng-Vachon model is in good agreement with experimental values. Maxwell-Eucken model shows slight deviation from experimental values at higher filler loading.

The variation of coefficient of thermal expansion of butyl rubber composites filled with silica and BZT are shown in Fig. 3.19. It is seen that the CTE of BR/S and BR/BZT composites decreases with filler loading as the CTE of the fillers, silica (0.5 ppm/^{o}C) and BZT (4.2 ppm/^{o}C) are lower than that of rubber matrix (191 ppm/^{o}C). In polymer-ceramic composite there is a region of tightly bound polymer chains in the immediate vicinity of the filler particles followed by a region of loosely bound polymer chains [65]. The filler particles will largely restrict the thermal expansion of polymer chains tightly bound to them. But the

thermal expansion of loosely bound polymer chains may not be that much constrained. The addition of more filler leads to the reduction in volume fraction of loosely bound polymer chains. Consequently the thermal expansion of the composite will get suppressed.

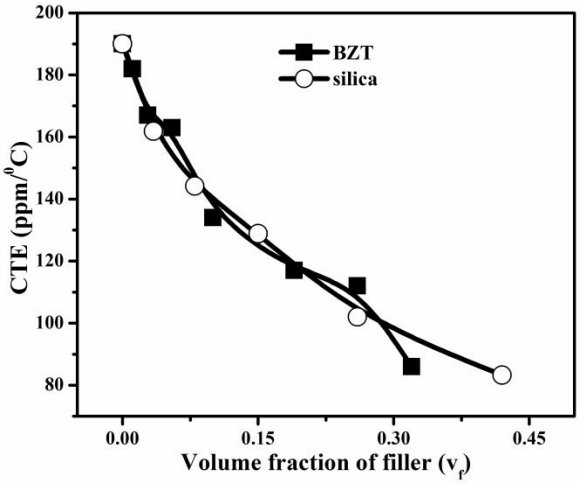

Fig. 3.19 Variation of coefficient of thermal expansion of BR/S and BR/BZT composites with ceramic loading

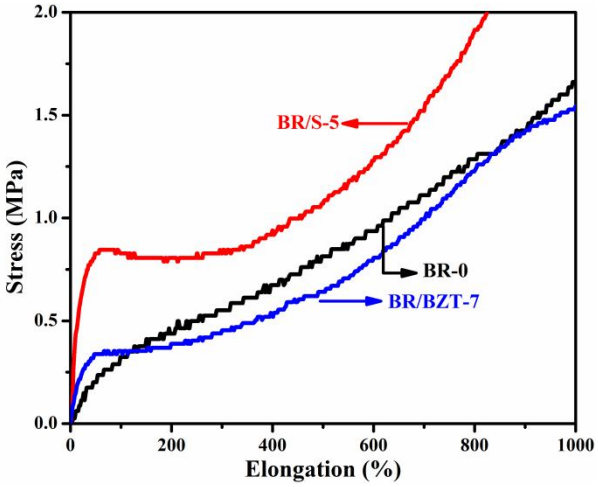

Fig. 3.20 Stress-strain curves of BR/S and BR/BZT composites

Figure 3.20 shows the stress-strain curves of BR-0, BR/S-5 and BR/BZT-7. The stress needed for elongation increases with filler content. The interfacial adhesion plays a major role in mechanical properties of the composites. Todorova et al. [66] reported that the interfacial adhesion increases with filler loading which in turn increases the effectiveness of the stress transfer from rubber chains. Salaeh et al. [67] reported that the mobility of molecular chains decreases due to the incorporation of ceramic particles and hence the increase in stiffness of the composite. From the figure it is clear that the silica filled composite shows higher reinforcement than that of BZT filled composite. Silica is reported to be good reinforcing filler for rubber composites [68, 69].

3.4 Effect of coupling agent on microwave dielectric properties of butyl rubber-BZT composites

In order to improve the compatibility between butyl rubber and ceramic of elastomer-ceramic composites, mercapto group based coupling agents are employed [70]. These are bifunctional silanes with different reactivity, where the double functionality allows them to react with the hydroxyl groups present on the surface of filler particles and the second sulfur based reactive groups interact with polymer macromolecules during the vulcanization step. Mercaptopropyltrimethoxy silane (MPTMS) coupling agent was used for the present investigation. Silane coupling agent acts as a bridge between butyl rubber and BZT ceramic and is shown in Fig. 3.21

Fig. 3.21 Silane coupling mechanism

The infrared spectrum of surface treated BZT is shown in Fig. 3.22. The peak in 620 cm^{-1} is the result of Ba-O bond vibrations. The peaks in 2920-2690 cm^{-1} range indicate $–CH_2$ stretching vibration of silane coupling agent. The peak in 1445 cm^{-1} indicates the scissoring vibration of $–CH_2$ groups. The peaks at around 1000 cm^{-1} (υ_{as}, Si-O) and 570 cm^{-1} (δ, Si-O-Si) attribute to the success of hydrolysis and condensation reactions (υ represents stretching, δ in-plane bending). This confirms the coating of MPTMS on BZT.

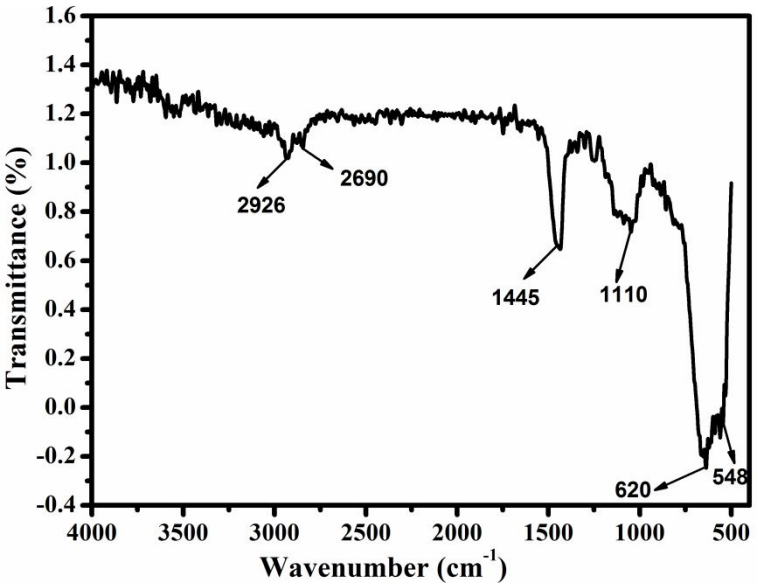

Fig. 3.22 FTIR spectra of MPTMS treated BZT

Table 3.3 Microwave dielectric properties of untreated and silane treated BZT–butyl rubber composites

Sample	ε_r at 5 GHz	tanδ at 5 GHz
BR/50BZT	2.77	0.0018
BR/50sBZT	2.82	0.0030
BR/100BZT	3.24	0.0019
BR/100sBZT	3.51	0.0052

The microwave dielectric properties of selected composition of BR/BZT and silane treated BZT loaded butyl rubber composites (BR/sBZT) are given in Table 3.3. From the Table 3.3 it is clear that the silane coupled composites does not exihibit much improvement in relative permittivity of the composites. The silane treated composite shows higher loss tangent than that of untreated one. This may be due to the presence of additional phases from coupling agent. Xu et al. observed a similar behaviour in aluminium/epoxy composites [71].

As far as microwave electronic packaging and substrate applications are concerned, a low loss material is preferred. Hence coupling agents are not used in our further works.

3.5 Conclusions

- The effect of low permittivity fillers such as alumina, silica and barium zinc tantalate on the dielectric, thermal and mechanical properties of butyl rubber composites was investigated. The influence of filler particle size on the performance of butyl rubber-alumina composites was also studied.
- The microstructure of the composites shows uniform dispersion of filler in the matrix and also some pores are present at higher filler loading.
- For 0.1 volume fraction of micron alumina loading, the composite have relative permittivity of 2.82 and loss tangent of 0.0023 at 5 GHz and for the same volume fraction of nano alumina content the composite have ε_r of 3.15 and tanδ of 0.0140 at 5 GHz. However, the nano alumina filled butyl rubber composites shows higher loss tangent than that of micron composite.
- The dielectric properties of the composites were studied at 1 MHz and 5 GHz and are found to be improved with ceramic loading. The butyl rubber-silica composites attained ε_r = 2.79, tanδ = 0.0039 for a optimum silica loading of 0.26 v_f and the butyl rubber-BZT composite have ε_r = 4.88, tanδ = 0.0022 for a optimum BZT loading of 0.26 v_f at 5 GHz.
- The thermal properties of the composite were also improved with filler content. The thermal conductivity and coefficient of thermal expansion of BR/AL composite is 0.21 $Wm^{-1}K^{-1}$ and 142 ppm/^oC and that of BR/nAL composite is 0.27 $Wm^{-1}K^{-1}$ and

100 ppm/^{o}C respectively for 0.1 v_f of filler loading. The water absorption of both composites for 0.1 v_f of filler loading are 0.065 vol% and 0.700 vol% respectively.

- The butyl rubber-silica composites attained CTE = 102 ppm/^{o}C, TC = 0.40 $Wm^{-1}K^{-1}$ and water absorption = 0.078 vol% for a optimum silica loading of 0.26 v_f. The butyl rubber-BZT composite have CTE = 112 ppm/^{o}C, TC = 0.30 $Wm^{-1}K^{-1}$ and water absorption= 0.047 vol% for an optimum BZT loading of 0.26 v_f.
- Various theoretical models were used to fit the experimental values of relative permittivity and thermal conductivity of all the composites.
- The stress-strain curves of all composite shows the mechanical flexibility of the composites. The butyl rubber-nano alumina composite shows better mechanical properties than that of micron composite due to the more homogenous dispersion of nano particles in the rubber matrix.
- The measured properties suggest that butyl rubber-micron Al_2O_3, butyl rubber-SiO_2 and butyl rubber-$Ba(Zn_{1/3}Ta_{2/3})O_3$ composites are suitable candidates for microwave substrate and electronic packaging applications.

3.6 References

1. C. D. Dimitrakopolous and P. R. L. Malenfant, *Adv. Mater.,* **14,** 99 (2002).
2. R. Morent, N. De Geyter, F. Axisa, N. De Smet, L. Gengembre, E. De Leersnyder, C. Leys, J. Vanfleteren, M. R. Machal, E. Schacht and E. Payen, *J. Phys. D: Appl. Phys.,* **40,** 7392 (2007).
3. J. A. Rogers and Y. G. Huang, *Proceedings of national academy of sciences.,* **106,** 10875 (2009).
4. J. D. Bolt, D. P Button and B. A. Yost, *Mater. Sci. Eng. A*, **109**, 207 (1989).
5. I. J. Youngs, G. C. Stevens and A. S. Vaughan, *J. Phys. D: Appl. Phys.,* **39**, 1267 (2006).
6. M. T. Sebastian and H. Jantunen, *Int. J. Appl. Ceram. Technol.,* **7,** 415 (2010).
7. H. Ohsato, T. Tsunooka, T. Sugiyama, K. Kakimoto and H. Ogawa, *J. Electroceram.,* **17,** 445 (2006).
8. M. T. Sebastian, Dielectric materials for wireless communication, Elsevier Publishers, Oxford, UK (2008).
9. K. P. Surendran, N. Santha, P. Mohanan and M. T. Sebastian, *Eur. Phys. J. B,* **41,** 301 (2004).
10. J. A. Bur, *Polymer,* **26,** 963 (1985).
11. S. Rimdusit and H. Ishida, *Polymer,* **41,** 7941 (2000).
12. D. P. Button, B. A. Yost, R. H. French, W. Y. Hsu, J. D. Belt, M. A. Subrahmanian, H.-M. Zhang, R. E. Geidd, A. J. Whittacker and D. G. Onn, Ceramic substrates and packages for electronic applications, Advances in Ceramics, American Ceramic Society, Westerville OH, **26,** 353 (1989).

13. N. Mohamad, A. Muchtar, M. J. Ghazali, D. H. J. Mohd and C. H. Azhari, *J. Appl. Polym. Sci.,* **115,** 183 (2010).
14. S. Rajesh, V. S. Nisa, K. P. Murali and R. Ratheesh, *J. Alloys Compd.*, **477,** 677 (2009).
15. J. Xu and C. P Wong, *Compos. Part A-Appl. Sci.,* **38**, 13 (2007).
16. H. He, R. Fu, Y. Shen, Y. Han and X. Song, *Comp. Sci. Tech.,* **67,** 2493 (2007).
17. P. Gonon and A. Sylvestre, *J. Mater. Sci. Mater. Electron.,* 12**,** 81 (2001).
18. M. G. Todd and F. G. Shi, *J. Appl. Phys.*, **94,** 4551 (2003).
19. L. Ramajo, M. S. Castro and M. M. Reboredo, *Composites Part A*, **38,** 1852 (2007)
20. H. Barron, Modern synthetic rubbers, Chapman & Hall Ltd, London (1949).
21. N. Mc N. Alford and S. J. Penn, *J. Appl. Phys.,* **80,** 5895 (1996).
22. N. Mohamad, A. Muchtar, M. J. Ghazali, H. M. Dahlan and C. H. Azhari, *Solid. State. Sci. and Technol.,* **17,** 133 (2009).
23. N. Mohamad, A. Muchtar, M. J. Ghazali, D. H. Mohd and C. H. Azhari, *Eur. J. Sci. Res.,* **24,** 538 (2008).
24. A. Nigrawal and N. Chand, *Prog. Nanotechnol. and Nanomater.,* **2,** 25 (2013).
25. K. P. Murali, S. Rajesh, O. Prakash, A. R. Kulkarni and R. Ratheesh, *Mater. Chem. Phys.,* **113,** 290 (2009).
26. L. K. Namitha, J. Chameswary, S. Ananthakumar and M. T. Sebastian, *Mater. Res. Bull.,* **48,** 4911 (2013).
27. W. Zhou, S. Qi, C. Tu, H. Zhao, C. Wang and J. Kou, *J. Appl. Polym. Sci.,* **104,** 1312 (2007).
28. W. Zhou, D. Yu, C. Wang, Q. An and S. Qi, *Polym. Eng. Sci.*, **48,** 1381 (2008).

29. Z. Li, M. C. Johnson, M. Sun, E. T. Ryan, D. J. Earl, W. Maichen, J. I. Martin, S. Li, C. M. Lew, J. Wang, M. W. Deem, M. E. Davis and Y. Yan, *Angew. Chem.*, **118,** 6477 (2006).
30. K. P. Murali, S. Rajesh, O. Prakash, A. R. Kulkarni and R. Ratheesh, *Composites Part A*, **40,** 1179 (2009).
31. M. G. Todd and F. G. Shi, *Microelectron. J.*, **33,** 627 (2002).
32. H. Couderc, I. Preda, M. Fréchette, S. Savoie, M. Reading, A. S. Vaughan and J. Castellon, Annual Report Conference on Electrical Insulation and Dielectric Phenomena (CEIDP) 511 (2012)
33. Y. C. Chen, H. C. Lin and Y. D. Lee, *J. Polym. Res.*, **10,** 247 (2003).
34. F. F. Hanna, A. A. Yehiab and A. F. Abou-Bakr, *Br. Polym. J.*, **5,** 83 (1973).
35. S. Kawashima, M. Nishida, I. Ueda and H. Ouchi, *J. Am. Ceram. Soc.*, **66,** 421 (1983).
36. K. M. Manu, S. Soni, V. R. K. Murthy and M. T. Sebastian, *J. Mater. Sci. Mater. Electron.*, **24,** 2098 (2013).
37. K. J. Nijesh, J. K. Stanly, K. P. Murali and R. Ratheesh, *Mater. Chem. Phys.*, **122,** 507 (2010).
38. L. K. Namitha, J. Chameswary, S. Ananthakumar and M. T. Sebastian, *Ceram. Int.*, **39,** 7077 (2013).
39. T. Hu, J. Juuti, H. Jantunen and T. Vilkman, *J. Eur. Ceram. Soc.*, **27,** 3997 (2007).
40. N. G. Devaraju, E. S. Kim and B. I. Lee, *Microelectron. Eng.*, **82,** 71 (2005).
41. V. S. Nisa, S. Rajesh, K. P. Murali, V. Priyadarsini, S. N. Potty and R. Ratheesh, *Compos. Sci. Technol.*, **68,** 106 (2008).

42. K. P. Murali, S. Rajesh, K. J. Nijesh and R. Ratheesh, *Int. J. Appl. Ceram. Technol.*, **7,** 475 (2010).

43. F. Claro and R. Rojas, *Phys. Rev. B,* **43,** 6369 (1991).

44. A. V. Goncharenko, V. Z. Lozovski and E. F. Venger, *Opt. Commun.,* **174,** 19 (2000).

45. N. Jayasundere and B. V. Smith, *J. Appl. Phys.*, **73,** 2462 (1993).

46. S. H. Xie, B. K. Zhu, X. Z. Wei, Z. K. Xu and Y. Y. Xu, *Composites Part A,* **36,** 1152 (2005).

47. M. A. Berger and R. L. Mc Cullough, *Compos. Sci. Technol.,* **22,** 81 (1985).

48. I. H. Tavman, *Int. Commun. Heat. Mass.*, **25,** 723 (1998).

49. S. Kemaloglu, G. Ozkoc and A. Aytac, *Thermochim. Acta.*, **499,** 40 (2010).

50. W. Zhou, S. Qi, H. Li and S. Shao, *Thermochim. Acta*., **452,** 36 (2007).

51. R. C. Progelhof, J. L. Throne and R. R. Ruetsch, *Polym. Eng. Sci.,* **16,** 615 (1976).

52. D. W. Richerson, Modern ceramic engineering: properties processing and use in design, Taylor and Francis, CRC Press, London (2006).

53. G. T. N. Tsao, *Ind. Eng. Chem.,* **53,** 395 (1961).

54. T. L. Li and S. L. C. Hsu, *J. Phys. Chem. B,* **114,** 6825 (2010).

55. C. Y. Chee, N. L. Song, L. C. Abdullah, T. S. Y. Choong, A. Ibrahim and T. R. Chantara, *J. Nanomater.,* **2012,** 1-6 (2012).

56. S. M. David, M. Blaszkiewicz and R. E. Newnham, *J. Am. Ceram. Soc.*, **73,** 2187 (1990).

57. C. J. Tsenoglou, S. Pavlidou and C. D. Papaspyrides, *Compos. Sci. Technol.,* **66,** 2855 (2006).

58. T. S. Laverghetta, Microwave materials and fabrication techniques, Artech House, Dedham MA (1985).

59. F. Xiang, H. Wang and X. Yao, *J. Eur. Ceram. Soc.*, **26,** 1999 (2006).

60. Y. Rao, J. Qu, T. Marinis and C. P. Wong, *IEEE Trans. Compon. Packag. Technol.*, **23,** 680 (2000).

61. Y. M. Poon and F. G. Shin, *J. Mater. Sci.*, **39,** 1277 (2004).

62. A. A. M. Ward, B. Stoll, W. V. Soden, S. Herminghaus and A. A. Mansour, *Macromol. Mater. Eng.*, **278,** 971 (2003).

63. L. L. Hench and J. K. West, Principles of electronic ceramics, Wiley, New York (1990).

64. Y. Beneviste and T. Miloh, Int. J. Eng. Sci., **24,** 1537 (1986).

65. R. K. Goyal, A. N. Tiwari, U. P. Mulik and Y. S. Negi, *Comp. Sci. Tech.*, **67,** 1802, (2007).

66. Z. Todorova, N. Dishovsky, R. Dimitrov, F. E. Tantawy, A. N. Aal, A. A. Hajry and M. Bououdina, *Polym. Compos.*, **29,** 109 (2008).

67. S. Salaeh, N. Muensit, P. Bomlai and C. Nakason, *J. Mater. Sci.*, **46,** 1723 (2011).

68. N. Rattanasoma, T. Saowaparkc and C. Deeprasertkul, *Polym. Test.*, **26,** 369 (2007).

69. K. Boonkerd, S. Chuayjuljit, D. Abdulraman and W. Jaranrangsup, *Rubber. Chem. Technol*., **85,** 1 (2012).

70. I. Mora-Barrantes, A. Rodrguez, L. Ibarra, L. Gonzalez and J. L. Valentın, *J. Mater. Chem.*, **21,** 7381 (2011).

71. J. Xu and C. P. Wong, *Composites Part A,* **38,** 13 (2007).

Chapter 4

Butyl Rubber-High Permittivity Ceramic (TiO_2, $Sr_2Ce_2Ti_5O_{15}$ and $SrTiO_3$) Composites

This chapter describes synthesis of high permittivity ceramic filled butyl rubber composites and dielectric, thermal and mechanical properties of all the composites were studied with filler loading. TiO_2, $Sr_2Ce_2Ti_5O_{15}$ and $SrTiO_3$ are the high permittivity ceramics used for the present investigation. The effect of filler particles size on these properties was investigated in butyl rubber-TiO_2 composites. The experimental relative permittivity and thermal conductivity of all composites were compared with theoretical models.

4.1 Introduction

Flexible electronic systems offer wide range of applications such as substrate, gate insulator of flexible organic thin film transistor or as a flexible waveguide [1-3]. Compared to flexible electronics built on non-stretchable materials, stretchable materials offer a wide range of advantages such as ability to reduce package size and weight, cost effective installation and dissipation of heat at a higher rate [4]. Moreover, these materials can cover curved surfaces and movable parts [5]. A flexible dielectric waveguide consists of a flexible core and a flexible cladding. The core should be a flexible low loss material with high relative permittivity and the cladding is also flexible low loss material but relative permittivity should be smaller than that of core [6]. Then only the fields of the guided mode would decrease rapidly with distance in the cladding. The requirements for a material to be used as a core of flexible dielectric waveguide are mechanical flexibility, high relative permittivity, low loss tangent, low coefficient of thermal expansion (CTE), high thermal conductivity etc. The continuous evolution of smaller, lighter and faster electronics necessitated the demand for new materials which can satisfy the requirements of present electronics. Recently elastomer-ceramic composites have been found to be most promising candidates for flexible electronic applications. These composite combines the stretchability and light weight of elastomer with good dielectric and thermal properties of ceramics. The permittivity of the polymer can be tailored to a greater extent by using high permittivity low loss fillers. A key advantage of composite is its ability to prepare a significant range of relative permittivity by controlling the ceramic mixture suitable for various applications. The research on the development of low loss millimeter wave guiding structures has attained much attention in recent years. Previous reports reveal that polymer based dielectric

waveguide was developed for flexible electronic applications. A flexible millimeter waveguide made from PTFE core and a foamed PTFE cladding is commercially available from W. L. Gore, Inc [7]. Shindo and Ohtomo developed another flexible guide with a polyethylene core, polyfoam cladding and a polyethylene jacket [8]. But these materials are bulky and have bending losses since the core and cladding has similar relative permittivity [9]. Recently Wang et al. developed Polyolefin elastomer-$SrTiO_3$ composite as the core of flexible dielectric wave guide but its thermal properties are not studied [3]. In order to develop low loss high relative permittivity flexible composites the ceramic used should have permittivity much higher than that of butyl rubber matrix. Ceramics such as TiO_2, $Sr_2Ce_2Ti_5O_{15}$ and $SrTiO_3$ having high permittivity are chosen for the present study.

The rutile form of TiO_2 is selected for the present study due to its excellent dielectric and thermal properties. The titanium dioxide crystallizes in three forms: rutile, brookite and anatase. Rutile is the stable form of titanium dioxide. TiO_2 has become the subject of many studies due to their remarkable optic and electronic properties. It is widely used in environmental applications such as self cleaning, antibacterial agent and waste water purification [10, 11]. The microwave dielectric properties of rutile was first reported by Cohen and has ε_r = 100, Q = 10,000 at 3.45 GHz and τ_f = +400 ppm/^oC [12]. Rutile is used to improve the dielectric and thermal properties of polymers [13-16]. Kashani et al. arranged titanium dioxide filler particles into a chain structure in a silicone rubber matrix by dielectrophoretic effect using an alternative electric field and the composite achieved an increased relative permittivity and reduced loss tangent in the orientation direction of filler particles [17]. The mechanical, thermophysical and diffusion properties of TiO_2 filled chlorobutyl rubber composites were studied by Saritha et al. [18].

$SrTiO_3$ (ST) is a well known ceramic which crystallizes in the ABO_3 cubic perovskite structure at room temperature and transforms into the tetragonal structure at temperatures less than 105 K. It has very large value of ε_r (=290) and low value (~ 10^{-3}) of tan δ [19]. The dielectric and mechanical properties of $SrTiO_3$ based PTFE and PEEK composites were investigated by Ratheesh et al. [20, 21] and found that these composites are suitable for microwave substrate applications. Eventhough $SrTiO_3$ filled polymer and elastomer composites are studied, the microwave dielectric properties of butyl rubber-$SrTiO_3$ composites are investigated for the first time.

$Sr_{2+n}Ce_2Ti_{5+n}O_{15+3n}$ (n=0-10) based ceramics and their composites have been studied extensively due to their high relative permittivity and relatively low loss tangent [22-26]. Among the $Sr_{2+n}Ce_2Ti_{5+n}O_{15+3n}$ series, $Sr_2Ce_2Ti_5O_{15}$ (SCT) is chosen for the present study. SCT ceramic has a high relative permittivity of 112, low loss of 10^{-4} at 7 GHz and a low CTE of 1.72 ppm/^oC [22, 23].

The present chapter deals with the detailed investigation of butyl rubber-high permittivity ceramic filler composites for the first time to understand their dielectric, thermal and mechanical performance for flexible electronic applications.

4.2 Butyl rubber-TiO_2 composites

The micron rutile is prepared as described in section 2.1.2.4 and nano rutile powder is procured from Sigma Aldrich. The nano rutile was heated at 100^oC for 24 hours before use. Butyl rubber-micron rutile (BR/RT) and butyl rubber-nano rutile (BR/nRT) composites were prepared in order to study the effect of filler particle size on dielectric, thermal and mechanical properties of butyl rubber composites. These composites were prepared by sigma

mixing as described in section 2.1.4.1. The sample designation and corresponding ceramic volume fraction are given in Table 4.1. The BR/RT composites were prepared with a volume fraction of micron rutile loading from 0-0.40 v_f. A maximum loading of 0.30 v_f of nano rutile is only possible in the case of BR/nRT composites due to the difficulty in processing at higher filler loadings [27]. The microstructure, dielectric, thermal and mechanical properties of both composites were characterized using techniques explained in section 2.2.

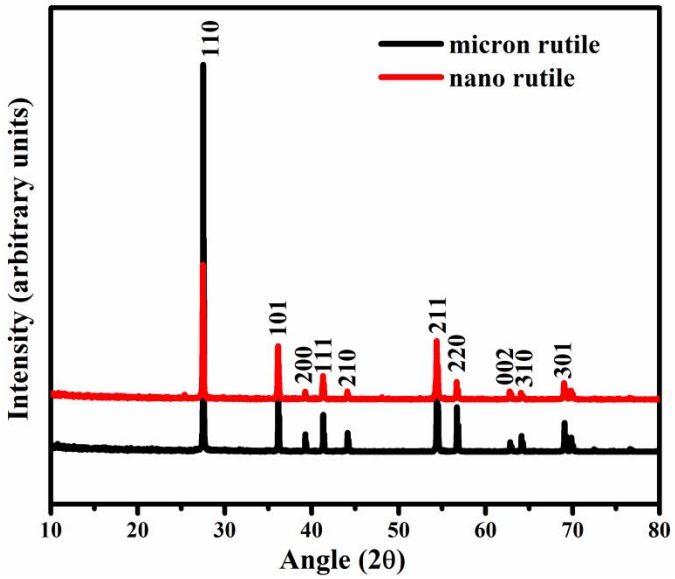

Fig. 4.1 XRD patterns of micron and nano rutile

Figure 4.1 shows the powder XRD pattern of micron and nano rutile. All the peaks are indexed based on JCPDS file no. 89-6975. The phase purity of both ceramics was obvious from Fig. 4.1.

The morphology of filler particles and composites are shown in Fig. 4.2. The micron rutile ceramic consists of flake like particles with an average size of 2 μm as shown in Fig. 4.2 (a). The nano rutile consists of agglomerated and irregularly shaped nano particles of average size 100 nm and is depicted in Fig. 4.2 (b). Figures 4.2 (c) and (d) show the fractured SEM images of BR/RT-5 and BR/NRT-5 respectively. A homogenous dispersion of filler particles in the matrix can be seen from both the figures eventhough some pores are present due to the agglomeration of filler particles at higher filler loading.

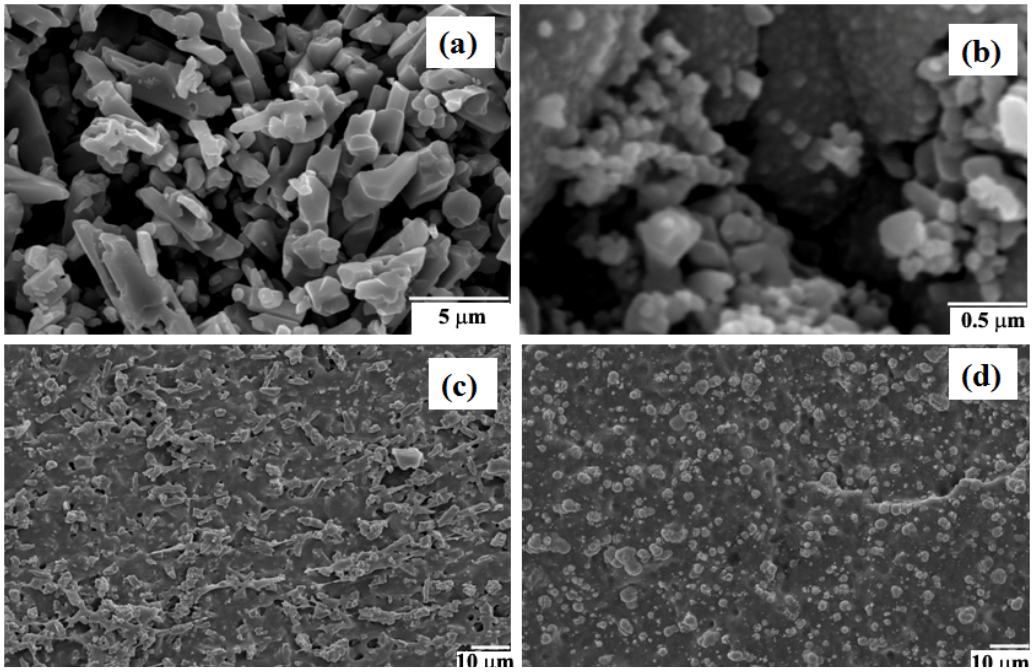

Fig. 4.2 SEM images of (a) micron rutile powder (b) nano rutile powder (c) fractured surface of BR+0.30 v_f of micron rutile and (d) BR+0.30 v_f of nano rutile composites

Table 4.1 Dielectric properties at 1 MHz and water absorption of BR/RT and BR/nRT composites

Composite material	Sample designation	Filler in phr[#] ()[$]	ε_r (1 MHz)	tan δ (1 MHz)	Water absorption (Vol%)
Butyl rubber-micron rutile composites	BR-0	0 (0.00)	2.44	0.0003	0.039
	BR/RT-1	10(0.021)	2.69	0.0015	0.048
	BR/RT -2	25 (0.052)	3.09	0.0017	0.049
	BR/RT -3	50 (0.090)	3.54	0.0023	0.052
	BR/RT -4	100 (0.180)	4.81	0.0051	0.059
	BR/RT -5	200 (0.300)	7.52	0.0060	0.065
	BR/RT -6	300 (0.400)	8.61	0.0066	0.078
Butyl rubber-nano rutile composites	BR/NRT-1	10(0.021)	2.63	0.0016	0.054
	BR/NRT -2	25 (0.052)	2.76	0.0039	0.062
	BR/NRT -3	50 (0.090)	3.14	0.0044	0.070
	BR/NRT -4	100 (0.180)	4.18	0.0059	0.079
	BR/NRT -5	200 (0.300)	6.23	0.0090	0.110

[#] parts per hundred rubber.

[$]The corresponding ceramic volume fraction is given in parenthesis.

Table 4.1 gives dielectric properties at 1 MHz and water absorption properties of both BR/RT and BR/nRT composites. The dielectric properties of both BR/RT and BR/nRT composites increase with filler loading. As the filler loading increases the connectivity

among the filler particles increases and hence the increase in ε_r. The relaxation of Maxwell-Wagner polarization is responsible for the increase in tan δ of heterogeneous systems at low frequencies. The presence of moisture content will affect the electrical properties of composites since water is a polar molecule. From the Table 4.1 it is evident that the volume % of moisture content of both composites increases with filler loading. The nano rutile particles absorb more moisture content due to its large surface area. Hence BR/nRT composites have more moisture content than that of BR/RT composites.

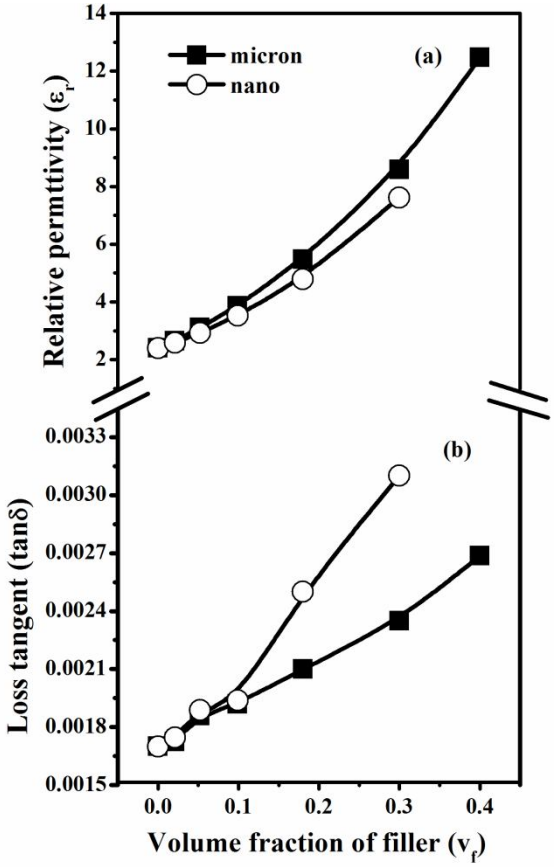

Fig. 4.3 Variation of (a) relative permittivity and (b) loss tangent of BR/RT and BR/nRT composites with filler content at 5 GHz

Figure 4.3 (a) and (b) shows the variation of relative permittivity and loss tangent of butyl rubber-micron rutile and butyl rubber-nano rutile composites as a function of filler loading at 5 GHz. The relative permittivity of both the composites increases with filler content which is expected since the relative permittivity of rutile is higher than that of butyl rubber matrix. It is worth to be note that the relative permittivity of micron rutile filled composite shows higher relative permittivity than that of nano composites. Generally the relative permittivity of nano composite is higher than that of micron composite. This unusual behavior may be due to the difference in morphology of micron rutile and nano rutile. Further detailed studies are needed to understand this unusual behavior of butyl rubber-rutile composites. It is also clear from the Fig. 4.3 that the loss tangent of both the composites increases with filler loading. The dipole relaxation of water molecules present in the composites contributed to the increase in loss tangent with filler content. It is also noted that the loss tangent of BR/nRT composite is higher than that of BR/RT composites. The increased lattice strain due to high surface area of nano rutile particles and higher moisture content [15,28] in the butyl rubber-nano rutile composites may be the cause of higher loss tangent of BR/nRT composites.

The prediction of effective relative permittivity of polymer-ceramic composites is very important for the engineering applications. The experimental relative permittivity of both BR/RT and BR/nRT composites was compared with those values calculated using equations (2.6) to (2.9) and is shown in Fig. 4.4. The measured relative permittivity of both butyl rubber-micron rutile and butyl rubber-nano rutile composites shows deviation from Maxwell–Garnett equation and Jayasundere-Smith equation. Maxwell-Garnett equation is valid only at very low filler loading and shows deviation at higher ceramic content [29]. The

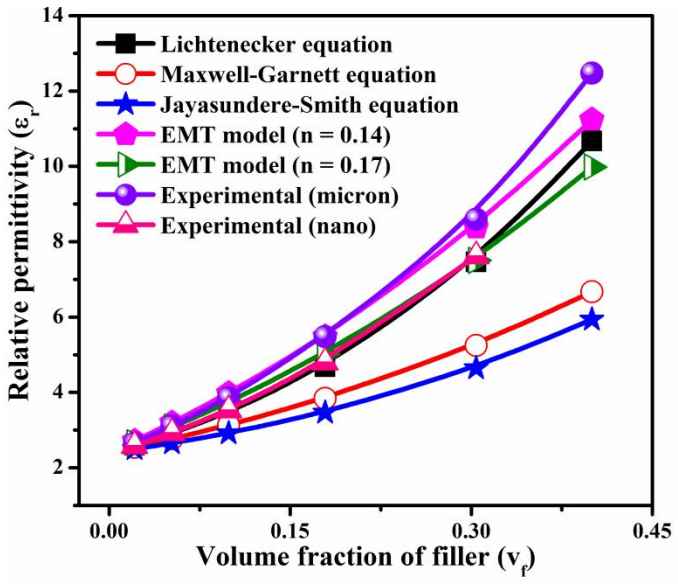

Fig. 4.4 Comparison of theoretical and experimental relative permittivity of BR/RT and BR/nRT composites at 5 GHz

Jayasundere-Smith equation also shows considerable deviation from experimental data. The filler particles are assumed to be spherical with an equal radius in Jayasundere–Smith model [30]. Since the micron rutile particles have flake like morphology (Fig. 4.2 (a)), it shows deviation from experimental ε_r. The nano particles show agglomeration tendency and are not identical spheres (Fig. 4.2 (b)), hence the measured relative permittivity of BR/nRT composite also shows deviation. The Lichtenecker equation holds well for butyl rubber-nano rutile composites. Ratheesh et al. used Lichtenecker equation and EMT model for PTFE-rutile nano composites [15]. This model is matching with BR/RT composites upto a micron rutile loading of 0.30 v_f and shows deviation at higher ceramic loading. This may be due to the agglomeration of filler particles at higher loading. The EMT model is suitable for predicting the effective relative permittivity of present composites since it involves a morphology factor 'n' [31]. The value of n for the BR/nRT composite is 0.17 and is almost matching with the n value reported for PTFE-rutile nano composites [15]. The n value for

BR/RT composite is 0.14 since the morphology of micron rutile powder is different from nano rutile powder. The morphology factor represents only the morphology of ceramic material. Hence the two different n values. This model also shows deviation at higher micron rutile loading and this may be due to the imperfect dispersion of filler particles at high loading.

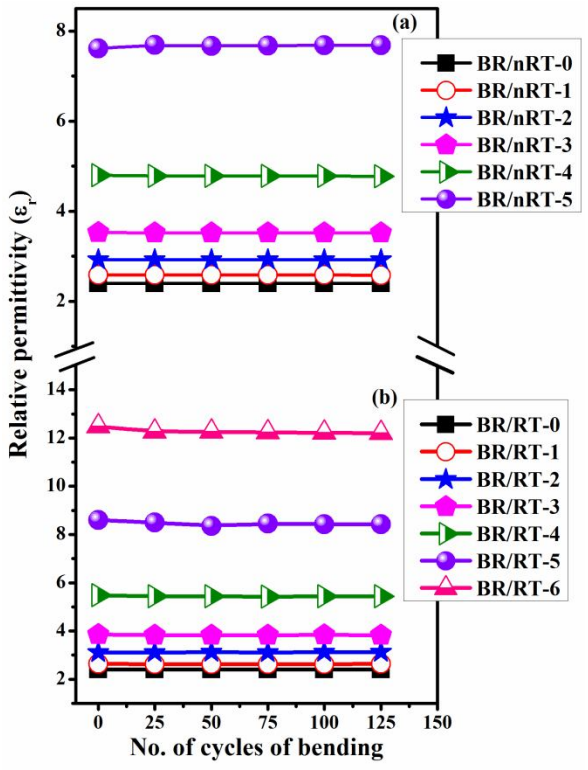

Fig. 4.5 Variation of relative permittivity of (a) BR/nRT and (b) BR/RT composites with bending

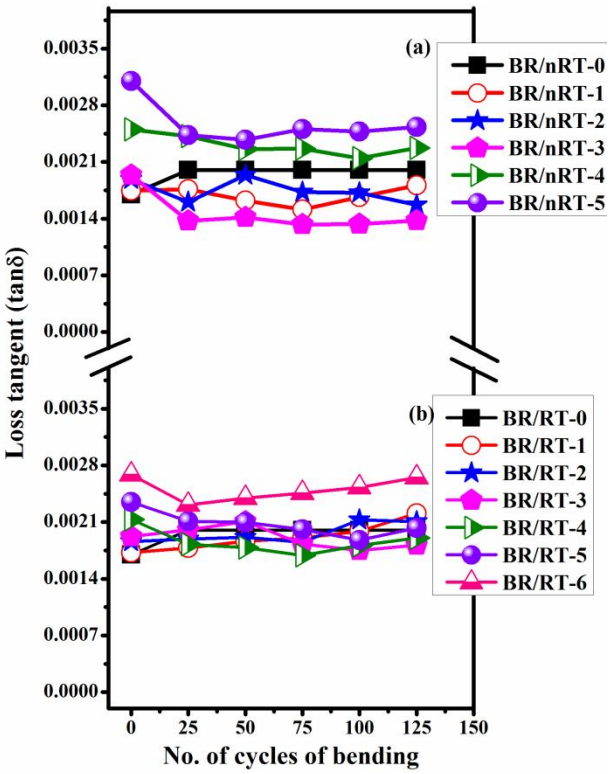

Fig. 4.6 Variation of loss tangent of (a) BR/nRT and (b) BR/RT composites with bending

Figures 4.5 & 4.6 show the effect of repeated bending on the microwave dielectric properties of butyl rubber-micron rutile and butyl rubber-nano rutile composites respectively. From the Fig. 4.5 (a) and (b), it is clear that the relative permittivity of both BR/nRT and BR/RT composites is independent of bending. The loss tangent of both composites shows only small variation with repeated bending as shown in Fig. 4.6 (a) and (b).

Figure 4.7 (a) and (b) shows the temperature variation of relative permittivity at 1 MHz of butyl rubber-nano rutile and butyl rubber-micron rutile composites respectively. It is worth to be noted that all the compositions of both composites were found to be almost thermally stable within the measured temperature range. It is found that the relative permittivity of the composites decrease with temperature and this may be due to the decrease in polarizability of dipoles with temperature and also due to the difference in CTE of rubber and filler [32].

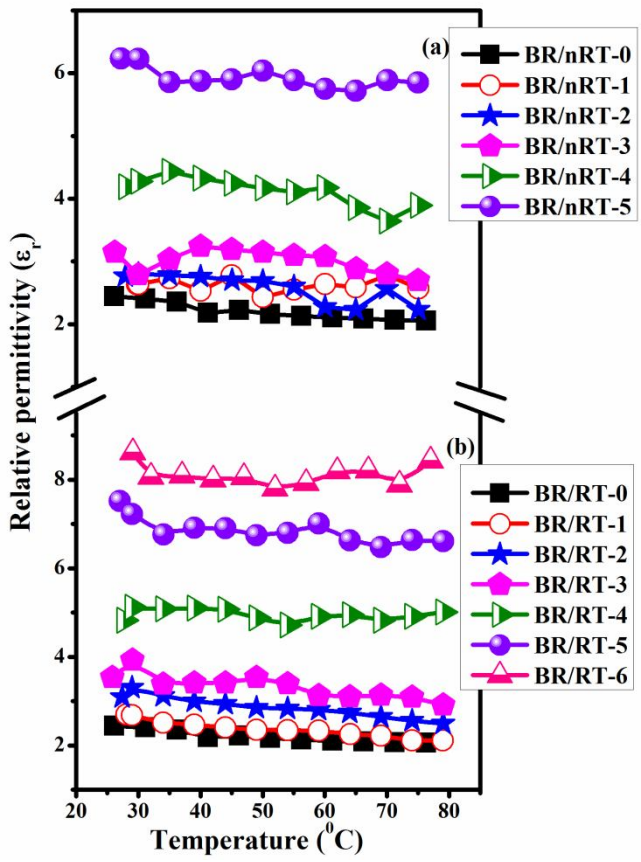

Fig. 4.7 Temperature dependence of ε_r at 1 MHz (a) BR/nRT and (b) BR/RT composites

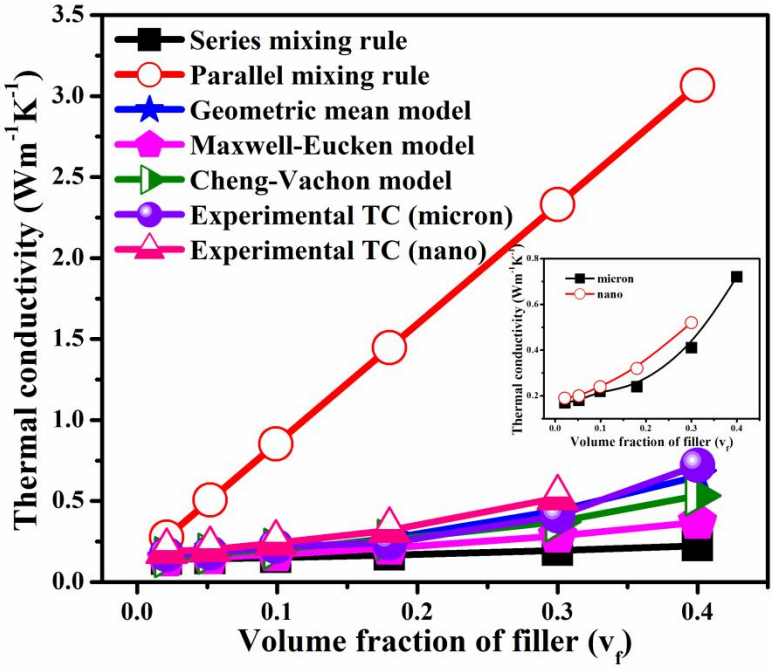

Fig. 4.8 shows the variation of thermal conductivity of BR/RT and BR/nRT composites with ceramic loading

The thermal properties of the composites are influenced by dispersion and orientation of the filler particles, the filler aspect ratio, the relative ratio of thermal conductivity of the filler and the matrix etc. Figure 4.8 shows the variation of thermal conductivity of butyl rubber-micron rutile and butyl rubber-nano rutile composites with ceramic loading. The thermal conductivity of both composites increases with filler loading since rutile has high thermal conductivity than that of butyl rubber matrix and also due to the formation of continuous thermally conductive chains as the filler-filler contact increases with ceramic loading [33]. The particle size also plays a major role in thermal properties of composites. From the inset plot in Fig. 4.8 it is evident that the TC of butyl rubber-nano rutile composites is higher than that of butyl rubber-micron rutile composites for the same filler content. The nano particles can achieve higher packing density of filler in matrix and thereby thermal conductivity increased for nano composites [34**]**. Meera et al. observed a higher TC

for 12–13 nm silica filled natural rubber composites than that of 190 nm TiO_2 filled natural rubber composites [35]. The comparison of experimental and predicted thermal conductivity of BR/RT and BR/nRT composites is also shown in Fig. 4.8. The experimental thermal conductivity was compared with those values calculated using equations (2.13) to (2.17). It is clear from figure that the experimental values of both the composites lies within the range of series and parallel model. The geometric mean model is in good agreement with experimental values of both the composites. The experimental values are found to be higher than that predicted by Maxwell-Eucken and Cheng-Vachon model. It is very difficult to predict the thermal conductivity of different materials due to the wide variations in filler geometry, orientation and dispersion. Hence the theoretical and experimental thermal conductivity values show deviation at higher filler contents.

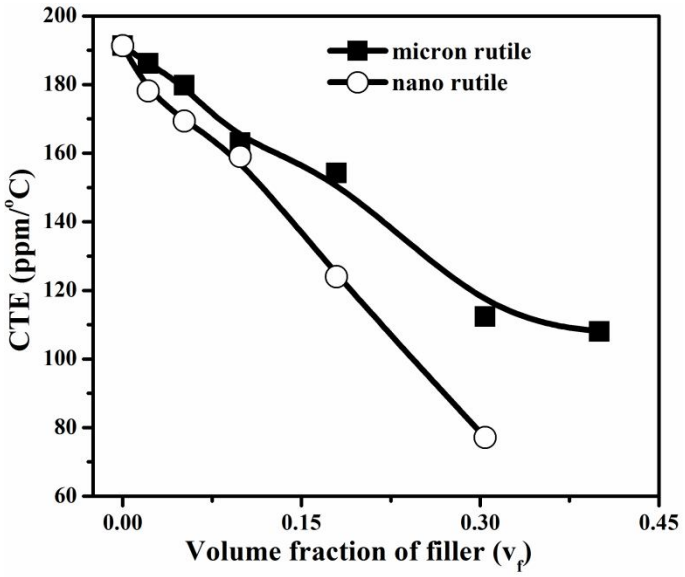

Fig. 4.9 Variation of coefficient of thermal expansion of BR/RT and BR/nRT composites withceramic loading

The variation of coefficient of thermal expansion of both BR/RT and BR/nRT composites with filler content is given in Fig. 4.9. The CTE of both composites were reduced

with ceramic addition as expected since the CTE of rutile (9.2 ppm/^{o}C) is less than that of rubber matrix (191 ppm/^{o}C). The free volume of polymer decreases as the ceramic loading increases and thereby thermal expansion of the composite is suppressed [36]. The lower coefficient of thermal expansion of BR/nRT composite compared to BR/RT composites is due to the presence of more physical crosslinking points and increased mechanical interaction between filler and matrix in the nano rutile filled butyl rubber composites [34].

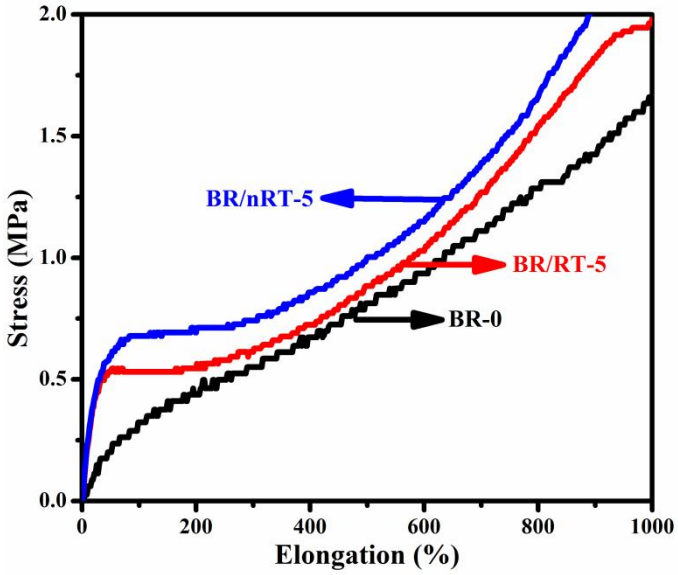

Fig. 4.10 Stress-strain curves of BR/RT and BR/nRT composites

Figure 4.10 shows the stress-strain curves of BR-0, BR/RT-5 and BR/nRT-5. From the figure it is clear that the stress needed for elongation increases with filler content. It is also evident that the stress needed for nano rutile filled butyl rubber composite is higher than that of micron rutile filled butyl rubber composites. Fu et al. reported that the particle size, particle-matrix interface adhesion and particle loading are the main factors which affect the mechanical properties of particulate filled polymer composites [37]. The more uniform dispersion of nano particles in the rubber matrix is responsible for the high stiffness of

BR/nRT-5 composite. Both the composites are not broken even upto an elongation of 1000%.

4.3 Butyl rubber-$Sr_2Ce_2Ti_5O_{15}$ and butyl rubber-$SrTiO_3$ composites

$Sr_2Ce_2Ti_5O_{15}$ and $SrTiO_3$ ceramics were prepared by conventional solid state route as described in section 2.1.2.5 and 2.1.2.6 respectively. BR/SCT and BR/ST composites were prepared as depicted in section 2.1.4.1. The sample designation and the corresponding ceramic volume fraction are given in Table 4.2. The composites were then hot pressed at 200^oC for 90 minutes under a pressure of 2 MPa. The phase purity of $Sr_2Ce_2Ti_5O_{15}$ and $SrTiO_3$ were confirmed by XRD analysis. The composites thus prepared were characterized for microstructure, dielectric, thermal and mechanical properties using techniques explained in section 2.2.

The phase purity of the ceramics $Sr_2Ce_2Ti_5O_{15}$ (SCT) and $SrTiO_3$ (ST) was analyzed by XRD and is shown in Fig. 4.11. The peaks were indexed based on the previous reports [23, 24] and JCPDS file 35-0734 for $Sr_2Ce_2Ti_5O_{15}$ and $SrTiO_3$ respectively and the phase purity of both ceramic powders were confirmed.

Figure 4.12 shows microstructure of $Sr_2Ce_2Ti_5O_{15,}$ $SrTiO_3$ ceramic and their composites with butyl rubber. The SEM images of $Sr_2Ce_2Ti_5O_{15}$ and $SrTiO_3$ ceramic powder was depicted in Fig. 4.12 (a) and (b) respectively. $Sr_2Ce_2Ti_5O_{15}$ particles are irregularly shaped with size less than about 10 μm and $SrTiO_3$ powder particles are upto 10 μm in size. Fig. 4.12 (c) and (d) shows the fractured surface of BR+ 0.43 v_f of SCT and (d) BR+0.42 v_f of ST respectively. It is clear from the figures that there is good adhesion between the filler and the matrix.

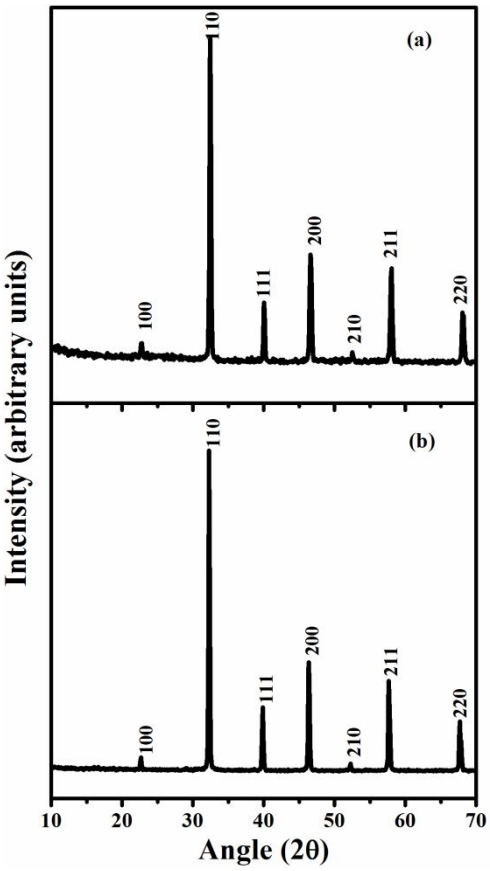

Fig. 4.11 XRD patterns of (a) $Sr_2Ce_2Ti_5O_{15}$ and (b) $SrTiO_3$

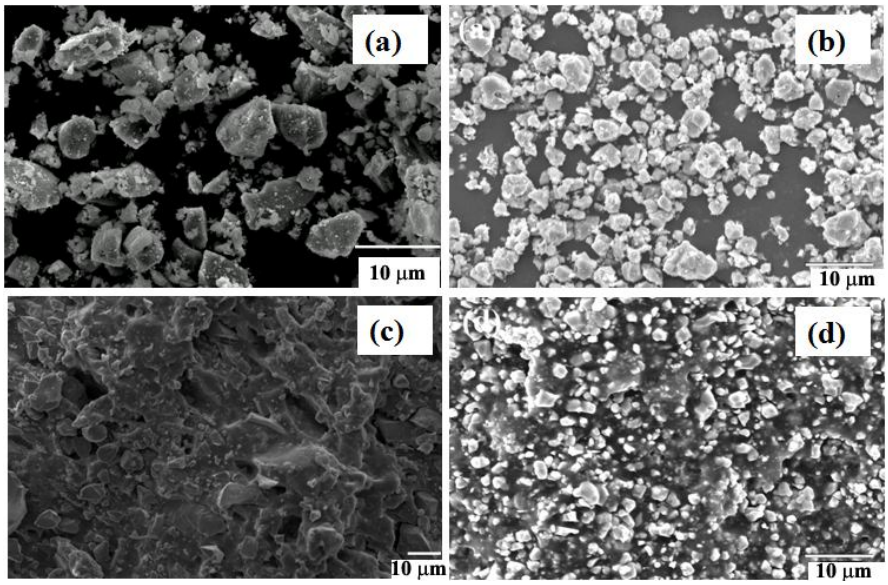

Fig. 4.12 SEM images of (a) $Sr_2Ce_2Ti_5O_{15}$and (b) $SrTiO_3$ (c) fractured surface of BR+ 0.43 v_f of SCT and (d) BR+0.42 v_f of ST composites

Table 4.2 gives the dielectric properties at 1 MHz and water absorption properties of BR/SCT and BR/ST composites. The dielectric properties of the composites is affected by a number of factors such as the porosity, size and shape of the filler particles, interface between the components and the effective dipole moment of the composites [38]. The value of ε_r increases with filler loading because ε_r of both fillers is relatively high. As the SCT loading increases from 0-0.43 v_f, the ε_r of BR/SCT composites increases from 2.44 to 8.76 and for BR/ST composites, the relative permittivity increases from 2.44 to 10.28 as the ST content increases from 0-0.42 v_f. At a lower concentration, the rubber matrix isolates filler particles from each other and their dielectric properties will not play a dominant role. But as the ceramic content increases, the particles will get into contact with each other leading to the formation of continuous networks. Consequently dipole-dipole interaction increases and results in increased values of ε_r [39]. Table 4.2 also shows the variation of the loss tangent of both composites with the filler content at 1 MHz. As the SCT loading increases from 0-0.43 v_f, the loss tangent of BR/SCT composites increases from 0.0003 to 0.0064 and as volume fraction of ST increases, tanδ increases from 0.0003 to 0.0060 at 1 MHz. In heterogeneous systems, the charge accumulation at the interfaces cause low frequency polarization called Maxwell-Wagner polarization. The relaxation of this interfacial polarization produces additional loss at low frequencies [40]. With the increase in filler volume fraction, the interfacial area is also increasing and hence the increase in loss. However, this interfacial effect is effective only at low frequencies. Moisture absorption is a major concern in polymer-ceramic composites when it comes to practical applications. It is evident from Table 4.2 that the volume % of moisture absorption increases gradually with the volume fraction of the filler for both the composites. However, the numerical values are very small ($\leq 0.081\%$).

Table 4.2 Dielectric properties at 1 MHz and water absorption of BR/SCT and BR/ST composites

Composite material	Sample designation	Filler in phr[#] ()[$]	ε_r (1 MHz)	tan δ (1 MHz)	Water absorption (Vol%)
Butyl rubber-$Sr_2Ce_2Ti_5O_{15}$ composites	BR-0	0 (0.00)	2.44	0.0003	0.039
	BR/SCT-1	10 (0.019)	2.51	0.0020	0.040
	BR/SCT-2	25 (0.045)	2.75	0.0050	0.042
	BR/SCT-3	50 (0.09)	3.10	0.0023	0.045
	BR/SCT-4	100 (0.16)	3.61	0.0025	0.050
	BR/SCT-5	200 (0.27)	5.38	0.0038	0.053
	BR/SCT-6	300(0.36)	7.45	0.0043	0.056
	BR/SCT-7	400(0.43)	8.76	0.0064	0.068
Butyl rubber-$SrTiO_3$ composites	BR/ST-1	10 (0.018)	2.45	0.0010	0.041
	BR/ST -2	25 (0.044)	2.50	0.0012	0.043
	BR/ST -3	50 (0.08)	3.22	0.0003	0.044
	BR/ST -4	100 (0.15)	3.82	0.0019	0.052
	BR/ST -5	200 (0.26)	6.25	0.0040	0.057
	BR/ST -6	300 (0.35)	8.26	0.0050	0.069
	BR/ST -7	400 (0.42)	10.28	0.0060	0.081

[#] parts per hundred rubber
[$] The corresponding ceramic volume fraction is given in parenthesis.

This may be due to the fact that the permeability of water through butyl rubber is low [41]. The good adhesion between matrix and filler may prevent the penetration of moisture through the interfaces also.

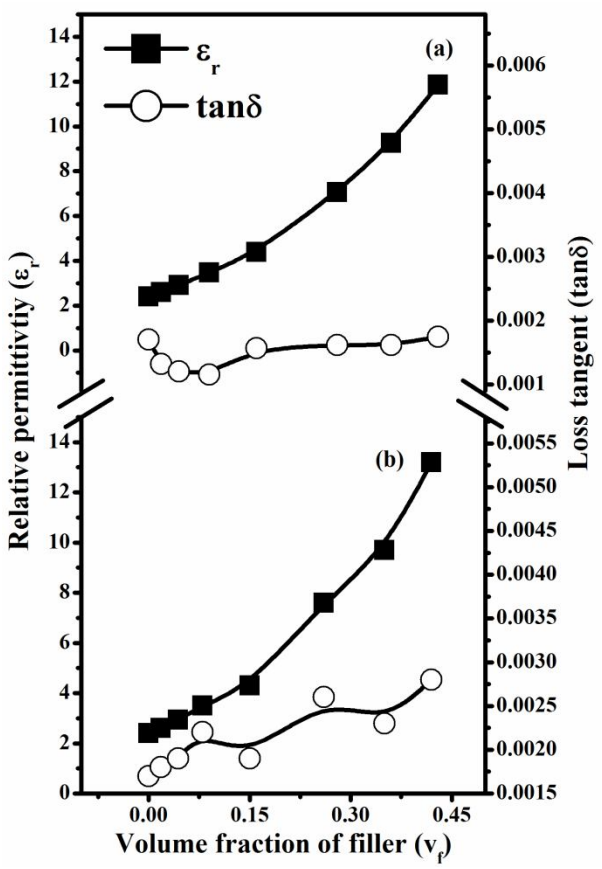

Fig. 4.13 Variation of relative permittivity and loss tangent of (a) BR/SCT and (b) BR/ST composites at 5 GHz

Figure 4.13 (a) and (b) shows the variation of microwave dielectric properties of butyl rubber-$Sr_2Ce_2Ti_5O_{15}$ and butyl rubber-$SrTiO_3$ composites as a function of ceramic loading respectively. It can be seen from the Fig. 4.13 that the relative permittivity of both composites increases with filler content. This may be due to the high relative permittivity of ceramic fillers, $Sr_2Ce_2Ti_5O_{15}$ (112) and $SrTiO_3$ (290) compared to rubber matrix (2.4) and also due to the increase in total polarizability of the composite material. It is also noted that the variation of loss tangent of both composites is small at 5 GHz. The loss tangent at microwave frequencies is due to the dipole relaxation of water molecules present in the composites which is evident from Table 4.2 [42]. The relative permittivity of both BR/SCT

and BR/ST composites at 5 GHz and at 1 MHz follows a same trend as that of BR/BZT composites. The relative permittivity increases from 2.40 to 11.00 and loss tangent varies from 0.0017 to 0.00175 with an increase of SCT loading form 0-0.43 v_f in butyl rubber. As the $SrTiO_3$ content increases from 0-0.42 v_f the ε_r and tan δ increases from 2.40 to 13.20 and 0.0017 to 0.0028 respectively for BR/ST composites at 5 GHz.

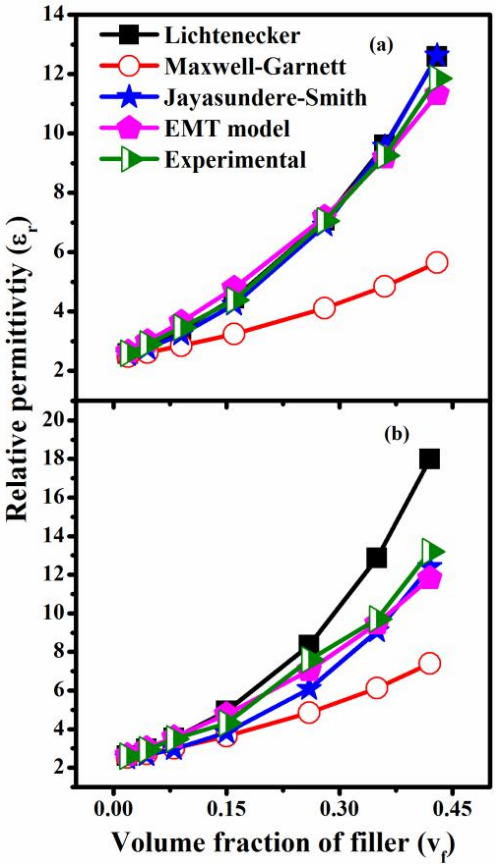

Fig. 4.14 Comparison of experimental and theoretical relative permittivity of (a) BR/SCT and (b) BR/ST composites at 5 GHz

Figure 4.14 (a) and (b)shows the comparison between experimental and theoretical relative permittivity of both BR/SCT and BR/ST composites respectively at 5 GHz. It is seen that for both the composites Maxwell-Garnett equation shows wide deviation from the experimental values. This may be due to the lack of consideration of correlations between the

dipolar excitations. Lichtenecker equation is in agreement with experimental relative permittivity of BR/SCT and BR/ST composites at low filler loading and shows deviation at higher loading. This prediction is valid for composites with near values of relative permittivities of filler and matrix and hence the deviation is more significant in the case of BR/ST composites. Since the ε_r of ST is higher than that of SCT, Lichtenecker equation shows much more deviation at higher loadings of ST in butyl rubber matrix. It is obvious from Fig. 4.14 that Jayasundere–Smith equation [30] is suitable for the prediction of ε_r of both composites. In the present study, it is clear from the SEM images (Fig. 4.12 (a) and (b)) that the filler particles are not identical spheres. Hence, the small deviation in the observed values of relative permittivity from the predicted values. The measured relative permittivity of both composites was also compared with EMT model proposed by Rao et al. [31]. The 'n' value for BR/SCT composite is 0.165 and that for BR/ST composite is 0.17. The n value of SCT is in agreement with PTFE-SCT composites reported by Subodh et al. [43]. It is observed that the EMT model holds good for both BR/SCT and BR/ST composites since it involves a shape factor.

The microwave dielectric properties of both composites after repeated bending by an angle of 180^o are shown in Fig. 4.15 and 4.16. Fig. 4.15 (a) indicates that the relative permittivity of BR/SCT composites is independent of bending. From the Fig. 4.15 (b) it is clear that composites up to 0.26 volume fraction of ST shows no remarkable variation in ε_r even after 125 cycles of bending. On the other hand, samples with higher filler loading show a small decrease in ε_r after 25 cycles and then the variation becomes marginal. It is also worth to note that the difference in the value of ε_r before and after 25 cycles of bending increases with the increase in the filler volume fraction. The loss tangent of SCT filled butyl

rubber composites shows marginal variation with bending which is clear from Fig. 4.16 (a). The variation of tan δ of BR/ST composites with repeated bending is shown in Fig. 4.16 (b) follows a similar trend as relative permittivity. In an undeformed sample, there would be a small amount of rubber trapped within the filler agglomerates losing its identity as elastomer. The cyclic deformations would release this trapped rubber making the matrix more homogeneous. Consequently the effective filler volume fraction would decrease [44]. The decrease in effective filler volume fraction and the homogenization of the matrix may be the reason for the initial decrease in ε_r and tan δ of BR/ST composites. At higher volume fractions of filler, since the possibility for particle agglomeration is high, this effect will be more distinguishable.

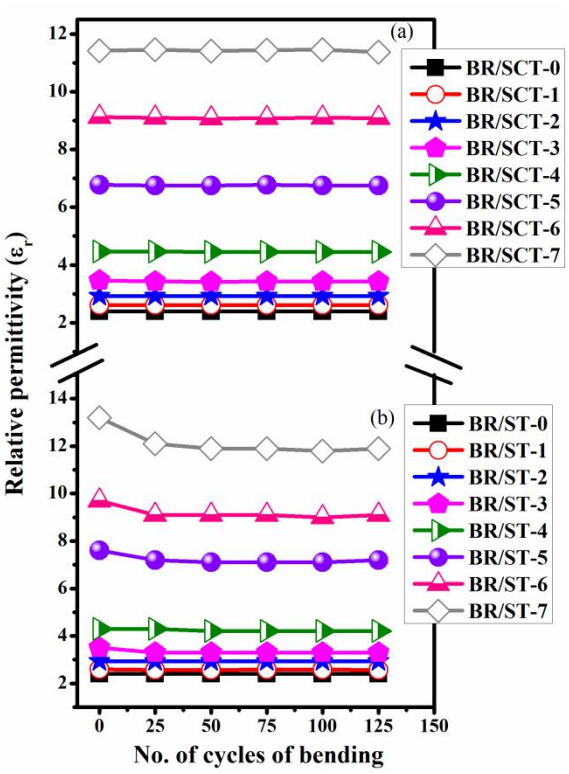

Fig.4.15 Variation of relative permittivity of (a) BR/SCT and (b) BR/ST composites with bending

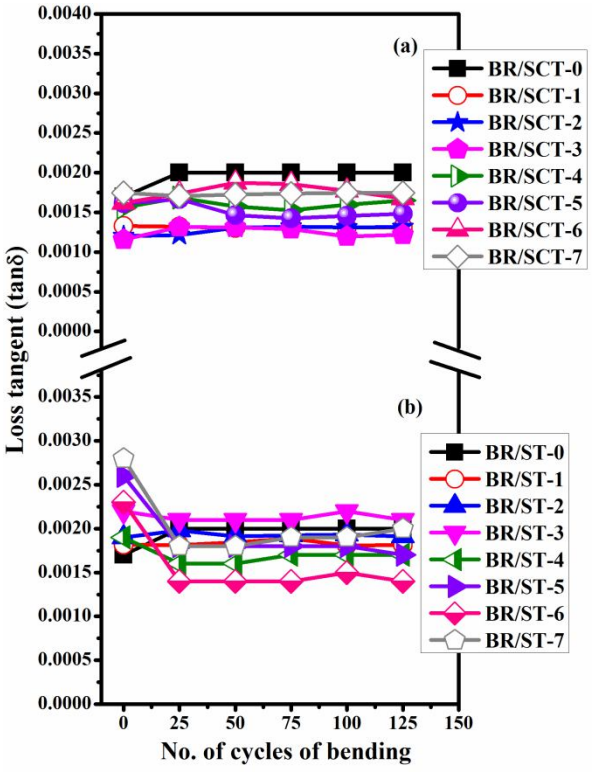

Fig.4.16 Variation of loss tangent of (a) BR/SCT and (b) BR/ST composites with bending

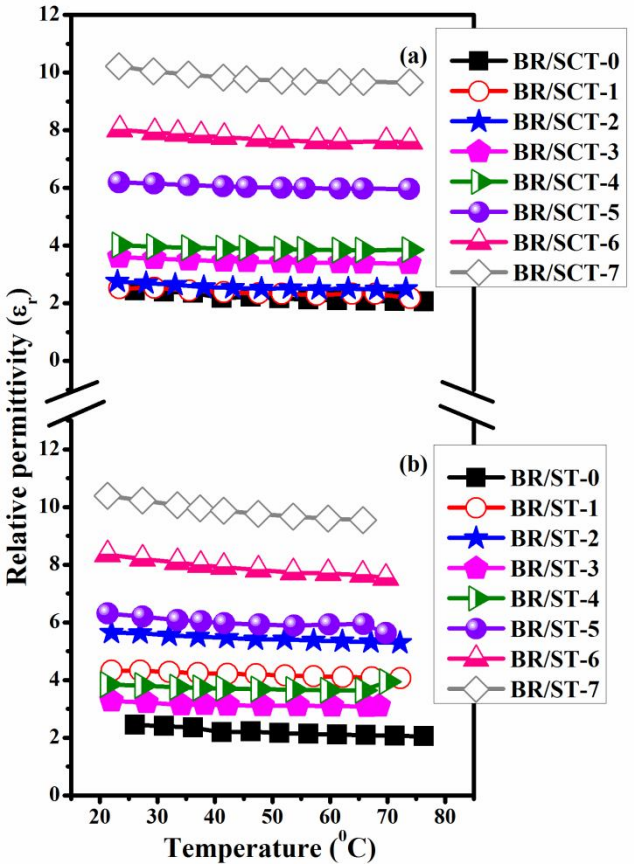

Fig. 4.17 Variation of relative permittivity of (a) BR/SCT and (b) BR/ST composites with temperature at 1 MHz

The temperature stability of dielectric properties is very important for microwave applications. The temperature dependence of ε_r at 1 MHz of both BR/SCT and BR/ST composite is depicted in Fig. 4.17. It can be observed that the relative permittivity of the composites with lower filler loading is almost constant throughout the measured temperature range. As the filler loading increases there is a decrease in relative permittivity with temperature. This may be due to the incipient ferroelectric nature of both SCT and ST ceramics. Incipient ferroelectrics are characterised by increasing permittivity on cooling due

to the softening of the lowest frequency polar optical phonon [24]. Subodh et al. have reported a similar behaviour in polyethylene- $Sr_9Ce_2Ti_{12}O_{36}$ composites [25].

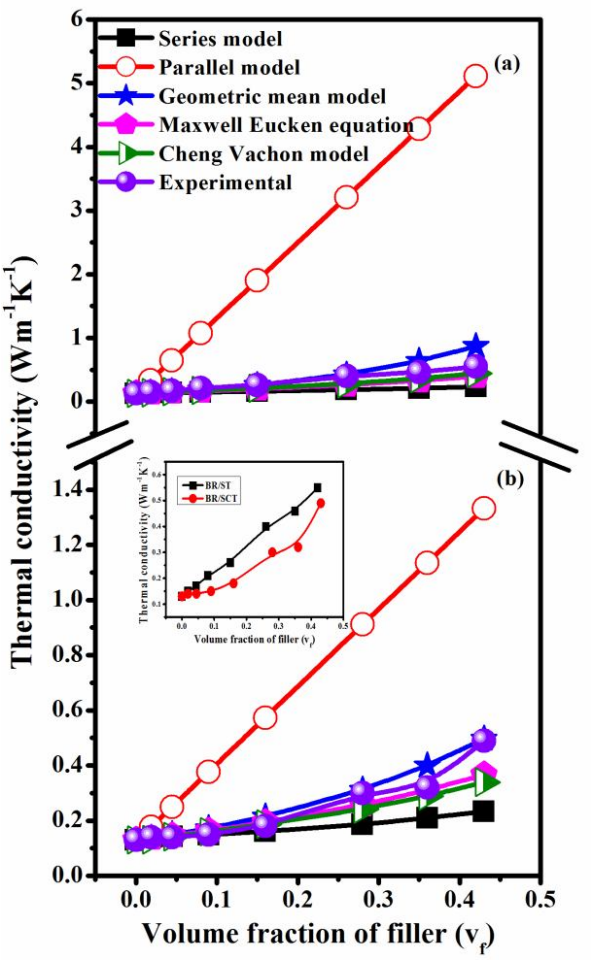

Fig. 4.18 Variation of thermal conductivity of (a) BR/SCT and (b) BR/ST composites with filler volume fraction

Ceramic fillers seem to improve the thermal conductivity of polymers as they act as conducting channels with lower thermal resistance than the matrix. Figure 4.18 (a) and (b) shows the variation of thermal conductivity of both BR/SCT and BR/ST composites with filler loading respectively and also shows comparison of TC values with those calculated from theoretical models. As the filler content increases, thermal conductivity of both

composites increases and $SrTiO_3$ filled butyl rubber composite shows much higher thermal conductivity than that of BR/SCT composites which is clear from inset graph. This may be due to the higher thermal conductivity of ST (12 $Wm^{-1}K^{-1}$) compared to SCT ceramic (2.93 $Wm^{-1}K^{-1}$). As the filler content increases, the filler particles will touch each other and thermally conductive networks were formed throughout the system and this leads to the rise in thermal conductivity of the composites [45]. As the SCT loading increases from 0-0.43 v_f the thermal conductivity of BR/SCT composites improved from 0.13 $Wm^{-1}K^{-1}$ to 0.49 $Wm^{-1}K^{-1}$ and that of BR/ST composites the thermal conductivity increases from 0.13 $Wm^{-1}K^{-1}$ to 0.55 $Wm^{-1}K^{-1}$ for the ST content increases from 0-0.42 v_f. Fig. 4.18 also compares the experimental thermal conductivity of both composites with theoretical models. From the figure it is clear that the experimental thermal conductivity of both composites are within the range of series and parallel models since these models give the lower and upper limits of thermal conductivity. The experimental thermal conductivity of both composites is in good agreement with all the predicted values of TC at low filler loading and shows deviations at higher filler content. As the volume fraction of ceramic increases, ceramic particles get agglomerated and thereby increasing the mismatch between the observed and theoretical values of thermal conductivity [46, 47].

The variation of CTE of both BR/SCT and BR/ST composites with ceramic content was shown in Fig. 4.19. The large value of CTE of polymers is caused by the low energy barrier to change the chain conformation and this high CTE precludes polymers from practical applications [48]. It is clear from Fig. 4.19 that the CTE of pure butyl rubber (191 ppm/^oC) is very much reduced by the addition of ceramic fillers SCT and ST which is having a very low CTE of 1.72 ppm/^oC and 9.4 ppm/^oC respectively. The increase in filler volume

fraction results in decreased free volume of polymer and hence reduced room for polymer expansion [49]. The CTE of BR/SCT-7 and BR/ST-7 composite is 30 ppm/^{o}C and 26 ppm/^{o}C respectively.

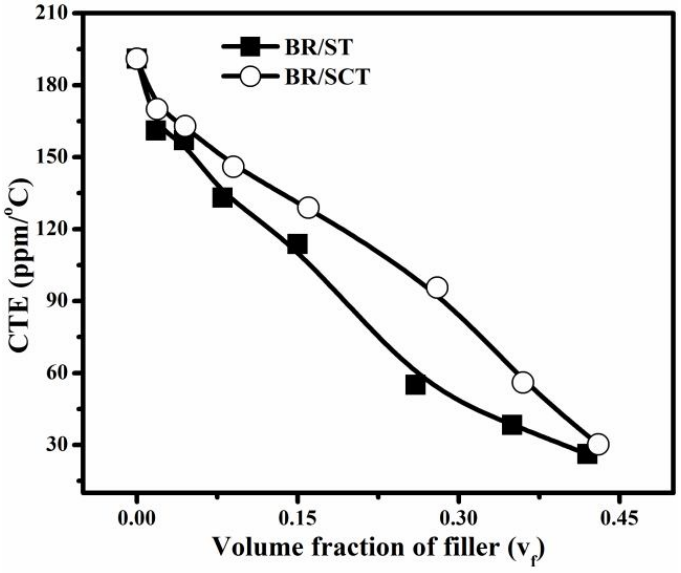

Fig. 4.19 Variation of CTE of BR/SCT and BR/ST composites with filler content

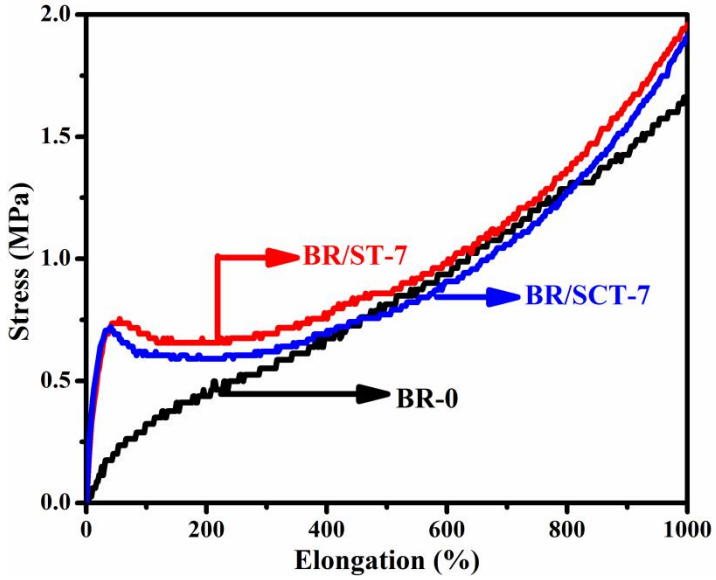

Fig. 4.20 Stress-strain curves of BR/SCT and BR/ST composites

The stress-strain curves of unloaded butyl rubber BR-0, BR/SCT-7 and BR/ST-7 are shown in Fig. 4.20. It has been reported that the stress-strain curves for particle filled rubber systems are affected by the crosslink density of the rubber matrix, the size of agglomerates and rubber-filler interactions [50]. From Fig. 4.20, it is clear that the stress for the same elongation is larger for ceramic filled composite as compared to unloaded butyl rubber. Increased filler loading leads to increase in the stiffness of the composite [51] and hence more stress is required for deformation. The stiffness is much higher for BR/ST-7 than that of BR/SCT-7 composite. This may be due to the more homogenous dispersion of ST particles in the matrix. Large elongations (1000%) of the samples without breaking indicate that the composites are flexible enough to meet the requirements.

4.4 Fabrication of flexible coplanar waveguide fed monopole antenna using BR/ST-4 substrate

There is an increasing demand for flexible antennas due to the proliferation of broadband wireless communication systems especially in the microwave region. The most widely used antenna in mobile communication systems is the monopole antenna [52]. In order to increase the antenna bandwidth of broadband planar monopole antennas, coplanar waveguide (CPW) feed is employed. In CPW feed both ground planes are very close to the conducting strip so there will be tight coupling between the ground and the conductor and have very less radiation losses compared to microstrip feed lines. The effective relative permittivity for the CPW feedlines is slightly higher since the fields are more confined in the dielectric substrate and this reduces the frequency corresponding to lower edge of banwidth. As the metallic geometry is on the same plane it can be easily realized in printed circuit structures [53].

A monopole antenna has been studied using BR+0.15 v_f of $SrTiO_3$ (BR/ST-4) composite having a relative permittivity of 4.3 similar to FR-4.The antenna dimensions were optimized using high frequency structure simulator (HFSS) to get good impedance matching. The optimized dimension of the resonating element is 35 mm length and 3 mm width. The antenna was fed with coplanar waveguide with a ground plane of 22 mm x 15 mm size and as the ground plane is on the same plane it can be easily fabricated. The copper cladding was done by hot pressing as per the simulated design. The detailed description of copper cladding of BR/ST-4 is given in section 2.2.12. The photograph of copper cladded BR/ST-4 is given in Fig. 4.21.

Fig. 4.21 Photograph of fabricated CPW fed monopole antenna

The simulated and measured reflection characteristics of BR/ST-4 are given in Fig. 4.22. It is evident from figure that the simulated and measured reflection characteristics are in good agreement. The measured sample has a return loss of -26.75 dB at 2.68 GHz.

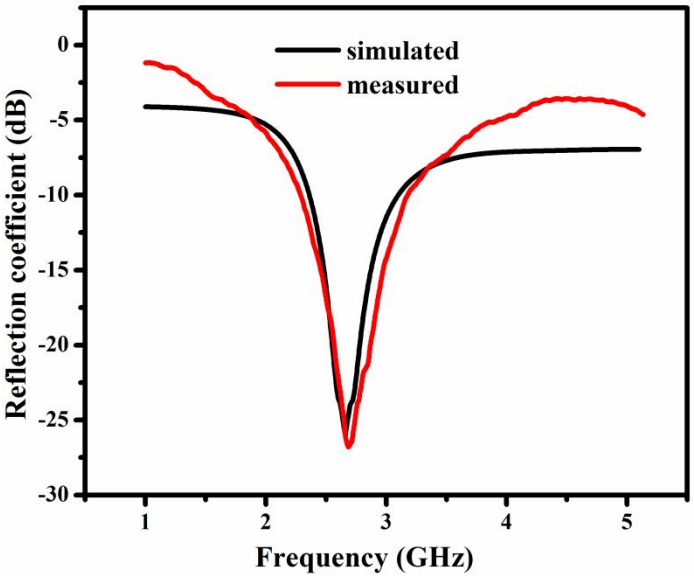

Fig. 4.22 Reflection characteristics of simulated and measured BR/ST-4 antenna

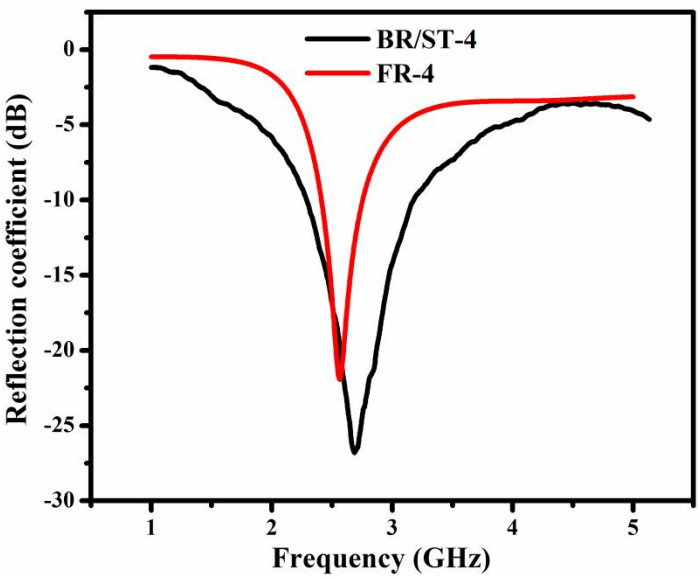

Fig. 4.23 Reflection characteristics of BR/ST-4 and FR-4

The measured return loss characteristics of BR/ST-4 are compared with the simulated return loss characteristics of FR-4 and are shown in Fig. 4.23. The band width of BR/ST-4 at -10 dB level is 16.9 % and that of FR-4 is 10.7 %. The BR/ST-4 has a higher gain of 1.71

dBi compared to FR-4 (1.59 dBi). The fabricated monopole has a higher band width and gain compared to FR-4 indicating the potential use of this antenna for communication applications.

4.5 Conclusions

- The high permittivity fillers such as TiO_2, $Sr_2Ce_2Ti_5O_{15}$ and $SrTiO_3$ ceramic reinforced butyl rubber composites were prepared by sigma mixing followed by hot pressing.
- The dielectric, thermal and mechanical properties of these composites were investigated as a function of filler loading and also the effect of filler particle size was studied in butyl rubber-rutile composites.
- The microstructural analysis of composites indicates the homogenous dispersion of filler particles in the butyl rubber matrix.
- Stress-strain curves of all composites show the flexibility of composites.
- The experimental relative permittivity and thermal conductivity of all the composites were compared with theoretical models.
- For 0.40 v_f of micron rutile loading, BR/RT composite has ε_r = 12.50 and tanδ= 0.0027 (at 5 GHz), CTE= 108 ppm/^oC, TC= 0.72 $Wm^{-1}K^{-1}$ and water absorption = 0.078 vol%. The BR/SCT composites have ε_r = 11.00 and tanδ= 0.00175 (at 5 GHz), CTE= 30 ppm/^oC and TC 0.49 $Wm^{-1}K^{-1}$ and water absorption of 0.068 vol% for 0.43 v_f of SCT content and BR/ST composites achieved a ε_r of 13.20 and tanδ of 0.0028 (at 5 GHz), CTE and TC of 26 ppm/^oC and 0.55 $Wm^{-1}K^{-1}$ respectively and

water absorption of 0.081 vol% for 0.42 v_f of $SrTiO_3$. All these composites can be used as the core of flexible dielectric waveguide applications.

- The measured properties indicate that all the other compositions of BR/RT, BR/nRT, BR/SCT and BR/ST composites can be used for cladding of flexible dielectric waveguide and also for microwave substrates and electronic packaging applications.
- A coplanar waveguide fed monopole antenna is fabricated using BR/ST-4 substrate which have better bandwidth compared to standard FR-4 substrate.

4.6 References

1. I. Park, S. H. Ko, H. Pan, C. P. Grigoropoulos, A. P. Pisano, J. M. J. Frechet, E. S. Lee and J. H. Jeong, *Adv. Mater.*, **20,** 489 (2008).
2. Y. G. Seol, H. Y. Noh, S. S. Lee, J. H. Ahn and N. E. Lee, *Appl. Phys. Lett.,* **93,** 013305 (2008).
3. F. Xiang, H. Wang and X. Yao, *J. Eur. Ceram. Soc.*, **27,** 3093 (2007).
4. A. Nathan and B. R. Chalamala, *Proc. IEEE.*, **93,** 1235 (2005).
5. A. C. Siegel, S. T. Phillips, M. D. Dickey, N. Lu, Z. Suo and G. M. Whitesides, *Adv. Funct. Mater.*, **20,** 28 (2010).
6. W. M. Bruno and W. B. Bridges, *IEEE Trans. Microwave Theory Tech.*, **36,** 882 (1988).
7. W. R. Gore Co, Product brochure.
8. S. Shindo and I. Ohtomo, *Tech. Rep. IECE Japan, MW 75-105*, 75 (1975).
9. J. Obrzut and P. F. Goldsmith, *IEEE Trans. Microwave Theory Tech.*, **38,** 324 (1990).
10. C. H. Kwon, H. Shin, J. H. Kim,W. S. Choia and K. H. Yoon, *Mater. Chem. Phys.,* **86,** 78 (2004).
11. A. A. Belhekar, S. V. Awate and R. Anand, *Catal. Commun.,* **3,** 453(2002).
12. S. B. Cohen, *IEEE Trans. Microwave. Theory. Tech.*, **16,** 218 (1968).
13. M. Crippa, A. Bianchi, D. Cristofori, M. DArienzo, F. Merletti, F. Morazzoni, R. Scotti and R. Simonutti, *J. Mater. Chem. C,* **1,** 484 (2013).
14. S. Rajesh, K. P. Murali, V. Priyadarsini, S. N. Potty and R. Ratheesh, *Mater. Sci. Eng. B,* **163,** 1 (2009).

15. S. Rajesh, V. S. Nisa, K. P. Murali and R. Ratheesh, *J. Alloys Compd.*, **477,** 677 (2009).

16. S. Nayak, B. Sahoo, T. K. Chaki and D. Khastgir, *RSC Adv.*, **3,** 2620 (2013).

17. M. R. Kashani, S. Javadi and N. Gharavi, *Smart. Mater. Struct.*, **19,** 035019 (2010).

18. A. Saritha, K. Joseph, A. Boudenne and S. Thomas, *Polym. Compos.*, **32,** 1681 (2011).

19. P. L. Wise, I. M. Reaney, W. E. Lee, T. J. Price , D. M. Iddles and D. S. Cannell, *J. Eur. Ceram. Soc.*, **21,** 2629 (2001).

20. S. Rajesh, K. P. Murali, K. V. Rajani and R. Ratheesh, *Int. J. Appl. Ceram. Technol.*, **6,** 553 (2009).

21. V. S. Nisa, S. Rajesh, K. P. Murali, V. Priyadarsini, S. N. Potty and R. Ratheesh, *Compos. Sci. Technol.*, **68,** 106 (2008).

22. G. Subodh and M. T. Sebastian, *Mater. Sci. Eng. B*, **136,** 50 (2007).

23. G. Subodh, J. James, M. T. Sebastian, R. M. Paniago, A. Dias and R. L. Moreira, *Chem. Mater.*, **19,** 4077 (2007).

24. S. Kamba, M. Savinov, F. Laufek, O. Tkac, C. Kadlec, S. Veljko, E. J. John, G. Subodh, M. T. Sebastian, M. Klementova, V. Bovtun, J. Pokorny, V. Goian and J. Petzelt, *Chem. Mater.*, **21,** 811 **(**2009).

25. G. Subodh, V. Deepu, P. Mohanan and M. T. Sebastian, *Appl. Phys. Lett.*, **95,** 062903 (2009).

26. G. Subodh, V. Deepu, P. Mohanan and M. T. Sebastian, *J. Phys. D Appl. Phys.*, **42,** 225501 (2009).

27. T. Hu, J. Juuti, H. Jantunen and T. Vilkman, *J. Eur. Ceram. Soc.*, **27,** 3997 (2007).

28. M. G. Todd and F. G. Shi, *Microelectron. J.*, **33,** 627 (2002).

29. W. Lamb, D. M. Wood and N. W. Ashcroft, *Phys. Rev. B,* **21,** 2248 (1980).

30. N. Jayasundere and B. V. Smith, *J. Appl. Phys.*, **73,** 2462 (1993).

31. Y. Rao, J. Qu, T. Marinis and C. P Wong, *IEEE Trans. Compon. Packag. Technol.*, **23,** 680 (2000).

32. L. L. Hench and J. K. West, Principles of electronic ceramics, Wiley, New York (1990).

33. L. Wang, F. Li and Z. Su, *J. Appl. Polym. Sci.*, **108,** 2968 (2008).

34. W. Zhou, D. Yu, C. Wang, Q. An and S. Qi, *Polym. Eng. Sci.*, **48,** 1381 (2008).

35. A. P. Meera, R. Tlili, A. Boudenne, L. Ibos, V. Poornima, S. Thomas and Y. Candau, *J. Elastomer Plast.*, **44,** 369 (2012).

36. R. K. Goyal, A. N. Tiwari and Y. S. Negi, *Composites Part B,* **47,** 70 (2013).

37. S. Fu, X. Feng, B. Lauke and Y. Mai, *Composites Part B*, **39,** 933 (2008).

38. Y. C. Chen, H. C. Lin and Y. D. Lee, *J. Polym. Res.*, **10,** 247 (2003).

39. Z. M. Dang, Y. F. Yu, H. P. Xu and J. Bai, *Comp. Sci. Tech.*, **68,** 171 (2008).

40. J. Liu, C. G. Duan, W. N. Mei, R. W. Smith and J. R. Hardy, *J. Appl. Phys.*, **98,** 093703 (2005).

41. H. Barron, *Modern synthetic rubbers,* Chapman & Hall Ltd, (1949).

42. F. Xiang, H. Wang and X. Yao, *J. Eur. Ceram. Soc.*, **26**, 1999 (2006).

43. G. Subodh, C. Pavithran, P. Mohanan and M. T. Sebastian, *J. Eur. Ceram. Soc.*, **27**, 3039 (2007).

44. A. A. M. Ward, B. Stoll, W. V. Soden, S. Herminghaus and A. A. Mansour, *Macromol. Mater. Eng.*, **278,** 971 (2003).

45. H. He, R. Fu, Y. Han, Y. Shen and D. Wang, *J. Electron. Packaging.,* **129,** 469 (2007).

46. H. He, R. Fu, Y. Han, Y. Shen and X. Song, *J. Mat. Sci.,* **42,** 6749 (2007).

47. D. Kumlutas, I. H. Tavman and M. T. Coban, *Comp. Sci. and Tech.,* **63,** 113 (2003).

48. Y. Q. Rao and T. N. Blanton, Macromolecules, **41,** 935 (2008).

49. R. K. Goyal, A. N. Tiwari, U. P. Mulik and Y. S. Negi, *Compos. Sci. Technol.,* **67,** 1802 (2007).

50. F. Yatsuyanagi, N. Suzuki, M. Ito and H. Kaidou, *Polym. J.,* **34,** 332 (2002).

51. H. Ismail, S. T. Sam, A. F. Mohd Noor and A. A. Bakar, *Polym. Plast. Technol. Eng.,* **46,** 641 (2007).

52. G. S. Gosal, Proc. of the Internationl Conference on Advances in Computer, Electronics and Electrical Engineering, 64-68 (2012).

53. V. A. Shameena, S. Jacob, S. Mridula, C. K Aanandan, K. Vasudevan and P. Mohanan, IEEE, (2011).

Chapter 5

Butyl Rubber–Very High Permittivity Ceramic [$BaTiO_3$ and $Ba_{0.7}Sr_{0.3}TiO_3$] Composites

The present chapter deals with preparation, characterization and properties of butyl rubber-very high permittivity ceramic composites. Very high permittivity ceramic fillers such as $BaTiO_3$ and $Ba_{0.7}Sr_{0.3}TiO_3$ are used for the preparation of butyl rubber composites. The influence of ceramic loading on dielectric, thermal and mechanical properties of the composites was investigated. The effect of filler particle size on these properties was studied in butyl rubber-$BaTiO_3$ composites. The experimental relative permittivity and thermal conductivity of the composites was compared with theoretical predictions.

5.1 Introduction

Currently electronic industry is in search of light weight, stretchable and deformable materials for microwave electronic applications [1]. Modern electronic industry requires systems that can be fitted into non-planar forms which can be folded and unfolded for packaging or storage [2,3]. Pliability provide the advantage of three-dimensional designs of conformal structures [4,5] and found applications from neural prosthetics in the medical field to microwave devices in electronics. In contrast to flexible electronics, stretchable electronics can be used for curved surfaces and movable parts such as the joints of a robot's arm, human medical prostheses etc. [6]. The stretchable circuits have the ability to withstand large levels of strain without fracture and also no deterioration in the electronic properties [1]. The soft and rubbery future of electronic industry needs new materials to satisfy their demands [7]. Polymers are widely used in electronic industry due to its excellent dielectric properties and easy machinability. The conventional polymers can be replaced by elastomers since stretchability is needed for many electronic applications.

The use of high permittivity ferroelectric ceramics in microwave devices is increasing in recent years because they possess frequency dependent permittivity. Low loss materials are needed for most high power applications [8]. The majority of microwave applications are related to high speed microelectronics, radar and communication systems and they need low loss high permittivity materials. The thermal properties such as thermal conductivity (TC) should be high and coefficient of thermal expansion (CTE) of materials should be low respectively for practical applications. Elastomer-ceramic composites can combine the advantages of both elastomer and ceramics which can satisfy diverse requirements of present electronic industry. Today elastomer-ceramic composites found applications ranging from

ultrathin health monitoring tapes to advanced imaging devices [9]. Many literatures are available in the field of dielectric properties of polymer-ferroelectric ceramic composites [10-12].

Barium titanate ($BaTiO_3$) is a well known ferroelectric ceramic chosen for the present work. It has a perovskite type structure with high relative permittivity (≈1000 to 2000), loss tangent (≈ 10^{-2}) and high breakdown strength [13]. $BaTiO_3$ is widely studied for its numerous scientific and industrial applications, such as in dielectric capacitors, transducers and tunable phase shifters [14]. It has a paraelectric cubic phase transition above its curie point of about 120^{o}C and has high relative permittivity at this temperature. Panomsuwan et al. reported the fabrication and dielectric properties of polybenzoxazine-$BaTiO_3$ composites at a frequency range of 1 kHz-10 MHz. The dielectric properties increases with filler loading and at 70% loading there is an abrupt rise in ε_r from 3.56 to 13.20 [15]. Epoxy-$BaTiO_3$-zinc oxide composites were prepared by Ioannou et al. and the dielectric properties were studied by broadband dielectric spectroscopy over a wide temperature and frequency range [16]. Popielarz et al. reported the dielectric properties of polymer-$BaTiO_3$ composites in the frequency range of 100 Hz to 10 GHz and a broad temperature range from -140^{o}C to 150^{o}C [17]. Pant et al. reported a comparative study of dielectric properties of composites of $BaTiO_3$ with two different polymers such as polyaniline and maleic resin in the X-band frequency [8]. Recently Salaeh et al. prepared flexible epoxidized natural rubber-$BaTiO_3$ composites and the influence of $BaTiO_3$ concentration on cure characteristics, mechanical, dielectric and morphological properties of the composites was investigated [18].

Since $BaTiO_3$ has high relative permittivity at its curie temperature, researchers made attempts to lower the curie temperature to room temperature by adding $SrTiO_3$. Barium

strontium titanate is a continuous solid solution of ferroelectric $BaTiO_3$ and paraelectric $SrTiO_3$ [19]. It is of considerable interest in the fields of electroceramics and microelectronics [20]. Among the series of solid solution of barium strontium titanate, $Ba_{0.7}Sr_{0.3}TiO_3$ (BST) is chosen for our study because at this Ba/Sr ratio curie point is close to room temperature. BST ceramic have very high relative permittivity (ε_r~2850 at 1 MHz) and loss tangent (tan δ~0.013 at 1 MHz) [21]. Polymer-barium strontium titanate composites were studied by various groups [22-24]. Wongwilawan et al. reported the dielectric properties of poly(benzoxazine/urethane)-$Ba_{0.3}Sr_{0.7}TiO_3$ composites and their microwave dielectric properties were studied at temperatures ranging from -50^{o}C to 150^{o}C in a frequency range of 300 MHz to 1 GHz [25]. Hu et al. investigated the dielectric properties of cyclic olefin copolymer-$Ba_{0.55}Sr_{0.45}TiO_3$ composites with different filler loadings with common and nano size ceramic powders at 1 GHz [26]. The effect of composite type on the dielectric properties at 10 kHz was studied by Wang et al. by preparing 0-3, 1-3 and 2-2 type structures of polymethylmethacrylate-$Ba_{0.6}Sr_{0.4}TiO_3$ composite [27]. Liou et al. studied the dielectric tunability of silicone rubber-$Ba_{0.65}Sr_{0.35}TiO_3$ composites with varying the volume fractions of ceramic content [28]. Even though dielectric properties of polymer-barium strontium titanate composites are available in the literature, the microwave dielectric properties of butyl rubber-BST composites are not yet reported.

The present chapter focuses on the effect of very high permittivity ferroelectric ceramic on dielectric, thermal and mechanical properties of butyl rubber-$BaTiO_3$ and butyl rubber-$Ba_{0.7}Sr_{0.3}TiO_3$ composites. This chapter also reports the effect of filler particle size of very high permittivity fillers on the above mentioned properties of butyl rubber-$BaTiO_3$ composites.

5.2 Butyl rubber–$BaTiO_3$ composites

Micron $BaTiO_3$ was prepared as described in section no. 2.1.2.7 and nano $BaTiO_3$ procured from Sigma Aldrich. The nano $BaTiO_3$ was heated at 100^oC for 24 hours before use. Butyl rubber-micron barium titanate (BR/BT) and butyl rubber-nano barium titanate (BR/nBT) composites were prepared in order to study the influence of filler particle size on dielectric, thermal and mechanical properties of butyl rubber composites. Both BR/BT and BR/nBT composites were prepared by a method described in section 2.1.4.1. The sample designation and corresponding ceramic volume fraction are given in Table 5.1. Both composites thus prepared were characterized for microstructure, dielectric, thermal and mechanical properties using techniques explained in section 2.2.

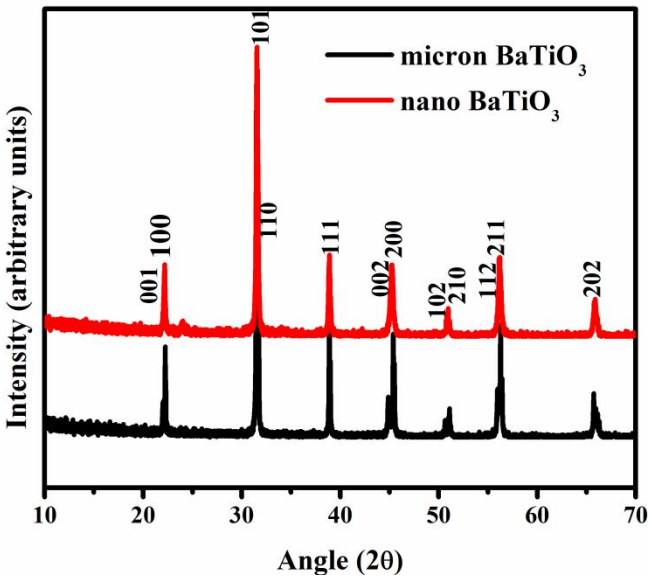

Fig. 5.1 XRD patterns of micron and nano $BaTiO_3$

Figure 5.1 shows the XRD patterns of micron $BaTiO_3$ and nano $BaTiO_3$. All the diffraction peaks were indexed based on the JCPDS file No. 83-1880. The phase formation of both ceramics was confirmed from the Fig. 5.1.

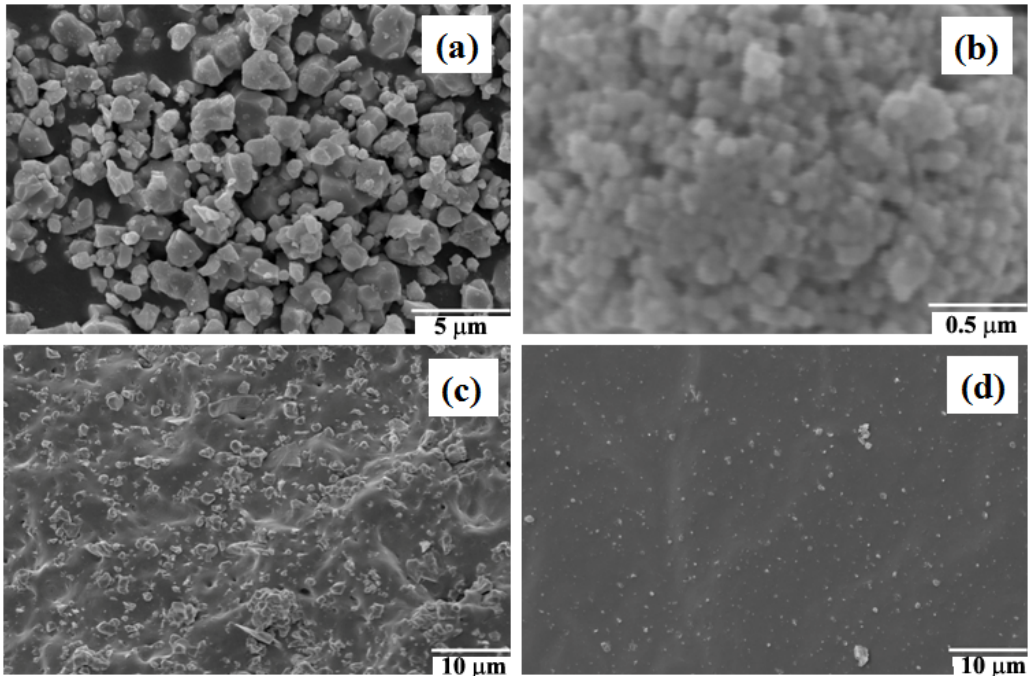

Fig. 5.2 SEM images of (a) micron $BaTiO_3$ powder (b) nano $BaTiO_3$ powder (c) fractured surface of BR+0.38 v_f of micron $BaTiO_3$ and (d) BR+0.24 v_f of nano $BaTiO_3$ composites

Figure 5.2 (a) and (b) shows SEM images of micron $BaTiO_3$ powder and nano $BaTiO_3$ powder respectively. Fig. 5.2 (c) and (d) shows the fractured surface of the BR+0.38 v_f of micron $BaTiO_3$ and BR+0.24 v_f of nano $BaTiO_3$ respectively. From Fig. 5.2 (c) it is clear that micron $BaTiO_3$ ceramic is uniformly distributed in the rubber matrix and some pores can be observed due to agglomeration of ceramic particles. The distribution of nano $BaTiO_3$ particles in the butyl rubber matrix is depicted from Fig. 5.2 (d).

Table 5.1 Dielectric properties at 1 MHz and water absorption values of BR/BT and BR/nBT composites

Composite material	Sample designation	Filler in phr[#] ()[$]	ε_r (1 MHz)	tan δ (1 MHz)	Water absorption (Vol%)
Butyl rubber-micron $BaTiO_3$ composites	BR-0	0 (0.00)	2.44	0.0003	0.039
	BR/BT-1	10 (0.02)	2.56	0.0009	0.040
	BR/BT -2	25 (0.04)	2.74	0.0011	0.045
	BR/BT -3	50 (0.07)	3.14	0.0015	0.046
	BR/BT -4	100 (0.13)	3.88	0.0016	0.048
	BR/BT -5	200 (0.24)	6.06	0.0020	0.057
	BR/BT -6	300 (0.32)	7.94	0.0021	0.068
	BR/BT -7	400 (0.38)	9.18	0.0023	0.120
Butyl rubber-nano $BaTiO_3$ composites	BR/nBT-1	10 (0.02)	2.63	0.0022	0.048
	BR/nBT-2	25 (0.04)	2.86	0.0033	0.052
	BR/nBT-3	50 (0.07)	3.37	0.0077	0.059
	BR/nBT-4	100 (0.13)	4.39	0.0080	0.078
	BR/nBT-5	200 (0.24)	7.02	0.0110	0.091

[#] parts per hundred rubber

[$] The corresponding ceramic volume fraction is given in parenthesis.

The dielectric properties at 1 MHz and water absorption values of both butyl rubber-micron $BaTiO_3$ and butyl rubber-nano $BaTiO_3$ composites are given in Table 5.1. The relative permittivity and loss tangent of both BR/BT and BR/nBT composites show an increasing trend with ceramic content since the relative permittivity and loss tangent of $BaTiO_3$ is higher than that of butyl rubber matrix. The dielectric properties of the composites are strongly affected by the presence of moisture content. The absorbed moisture interacts with polymer matrix and also at the filler-matrix interface [29] and thus affects the dielectric properties of composites. The volume% of moisture absorption of both BR/BT and BR/nBT composites with filler loading is also given in Table 5.1. The moisture absorption values are found to be increased with ceramic content. This may be due to the hydrophilic nature of ceramic particles.

Figure 5.3 (a) shows the variation of relative permittivity of BR/BT and BR/nBT composites with ceramic content at 5 GHz. The ε_r of both the composites show the same trend as that of 1 MHz. It is worth to be noted that the nano $BaTiO_3$ filled butyl rubber composite shows higher relative permittivity than micron composites. This may be due to the presence of higher moisture content in the nano composite since the relative permittivity of water is high (ε_r~ 80). The interface region between the filler and matrix is large in the case of nano composites which also contribute to high relative permittivity [30]. The relative permittivity of BR/BT composite is 7.03 for ceramic loading of 0.24 v_f and that of BR/nBT composite is 8.79 for the same loading of nano $BaTiO_3$. Eventhough the ε_r of $BaTiO_3$ is very high than that of matrix, the composite cannot attain higher relative permittivity. The relative permittivity of polymer-ferroelectric ceramic composite cannot exceed 100 even at maximum filler loading [31] since the 0-3 type composite follow an exponential relationship between

relative permittivity of composite and the volume fraction of the filler. Logarithm of the relative permittivity of such composites ($\varepsilon'_{composite}$) is linearly proportional to the volume fraction of the filler (ϕ_{filler}) with the slope dependent of the dielectric properties of both components (Equation (5.1)).

$$\log \varepsilon'_{composite} = \phi_{filler} \log(\varepsilon'_{filler}/\varepsilon'_{polymer}) + \log \varepsilon'_{polymer} \qquad (5.1)$$

In general it is difficult to prepare polymer composite with ceramic loading higher than 0.40 v_f. In order to get a polymer composite with relative permittivity higher than 100 based on typical polymers with relative permittivity of the order of 5, the relative permittivity of the filler must be higher than 9000 [31]. Xie et al. prepared core shell structured polymethylmethacrylate-$BaTiO_3$ nano composites by in situ atom transfer radical polymerization of methyl methacrylate from the surface of $BaTiO_3$ nano particles. For 76.88 wt% $BaTiO_3$ content, the composite achieved a ε_r of 13.46 and tan δ of 0.00372 at 1 kHz [32]. The variation of loss tangent of both BR/BT and BR/nBT composites with filler loading is also shown in Fig. 5.3 (b). The loss tangent of both composites increases with filler volume fraction since the loss tangent of $BaTiO_3$ is higher than that of butyl rubber. The tan δ of butyl rubber-nano barium titanate composite is higher than that of butyl rubber-micron barium titanate composites. This is due to the presence of higher water content in the nano composites due to the larger surface area and reactivity of nano particles. Structural defects like lattice strain are also responsible for the higher loss tangent of nano composites [33]. The tan δ of micron composite is 0.0140 for a filler loading of 0.24 v_f and that of nano composite is 0.0190 for the same filler loading.

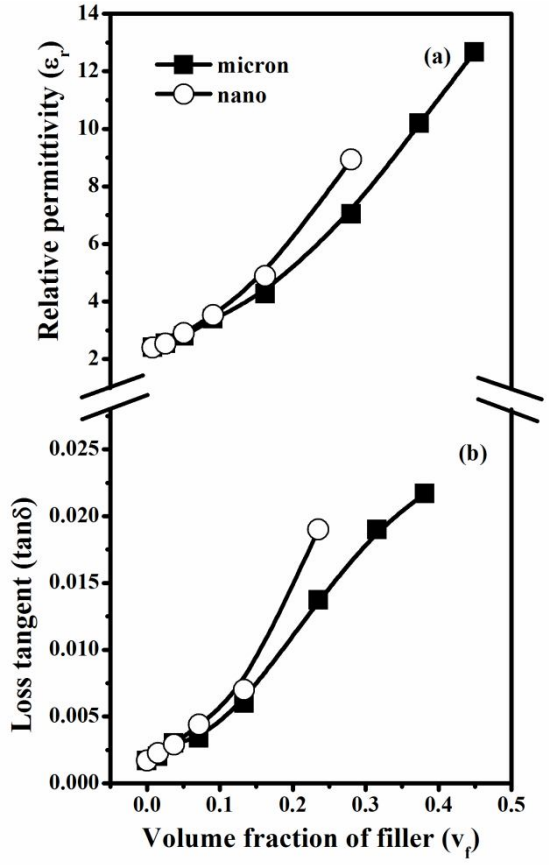

Fig. 5.3 Variation of (a) relative permittivity and (b) loss tangent of BR/BT and BR/nBT composites at 5 GHz

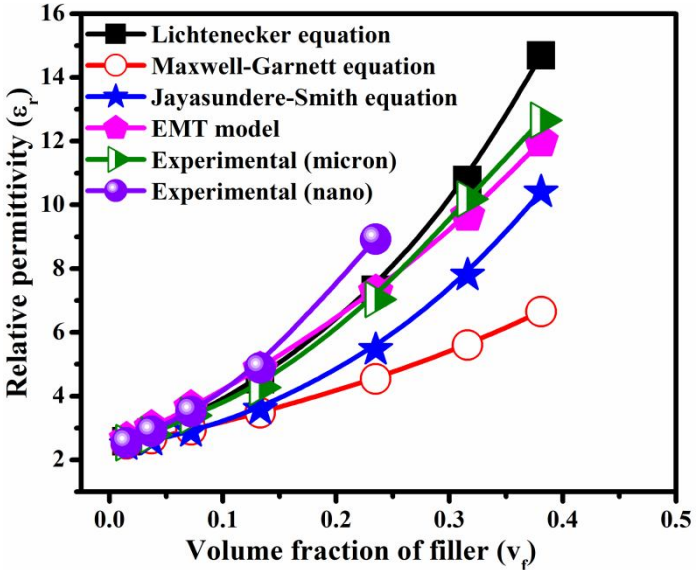

Fig. 5.4 Comparison between experimental and theoretical relative permittivity of BR/BT and BR/nBT composites at 5 GHz

Figure 5.4 shows the comparison between experimental and theoretical values of relative permittivity at 5 GHz for both butyl rubber-micron $BaTiO_3$ and butyl rubber-nano $BaTiO_3$ composites. The experimental ε_r of both BR/BT and BR/nBT composites are in agreement with Lichtenecker equation and EMT model at low filler loadings. The ε_r of BR/BT composites shows deviation from both models after a filler loading of 0.24 v_f of $BaTiO_3$ content. The relative permittivity of BR/nBT composites are matching with Lichtenecker and EMT model upto a loading of 0.13 v_f of nano $BaTiO_3$ and shows deviation at higher filler loading. The deviation at higher filler loading may be due to the non-homogenous dispersion of filler particles in the rubber matrix. The relative permittivity of both the composites was also compared with Maxwell-Garnett and Jayasundere-Smith equation and the observed values are not matching with both theoretical models.

Figure 5.5 and 5.6 shows the effect of bending on dielectric properties of BR/BT and BR/nBT composites at 5 GHz. The relative permittivity of both composites is almost independent of bending and is clear from Fig. 5.5 (a) and (b). It is also evident from Fig. 5.6 (a) and (b) that the loss tangent of both BR/BT and BR/nBT composites showing a slight variation with mechanical bending but the variation is marginal. Vrejoiu et al. observed a similar behaviour in PFCB (perfluorocyclobutene (poly 1,1,1-triphenyl ethane per-fluorocyclobutyl ether)-$BaTiO_3$ composites [34]. They observed that repeated mechanical bending upto 50 cycles does not change ε_r and tan δ of the composites.

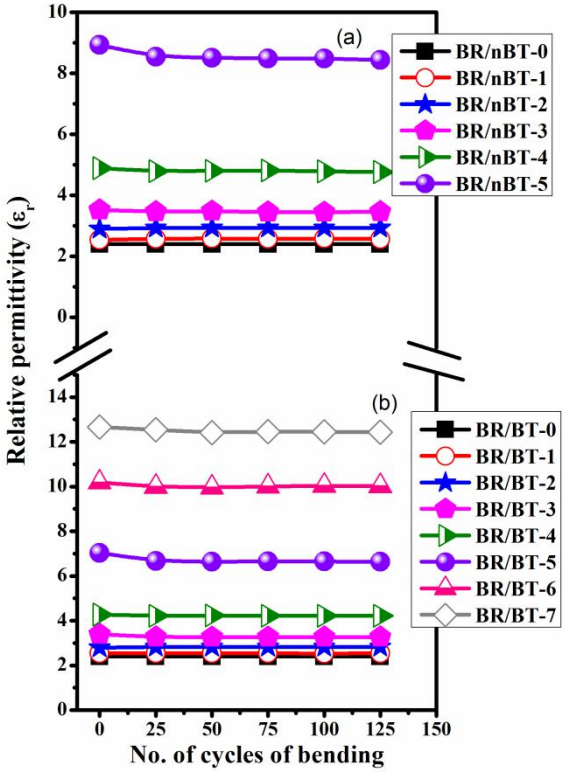

Fig. 5.5 Variation of relative permittivity of (a) BR/nBT and (b) BR/BT composites with bending

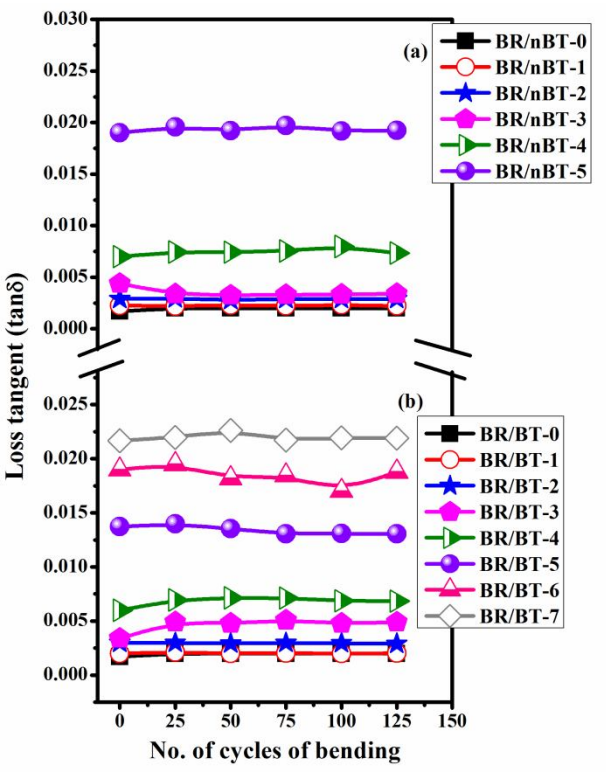

Fig. 5.6 Variation of loss tangent of (a) BR/nBT and (b)BR/BT composites with bending

Figure 5.7 (a) and (b) shows temperature variation of relative permittivity of both BR/nBT and BR/BT composites at 1 MHz respectively. The drift in relative permittivity with temperature should be small for practical applications. The relative permittivity of all the compositions of butyl rubber-micron $BaTiO_3$ and butyl rubber-nano $BaTiO_3$ composites are almost stable in the measured temperature range. From the Fig. 5.7 (a) and (b) it is clear that as the temperature increases, the relative permittivity of composites shows a slight decrease like other butyl rubber composites.

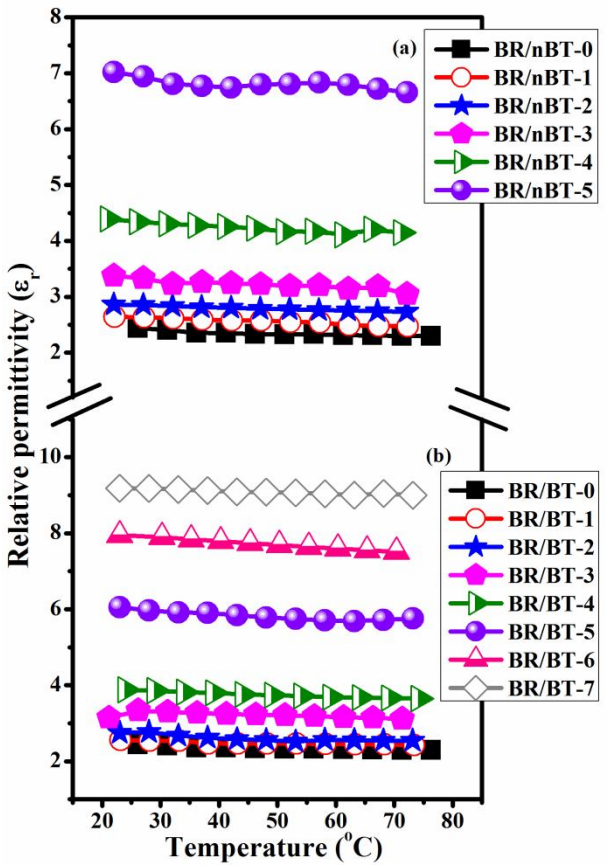

Fig. 5.7 Variation of relative permittivity of (a) BR/nBT and (b) BR/BT composites with temperature at 1 MHz

Figure 5.8 shows the variation of thermal conductivity of BR/BT and BR/nBT composites with ceramic loading. As the ceramic loading increases the thermal conductivity of both composite increases since the thermal conductivity of $BaTiO_3$ (2.6 $Wm^{-1}K^{-1}$) is higher than the butyl rubber (0.13 $Wm^{-1}K^{-1}$). As the filler loading increases, distance between the filler particles decreases and thus filler become the main channels for thermal conduction. Hence thermal conductivity of both composites increases with filler content [35]. It is also worth to note that the nano composite have higher thermal conductivity than that of micron

composite. As the particle size decreases the number of particles increases at the same volume fraction of filler. This will leads to the formation of more number of thermally conductive pathways in the nano composite [36]. Hence the thermal conductivity of BR/nBT composite is higher than that of BR/BT composites. The butyl rubber-micron barium titanate composite with ceramic loading of 0.24 v_f have a thermal conductivity of 0.31 $Wm^{-1}K^{-1}$and that of butyl rubber-nano barium titanate composite is 0.36 $Wm^{-1}K^{-1}$. Fig. 5.8 also shows the comparison between experimental and theoretical thermal conductivity of both composites. The series and parallel mixing rule of both composites shows the same trend as that of previous chapters. All the other theoretical models are matching with thermal conductivity of BR/nBT composites at low filler loading and show deviation at higher nano $BaTiO_3$ content. The thermal conductivity of butyl rubber–micron $BaTiO_3$ composites are in agreement with Cheng-Vachon and geometric mean model. Maxwell-Eucken equation holds good at low filler loading and deviates at higher micron $BaTiO_3$ content [37].

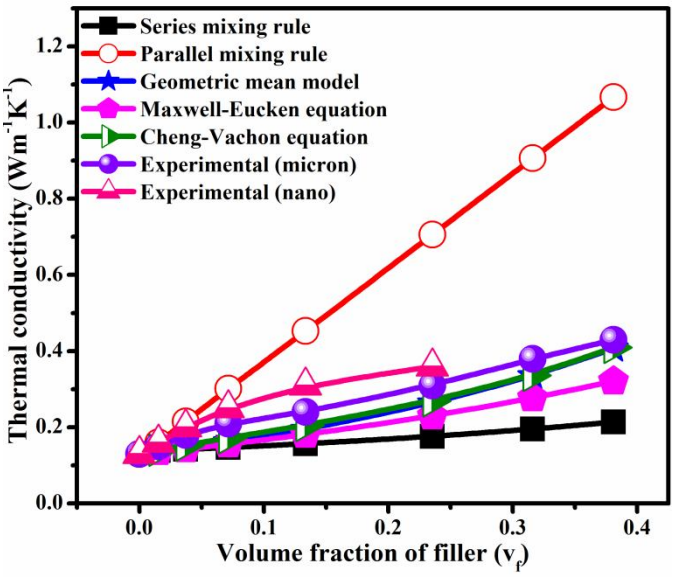

Fig. 5.8 Variation of thermal conductivity of BR/BT and BR/nBT composites

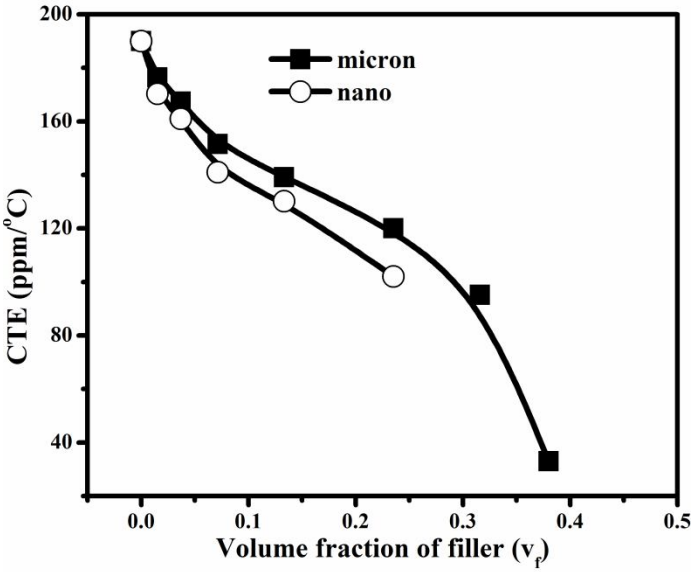

Fig. 5.9 Variation of CTE of BR/BT and BR/nBT composites

The variation of CTE of BR/BT and BR/nBT composites with volume fraction of filler content is shown in Fig. 5.9. It is clear from the figure that the thermal expansion of both composites were lowered with the addition of ceramic particles. The presence of ceramic imparts constraints on the mobility of polymer chains and thereby CTE is decreased [38]. It is worth to be noted that the nano composites show higher reduction of CTE than that of BR/BT composites like other butyl rubber nano composites.

Figure 5.10 shows the stress-strain curves of BR/BT-7 and BR/nBT-5. As the filler loading increases the stress needed for elongation and also stiffness of the composite increases [39]. From the Fig. 5.10 it is clear that the nano composite is slightly stiffer than micron composite. Both the composites were not broken upto an elongation of 1000% which indicates the mechanical flexibility of the composites.

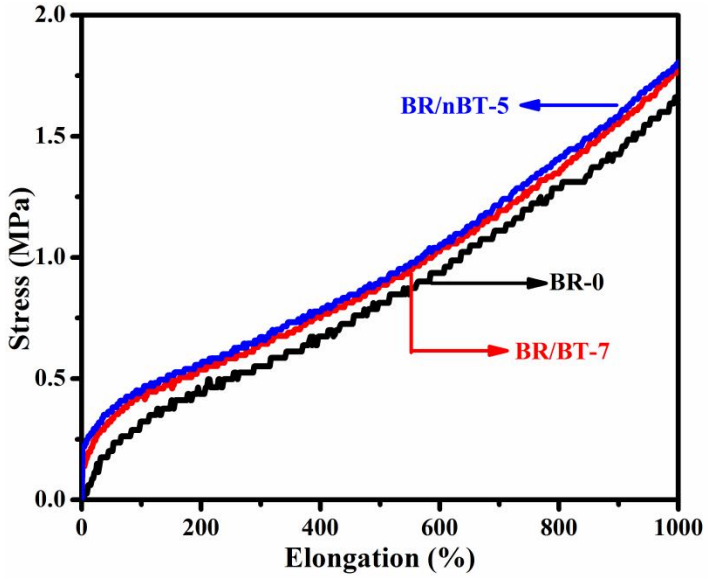

Fig. 5.10 Stress-strain curves of BR/BT and BR/nBT composites

5.3 Butyl rubber-$Ba_{0.7}Sr_{0.3}TiO_3$ composites

$Ba_{0.7}Sr_{0.3}TiO_3$ was prepared by solid state ceramic route as described in section 2.1.2.8. Butyl rubber-$Ba_{0.7}Sr_{0.3}TiO_3$ (BR/BST) composites were prepared by sigma mixing as described in section 2.1.4.1. The sample designation and the corresponding ceramic volume fraction are given in Table 5.2. The composites thus prepared were characterized for microstructure, dielectric, thermal and mechanical properties using techniques explained in section 2.2.

Figure 5.11 shows the XRD pattern of $Ba_{0.7}Sr_{0.3}TiO_3$ ceramic powder sintered at 1300^oC for 4 hours. The powder diffraction patterns of $Ba_{0.7}Sr_{0.3}TiO_3$ were indexed based on

the JCPDS file no. 44-0093. A single phase of the tetragonal system was confirmed from the XRD

Figure 5.12 (a) shows the SEM image of BST powder which is irregularly shaped. Fig. 5.12 (b) shows the fractured surface of the BR+0.39 v_f of BST composite. A uniform dispersion of filler particles in the matrix can be depicted from Fig. 5.12 (b).

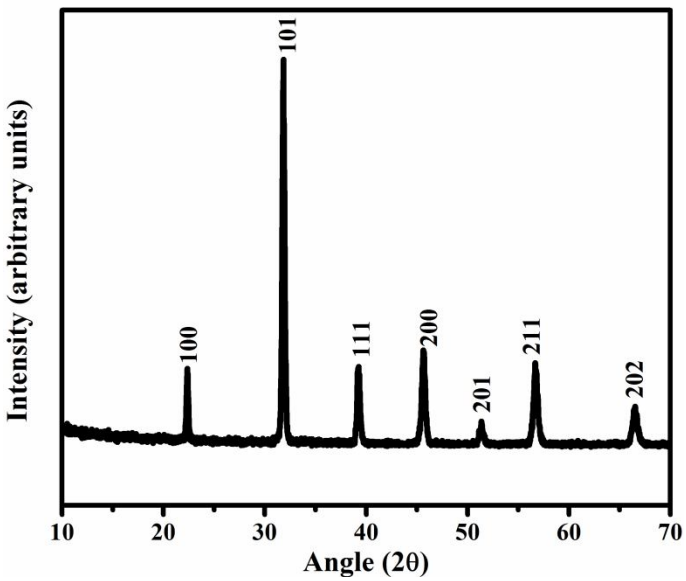

.

Fig. 5.11 XRD pattern of $Ba_{0.7}Sr_{0.3}TiO_3$

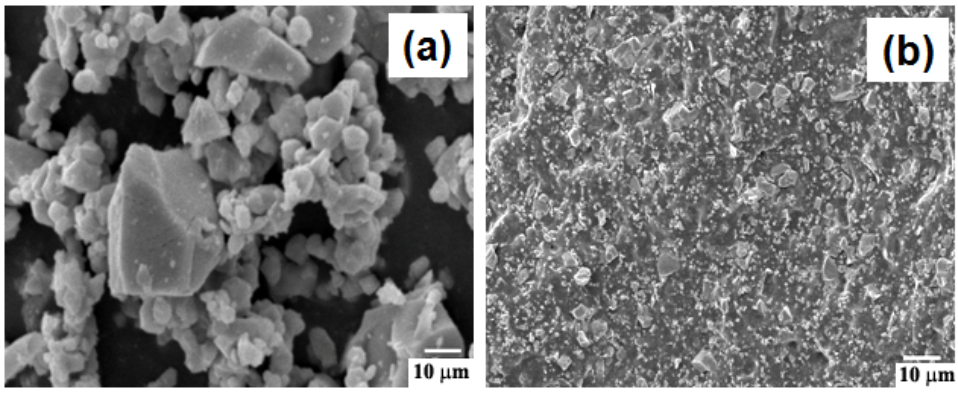

Fig. 5.12 SEM images of (a) BST powder and (b) fractured surface of BR+0.39 v_f of BST composite

Table 5.2 Dielectric properties at 1 MHz and water absorption of BR/BST composites

Composite material	Sample designation	Filler in phr[#] ()[$]	ε_r (1 MHz)	tan δ (1 MHz)	Water absorption (Vol%)
Butyl rubber-$Ba_{0.7}Sr_{0.3}TiO_3$ composites	BR-0	0 (0.00)	2.44	0.0003	0.039
	BR/BST-1	10 (0.02)	2.48	0.0014	0.042
	BR/BST -2	25 (0.04)	2.67	0.0019	0.048
	BR/BST -3	50 (0.07)	3.06	0.0024	0.051
	BR/BST -4	100 (0.14)	3.77	0.0025	0.054
	BR/BST -5	200 (0.24)	6.32	0.0034	0.055
	BR/BST -6	300 (0.32)	9.35	0.0036	0.056
	BR/BST -7	400 (0.39)	10.18	0.0044	0.060

[#] parts per hundred rubber

[$]The corresponding ceramic volume fraction is given in parenthesis.

Table 5.2 gives the dielectric and water absorption properties of BR/BST composites for different volume fractions of filler content. The effective dielectric properties are mainly influenced by the interface regions [40]. Interface regions exist between elastomer and ceramic particles. As the filler content increases the interfacial area increases and influence the dielectric properties significantly. The relative permittivity and loss tangent of the composite is found to increase with filler loading. The ε_r increases from 2.44 to 10.18 and loss tangent from 0.0003 to 0.0044 as the BST loading increases from 0-0.39 v_f. It is also clear from the Table 5.2 that the water absorption of the composite increases with the increase in filler content. The volume % of water absorption of BR/BST composite is 0.060

for the maximum filler loading of 0.39 v_f and is within the limit of practical electronic applications.

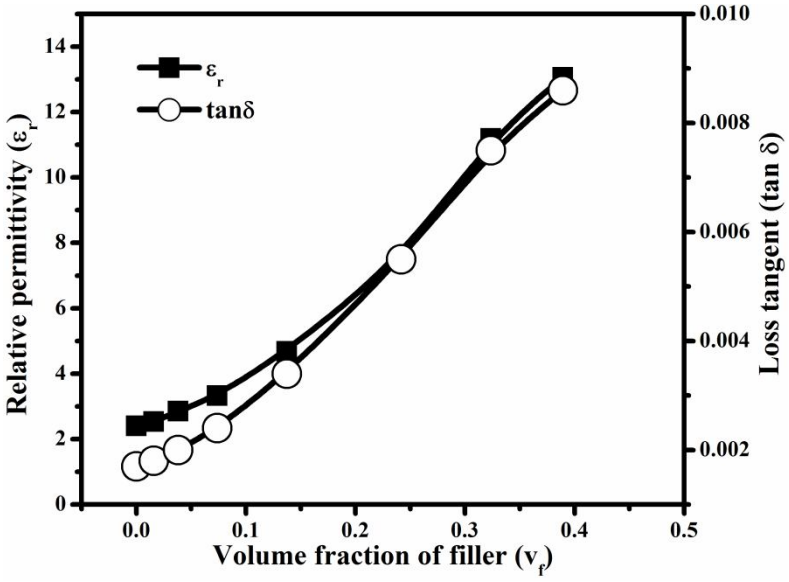

Fig. 5.13 Variation of relative permittivity and loss tangent of BR/BST composites at 5 GHz

Figure 5.13 shows the variation of relative permittivity and loss tangent of the BR/BST composites with filler loading at 5 GHz. Since the ε_r of BST is higher than that of butyl rubber matrix, the relative permittivity of BR/BST composite increases with filler loading. As the filler content increases, dipole-dipole interaction increases which contributes to the increase of relative permittivity [41]. The relative permittivity of BR/BST composites at 5 GHz is higher than that at 1 MHz as in previous chapters. The ε_r of the present composite increases from 2.40 to 13.10 as the filler loading increases from 0-0.39 v_f. The relative permittivity of BR/BST composites also does not exceed 100 and this may be due to the logarithmic relation explained in BR/BT composites [31]. Hu et al. prepared PPS-BST composites and their dielectric properties were studied as a function of BST loading upto 70 wt%. The relative permittivity increases from 3.20 to 13.50 and loss tangent from 0.0010 to

0.0025 at 1 GHz [23]. It is also evident from Fig. 5.13 that the loss tangent of the present composites increases with filler volume fraction. The dipole relaxation of water molecules present in the composite may be responsible for the increase in loss tangent in the microwave frequency. The loss tangent increases from 0.0017 to 0.0090 as BST content increases from 0-0.39 v_f.

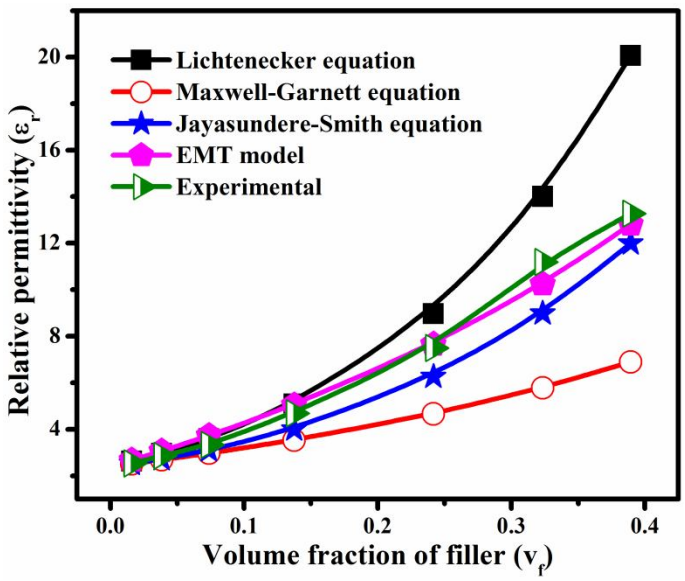

Fig. 5.14 Comparison of experimental and theoretical ε_r of BR/BST composites at 5 GHz

Figure 5.14 shows the comparison of the experimental values of ε_r with theoretical models given by equations (2.6) to (2.9). From the figure it is clear that Lichtenecker and Maxwell-Garnett equation hold good for low filler contents. Both Lichtenecker and Maxwell-Garnett models are based on the assumption that spheroidal fillers are ideally dispersed in the matrix [42, 43]. The BST particles in the present investigation are irregularly shaped which is evident from SEM image Fig. 5.12 (a) and hence the large deviation at higher BST loadings. The Jayasundere-Smith equation shows slight deviation from experimental values. The experimental relative permittivity is very well matching with EMT

model [44]. The value of n for BR/BST composite is found to be 0.17. Since EMT model includes a shape factor there is no restriction with the shape of the ceramic particles. Hence it is in good agreement with experimental values.

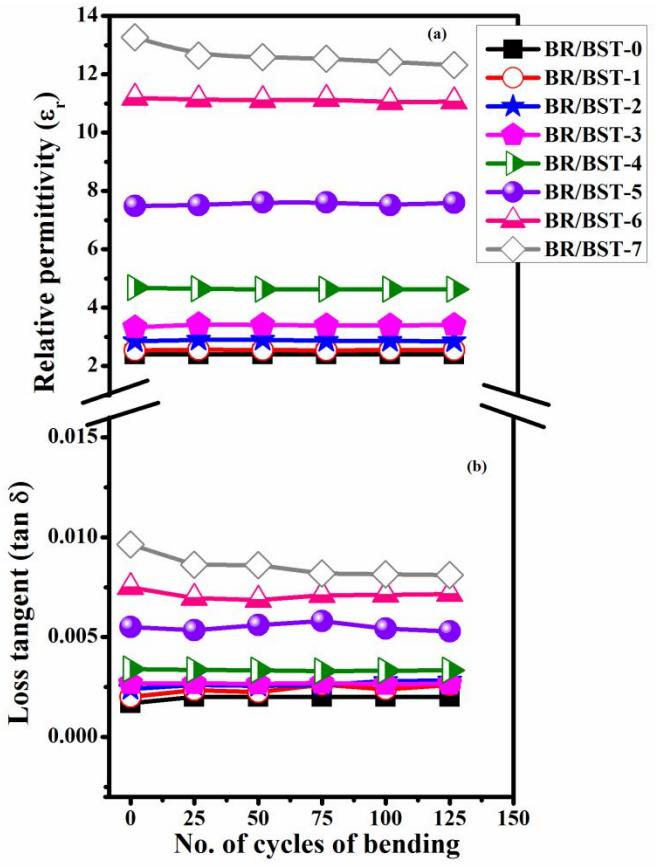

Fig. 5.15 Variation of (a) relative permittivity and (b) loss tangent of BR/BST composites with bending

Figure 5.15 shows the variation of microwave dielectric properties of BR/BST composites after repeated bending of samples by an angle of 180°. From the figure it is clear that the relative permittivity of the composites are almost independent of bending upto 0.32 v_f and after that it slightly decreases after 25 cycles of bending. The loss tangent of the BR/BST composites is almost constant throughout the repeated bending upto a filler loading of 0.24 v_f and the loss tangent shows a slight variation after a filler loading of 0.24 v_f. The

deviation at higher filler loading may be due to the particle agglomeration at higher filler content.

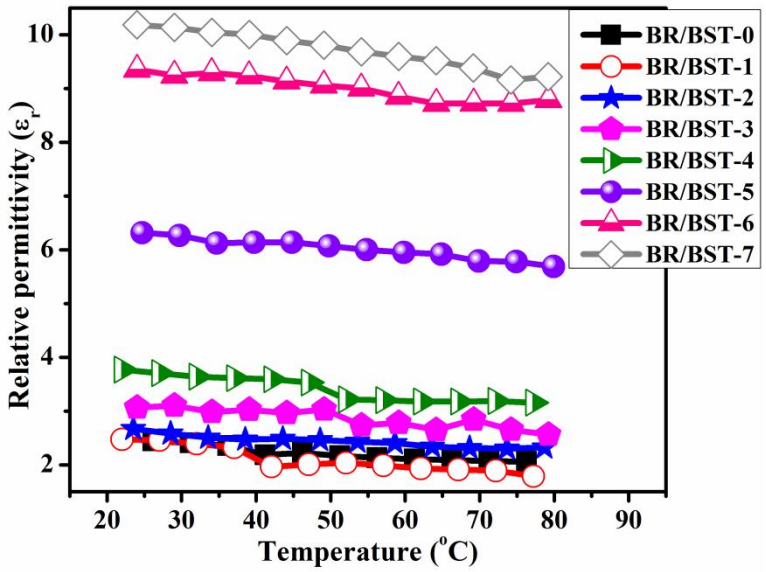

Fig. 5.16 Variation of relative permittivity of BR/BST composites with temperature at 1 MHz

Figure 5.16 shows the temperature dependence of relative permittivity of BR/BST composites with different volume fractions of ceramic loading. The relative permittivity of polymer composites should be stable within the operational temperature range of electronic devices for practical applications. From the figure it is clear that all the BR/BST composites are almost stable within the measured temperature range. The polarizability of dipoles is disturbed with increase in temperature and also the difference in CTE of rubber and filler may be responsible for the decrease in relative permittivity of the composites with temperature [45, 46].

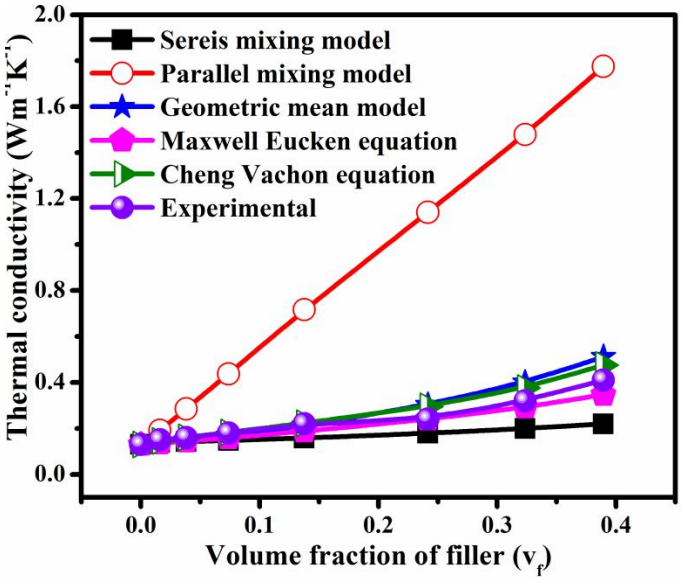

Fig. 5.17 Variation of thermal conductivity of BR/BST composites with BST content

The heat generated from the microelectronic product must be dissipated away in time to avoid over heat occurrence. Since the thermal conductivity of polymeric packaging materials is low, cooling is restricted in most modern electronic devices. Hence the thermal conductivity of polymers should be improved. The interfacial physical contact between polymer and filler is very critical for a polymer-ceramic composite [47]. Fig. 5.17 shows the variation of thermal conductivity of BR/BST composites with filler loading. The thermal conductivity of the composite increases obviously with the increase in filler loading since the thermal conductivity of BST (4.36 $Wm^{-1}K^{-1}$) is higher than that of butyl rubber matrix (0.13 $Wm^{-1}K^{-1}$). The filler particles at low volume fraction will disperse randomly in the rubber matrix and a little increase of thermal conductivity is observed. As the filler loading increases the filler particles begin to touch each other and form a thermally conducting path in the whole system and leads to an enhancement in thermal conductivity [48]. The thermal

conductivity of present composite improved from 0.13 to 0.41 $Wm^{-1}K^{-1}$ as the filler loading increases from 0-0.39 v_f. Comparison of thermal conductivity of BR/BST composites with various theoretical models [49] is also shown in Fig. 5.17. The experimental thermal conductivity values are within the range of values calculated from series and parallel mixing model. It is clear from the Fig. 5.17 that the thermal conductivity of BR/BST composite is in agreement with theoretical predictions such as geometric mean model, Maxwell-Eucken and Cheng-Vachon equation at low filler contents and shows deviation at higher BST loading.

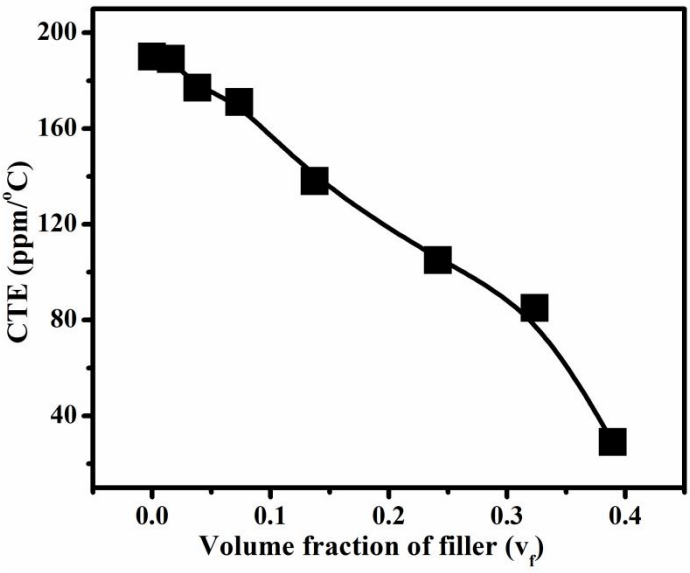

Fig. 5.18 Variation of CTE of BR/BST composites with filler content

Figure 5.18 shows the variation of coefficient of thermal expansion of BR/BST composites with filler content. The CTE of pure rubber matrix is 191 ppm/^oC. As the filler volume fraction increases, the CTE decreases. When a composite is heated, the polymer matrix will expand more than that of ceramic fillers. The expansion of matrix will be reduced if the interfaces are capable of transmitting stress. The polymer chains get arrested in the presence of ceramic and unable to expand with temperature. Hence the CTE of a composite

is reduced with increase in filler content and composite with strong interface exhibits an additional reduction of CTE [50, 51].

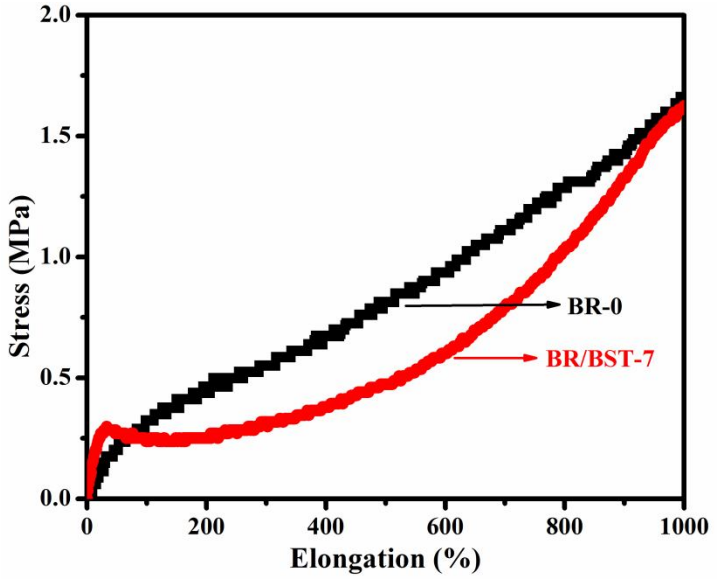

Fig. 5.19 Stress-strain curves of BR/BST composites

The mechanical flexibility is a prime requirement for a material to be used for flexible applications. The mechanical properties of the elastomer are generally improved by the addition of ceramic particles. Fig. 5.19 shows the stress-strain characteristics of BR/BST composites. The stiffness of the composites increases with filler content. The BR/BST-7 composite is not broken even upto an elongation of 1000%. This shows the good flexibility of the composite.

5. 4 Conclusions

- Butyl rubber-very high permittivity ceramic filler composites were prepared and their dielectric, thermal and mechanical properties were studied as a function of ceramic loading.

- Effect of ceramic particle size on these properties was investigated in butyl rubber-$BaTiO_3$ composites and the nano $BaTiO_3$ filled butyl rubber composites have slightly high ε_r and tan δ compared to micron composites.
- The microstructure of the composites shows the uniform dispersion of ceramic particles in the butyl rubber matrix.
- Stress-strain curves reveal the mechanical flexibility of the composites.
- The experimental relative permittivity and thermal conductivity of the composites were compared with theoretical predictions.
- BR/BT composite have ε_r = 12.70 and tan δ = 0.0220 (at 5 GHz), CTE= 33 ppm/^oC, TC=0.43 $Wm^{-1}K^{-1}$ and water absorption = 0.120 vol% for a $BaTiO_3$ ceramic loading of 0.38 v_f and that of BR/BST composite achieved a ε_r = 13.10 and tan δ = 0.0090 (at 5 GHz), TC=0.41 $Wm^{-1}K^{-1}$, CTE= 29 ppm/^oC and water absorption = 0.060 vol% for a BST ceramic loading of 0.39 v_f. Both these composites are suitable candidates for core of flexible dielectric waveguide applications.

5.5 References

1. D. H. Kim and J. A. Rogers, *Adv. Mater.,* **20,** 4887 (2008).
2. A. C. Siegel, S. T. Phillips, M. D. Dickey, N. Lu, Z. Suo and G. M. Whitesides, *Adv. Funct. Mater.,* **20,** 28 (2010).
3. E. Apaydin, Microfabrication techniques for printing on PDMS elastomers for antenna and biomedical applications, Dissertation, The Ohio State University (2009).
4. R. K. Kramer, C. Majidi, R. Sahai and R. J. Wood, IEEE/RSJ International conference on intelligent robots and systems, San Francisco, CA, USA, 1919 (2011).
5. Y. G. Seol, H. Y. Noh, S. S. Lee, J. H. Ahn and N. E. Lee, *Appl. Phys. Lett.,* **93,** 013305 (2008).
6. T. Sekitani, Y. Noguchi, K. Hata, T. Fukushima, T. Aida and T. Someya, *Science Magazine*, **321,** 1468 (2008).
7. J. A. Rogers and Y. G. Huang, *Proceedings of National Academy of Sciences*, **106,** 10875 (2009).
8. H. C. Pant, M. K. Patra, A. Verma, S. R. Vadera and N. Kumar, *Acta Mater.,* **54,** 3163 (2006).
9. F. Wang, W. Li, H. Jiang, M. Xue, J. Lu and J. Yao, *J. Appl. Phys.,* **107,** 043528 (2010).
10. H. Tang, J. Zhong, J. Yang, Z. Ma and X. Liu, *J. Electron. Mater.,* **40,** 141 (2011).
11. A. Biswas, I. S. Bayer, P. C. Karulkar, A. Tripathi, D. K. Avasthi, M. G. Norton and J. B. Szczech, *Appl. Phys. Lett.,* **91,** 212902 (2007).

12. T. Zhou, J. W. Zha, R. Y. Cui, B. H. Fan, J. K. Yuan and Z. M. Dang, *Appl. Mater. Interfaces.*, **3,** 2184 (2011).

13. S. F. Wang, Y. R. Wang, K. C. Cheng and Y. P. Hsaio, *Cerm. inter.*, **35,** 265 (2009).

14. B. Agoudjil, L. Ibos, Y. Candau and J. C. Majeste, *J. Phys. D: Appl. Phys.*, **41,** 055407 (2008).

15. G. Panomsuwan, S. Kaewwatal, H. Manuspiyal and H. Ishida, Proceedings of the 2nd IEEE International conference on nano/micro engineered and molecular systems, Bangkok, Thailand, 497 (2007).

16. G. Ioannou, A. Patsidis and G. C. Psarras, *Composites Part A*, **42,** 104 (2011).

17. R. Popielarz, C. K. Chiang, R. Nozaki and J. Obrzut, *Macromolecules*, **34,** 5910 (2001).

18. S. Salaeh, G. Boiteux, P. Cassagnau and C. Nakason, *Int. J. Appl. Ceram. Technol.*, Article in press (2013).

19. E. N. Bunting, G. R. Shelton and A. S. Creamer, *J. Amer. Ceramic. Soc.*, **30,** 114 (1947).

20. R. J. Fleming, A. Ammala, P. S. Casey and S. B. Lang, *IEEE. T. Dielect. El. In.*, **18,** 15 (2011).

21. B. R. Priya Rani and M. T. Sebastian, *J. Mater. Sci: Mater. Electron.*, **19,** 39 (2008).

22. F. Xiang, H. Wang, K. Li, Y. Chen, M. Zhang, Z. Shen and X. Yao, *Appl. Phys. Lett.*, **91,** 192907 (2007).

23. T. Hu, J. Juuti and H. Jantunen, *J. Eur. Ceram. Soc.,* **27,** 2923 (2007).

24. V. K. Palukuru, K. Sanoda, V. Pynttari, T. Hu, R. Makinen, M. Mantysalo, J. Hagberg and H. Jantunen, *Int. J. Appl. Ceram. Technol.,* **8,** 940 (2011).

25. S. Wongwilawan, H. Ishida and H. Manuspiya, *Ferroelectrics.,* **452,** 84 (2013).

26. T. Hu, J. Juuti, H. Jantunen and T. Vilkman, *J. Eur. Ceram. Soc.,* **27,** 3997 (2007).

27. H. Wang, F. Xiang and K. Li, *Int. J. Appl. Ceram. Technol.,* **7,** 435 (2010).

28. J. W. Liou and B. S. Chiou, *J. Phys. Condens. Matter.***, 10,** 2773 (1998).

29. H. Zhao and R. K. Y. Li, *Composites Part A,* **39,** 602 (2008).

30. K. P. Murali, S. Rajesh, O. Prakash, A. R. Kulkarni and R. Ratheesh, *Composites Part A,* **40,** 1179 (2009).

31. R. Popielarz and C. K. Chiang, *Mater. Sci. Eng. B,* **139,** 48 (2007).

32. L. Xie, X. Huang, C. Wu and P. Jiang, *J. Mater. Chem.,* **21,** 5897 **(**2011).

33. K. P. Murali, S. Rajesh, K. J. Nijesh and R. Ratheesh, *Int. J. Appl. Ceram. Technol.,* **7,** 475 (2010).

34. I. Vrejoiu, J. D. Pedarnig, M. Dinescu, S. B. Gogonea and D. Bäuerle, *Appl. Phys. A.,* **74,** 407 (2002).

35. W. Ling, A. Gu, G. Liang and L. Yuan, *Polym. Compos.,* **31,** 307 (2010).

36. W. Zhou, S. Qi, H. Li and S. Shao, *Thermochim. Acta.,* **452,** 36 (2007).

37. E. F. Jaguaribe and D. E. Beasley, *Int. J. Heat. Mass. Transfer.*, **27,** 399407 (1984).

38. R. K. Goyal, P. Jadhav and A. N. Tiwari, *J. Electron. Mater.,* **40,** 1377 (2011).

39. N. Suzuki, F. Yatsuyanagi, M. Ito and H. Kaidou, *J. Appl. Polym. Sci.,* **86,** 1622 (2002).

40. M. G. Todd and F. G. Shi, *Microelectron. J.*, **33,** 627 (2002).

41. D. H. Kuo, C. C. Chang, T. Y. Su, W. K. Wang and B. Y. Lin, *Mater. Chem. Phys.,* **85,** 201 (2004).

42. A. V. Goncharenko, V. Z. Lozovski and E. F. Venger, *Opt. Commun.,* **174,** 19 (2000).

43. F. Claro and R. Rojas, *Phys. Rev. B,* **43,** 6369 (1991).

44. Y. Rao, J. Qu, T. Marinis and C. P. Wong, *IEEE Trans. Compon. Packag. Technol.,* **23,** 680 (2000).

45. S. H. Xie, B. K. Zhu, X. Z. Wei, Z. K. Xu and Y. Y. Xu, *Composites Part A,* **36,** 1152 (2005).

46. M. A. Berger and R. L. Mc Cullough, *Compos. Sci. Technol.,* **22,** 81 (1985).

47. G. W. Lee, M. Park, J. Kim, J. I. Lee and H. G. Yoon, *Composites Part A,* **37,** 727 (2006).

48. S. Kemaloglu, G. Ozkoc and A. Aytac, *Thermochim. Acta.*, **499,** 40 (2010).

49. R. C. Progelhof, J. L. Throne and R. R. Ruetsch, *Polym. Eng. Sci.*, **16,** 615 (1976).

50. L. Holliday and Robinson, *J. Mater. Sci.*, **8,** 301 (1973).

51. R. K. Goyal, A. N. Tiwari, U. P. Mulik and Y. S. Negi, *Compos. Sci. Technol.*, **6,** 1802 (2007).

Chapter 6

Conclusions and Scope for Future Work

This chapter summarizes the results of thesis and also directions for future work

Flexible electronics is a current active research area in the microelectronic industry. A new generation of flexible circuit connectors could produce a new class of electronic applications, such as stretchable thermometers, biomedical devices and electronic clothing etc. The future of electronic appliances should be flexible and stretchable in order to meet the demand of today's electronic industry. This growing demand of new generation electronic industry is to be satisfied by the development of new high performance materials. The present investigation deals with synthesis, characterization and properties of butyl rubber composites with low, high and very high ceramic fillers and also the effect of particle size on dielectric, thermal and mechanical properties of selected composites. The investigations carried out can be divided into 6 chapters.

The first chapter gives a general introduction about flexible electronics and dielectrics. The recent developments in flexible electronics and also the importance of elastomer-ceramic composites in today's electronic world are cited in this chapter. The chapter 2 deals with a brief description of the synthesis methods and characterization techniques of ceramic powder and their composites with butyl rubber used in the present work.

The synthesis, characterization and properties of butyl rubber-low permittivity ceramic composites are discussed in chapter 3. The low permittivity ceramic fillers used are Al_2O_3, SiO_2 and $BaZn_{1/3}Ta_{2/3}O_3$. The dielectric, thermal and mechanical properties of the composites is investigated as a function of ceramic loading. The effect of particle size on these properties is studied in butyl rubber-alumina composites. The XRD analysis of

ceramics revealed that the ceramics used are phase pure. The microstructure of the composites shows the dispersion of filler in the matrix and also the presence of some pores at higher filler loading. The dielectric properties of the composites are studied at 1 MHz and 5 GHz and are found to be improved with ceramic loading. For 0.1 volume fraction of micron alumina loading, the composite have relative permittivity (ε_r) of 2.82 and loss tangent (tanδ) of 0.0023 at 5 GHz and for the same volume fraction of nano alumina content the composite have ε_r of 3.15 and tanδ of 0.0140 at 5 GHz. The thermal properties of the composites also improved with filler content. The thermal conductivity (TC) and coefficient of thermal expansion (CTE) of BR/AL composite is 0.21 $Wm^{-1}K^{-1}$ and 142 ppm/^oC and that of BR/nAL composite is 0.27 $Wm^{-1}K^{-1}$ and 100 ppm/^oC respectively for 0.1 v_f of filler loading and for the same filler loading, the water absorption of both composites are 0.065 vol% and 0.700 vol% respectively. The butyl rubber-silica composites attained ε_r = 2.79, tanδ = 0.0039 for an optimum silica loading of 0.26 v_f and the butyl rubber-BZT composite have ε_r = 4.88, tanδ = 0.0022 for an optimum BZT loading of 0.26 v_f at 5 GHz. The butyl rubber-silica composite has CTE = 102 ppm/^oC, TC = 0.40 $Wm^{-1}K^{-1}$ and water absorption = 0.078 vol% for an optimum silica loading of 0.26 v_f. The butyl rubber-BZT composite have CTE = 112 ppm/^oC, TC = 0.30 $Wm^{-1}K^{-1}$ and water absorption= 0.047 vol% for an optimum BZT loading of 0.26 v_f. Various theoretical models are used to fit the experimental values of relative permittivity and thermal conductivity of all the composites. The stress strain curves of all composites show the mechanical flexibility of the composites. The butyl rubber-nano alumina composite shows better mechanical properties than that of micron composite, but BR/AL, BR/S and BR/BZT composites have better microwave dielectric properties. Hence

BR/AL, BR/S and BR/BZT composites are possible candidates for microwave substrate and electronic packaging applications.

The effect of high permittivity fillers such as TiO_2, $Sr_2Ce_2Ti_5O_{15}$ and $SrTiO_3$ on dielectric, thermal and mechanical properties of butyl rubber composites are given in chapter 4. The influence of filler particle size on the above mentioned properties is investigated in butyl rubber-rutile composites. The dispersion of filler particles in the butyl rubber matrix is depicted in microstructure analysis of composites. The dielectric properties of the composites both at 1 MHz and 5 GHz are investigated. For 0.40 v_f of micron rutile loading, BR/RT composite showed ε_r = 12.50 and tanδ= 0.0027 (at 5 GHz), CTE= 108 ppm/^oC, TC= 0.72 $Wm^{-1}K^{-1}$ and water absorption = 0.078 vol%. The BR/SCT composites have ε_r = 11.00 and tanδ= 0.00175 (at 5 GHz), CTE= 30 ppm/^oC and TC 0.49 $Wm^{-1}K^{-1}$ and water absorption of 0.068 vol% for 0.43 v_f of SCT content and BR/ST composites achieved a ε_r of 13.20 and tanδ of 0.0028 (at 5 GHz), CTE and TC of 26 ppm/^oC and 0.55 $Wm^{-1}K^{-1}$ respectively and water absorption of 0.081 vol% for 0.42 v_f of $SrTiO_3$. Stress strain curves of all composites indicate good mechanical flexibility of composites. All the above mentioned composites can be used as the core of flexible dielectric waveguide applications. The measured properties indicate that all the other compositions of BR/RT, BR/nRT, BR/ST and BR/SCT composites can be used as cladding of flexible dielectric waveguide, microwave substrates and electronic packaging applications. The experimental values of relative permittivity and thermal conductivity of all the composites are compared with theoretical models. A coplanar waveguide fed monopole antenna was fabricated using butyl rubber + 0.15 v_f of $SrTiO_3$ and have better bandwidth and return loss compared to FR-4 substrate.

Chapter-6

Chapter 5 discusses the synthesis, characterization and properties of butyl rubber-very high permittivity ceramic composites. The ferroelectric fillers like $BaTiO_3$ and $Ba_{0.7}Sr_{0.3}TiO_3$ are the very high permittivity ceramics used in the present study. The dielectric, thermal and mechanical properties of the composites are studied as a function of ceramic volume fraction and the influence of ceramic particle size is investigated in butyl rubber- barium titanate composites. BR/BT composite achieved a ε_r = 12.70 and tanδ = 0.0220 (at 5 GHz), TC=0.43 $Wm^{-1}K^{-1}$, CTE= 33 ppm/^oC and water absorption = 0.120 vol% for a $BaTiO_3$ ceramic loading of 0.38 v_f and that of BR/BST composite have ε_r = 13.10, tanδ = 0.0090, TC=0.41 $Wm^{-1}K^{-1}$, CTE= 29 ppm/^oC and water absorption = 0.060 vol% for a BST ceramic loading of 0.39 v_f. Both these composites are suitable candidates for core of flexible dielectric waveguide applications. Several theoretical models are used to fit the experimental values of relative permittivity and thermal conductivity of all the composites.

Scope for future work

- Development of butyl rubber composites in 1,3-type connectivity and investigate the microwave dielectric properties
- Fabrication of flexible waveguide using suitable butyl rubber composites developed.
- Development of butyl rubber composites with giant permittivity fillers like calcium copper titanate for flexible capacitor applications.
- Improvement of thermal conductivity of composites by adding high thermal conductivity ceramics such as aluminium nitride, silicon nitride etc.

****

List of publications

Publications in SCI journals

1. **Janardhanan Chameswary** and Mailadil T. Sebastian, Development of butyl rubber–rutile composites for flexible microwave substrate applications, *Ceram. Int.*, **40,** 7439-7448 (2014).
2. **Janardhanan Chameswary** and M. T. Sebastian, Effect of $Ba(Zn_{1/3}Ta_{2/3})O_3$ and SiO_2 ceramic fillers on the microwave dielectric properties of butyl rubber composites, *J. Mater. Sci. Mater. Electron.*, **24,** 4351-4360 (2013).
3. **Janardhanan Chameswary**, Lathikumari Krishnankutty Namitha, Methalayil Brahmakumar, and Mailadil Thomas Sebastian, Material characterization and microwave substrate applications of alumina-filled butyl rubber composites, *Int. J. Appl. Ceram. Technol.*, 1–8 (2013), DOI:10.1111/ijac.12067.
4. **Janardhanan Chameswary** and Mailadil Thomas Sebastian, Butyl rubber–$Ba_{0.7}Sr_{0.3}TiO_3$ composites for flexible microwave electronic applications, *Ceram. Int.*, **39,** 2795–2802 (2013).
5. Lathikumari Krishnankutty Namitha, **Janardhanan Chameswary** and Mailadil Thomas Sebastian, Effect of micro- and nano-fillers on the properties of silicone rubber-alumina flexible microwave substrate, *Ceram. Int.*, **39,** 7077–7087 (2013).
6. **Janardhanan Chameswary**, Dhanesh Thomas, Ganesanpotti Subodh, Soumya, Harshan, Jacob Philip and Mailadil Thomas Sebastian, Microwave dielectric properties of flexible butyl rubber– strontium cerium titanate composites, *J. Appl. Polym. Sci.*, **124,** 3426–3433 (2012).

7. Dhanesh Thomas, **Janardhanan Chameswary** and Mailadil Thomas Sebastian, Mechanically flexible butyl rubber–$SrTiO_3$ composites for microwave applications, *Int. J. Appl. Ceram. Technol.*, **8,** 1099 –1107 (2011).
8. **Janardhanan Chameswary**, Sherin Thomas and Mailadil Thomas Sebastian, Microwave dielectric properties of $Co_2La_4Ti_3Si_4O_{22}$ ceramics, *J. Am. Ceram. Soc.*, **93,** 1863–1865 (2010).
9. **Janardhanan Chameswary**, K. Jithesh, S. George, R. Sujith, P. Mohanan and M. T.Sebastian, PTFE-SWNT composites for microwave absorption application, *Mater. Lett.*, **64,** 743-745 (2010).
10. L. E. Yahaya, K.O. Adebowale, A. R. R. Menon, S. Rugmini, B. I. Olu-Owolabi and **Janardhanan Chameswary**, Natural rubber/organoclay nanocomposites: Effect of filler dosage on the physicomechanical properties of vulcanizates, African Journal of Pure and Applied Chemistry, **4,** 198-205 (2010).

Conference proceedings

1. **J. Chameswary** and M. T. Sebastian, Effect of nano silica filler on the microwave dielectric properties of butyl rubber composites, Nano india-2013.
2. **J. Chameswary** and M. T. Sebastian, Butyl Rubber–Nano Strontium Titanate Composite for Microwave Flexible Electronic Applications, International Conference on Frontiers in Materials Science and Environment (ICFMS)-2012.
3. **J. Chameswary** and M. T. Sebastian, Microwave Dielectric Characteristics of Butyl Rubber- Barium Titanate Composites, CICMT-2012.
4. L. K. Namitha, **J. Chameswary,** S. Ananthakumar and M.T. Sebastian, Microwave dielectric properties of flexible silicone rubber and butyl rubber

composites with aluminium nitride, 2nd International Conference on Advanced Functional Materials ICAFM-2014.

5. K. Anlin Lazar, **J. Chameswary** and M. T. Sebastian, Effect of dopant addition on the dielectric properties of lithium rare earth silicate ceramics, International Conference on Multifuctional Materials (ICMM)-2010.
6. **J. Chameswary,** Sherin Thomas and M. T. Sebastian, Microwave dielectric properties of novel rare earth based titanium silicate ceramics, International Conference on Electroceramics (ICE)-2009.
7. T. S. Sasikala, **J. Chameswary,** C. Pavithran, M. T.Sebastian, Preparation and Dielectric properties of Forsterite loaded Polymer Composites for Microelectronic Applications, International Conference on Advanced Functional Materials (ICAFM)-2009.
8. **J. Chameswary** and A. R. R. Menon, Multifunctional pressure sensitive adhesives based on blends of natural rubber, polychloroprene rubber and phosphorylated cashew nut shell liquid prepolymer, 21st Kerala Science Congress-2009.